Master thesis and internship[BR]- Master's thesis : Thermo-mechanical modeling of composite materials subjected to fire[BR]- Integration Internship

Auteur : Dethier, Victor
Promoteur(s) : Noels, Ludovic
Faculté : Faculté des Sciences appliquées
Diplôme : Master en ingénieur civil en aérospatiale, à finalité spécialisée en "aerospace engineering"
Année académique : 2021-2022
URI/URL : http://hdl.handle.net/2268.2/14528

Thermo-mechanical modeling of composite materials subjected to fire

Master's thesis carried out to obtain the degree of
Master of Science in Aerospace Engineering

Author: Victor DETHIER

Internship supervisor: Michaël BRUYNEEL (GDTech)

Academic advisor: Prof. Ludovic NOELS

Abstract

Composite materials, and especially Polymer Matrix Composites, are increasingly used in engineering applications such as in aerospace or marine structures. The environments in which they are used can be prone to fire events. However, the fire resistance of Polymer Matrix Composites is rather poor. This is explained by the fact that the polymer matrix reacts to fire and undergoes pyrolysis. Premature failures are therefore occurring. It is thus important to be able to model the thermo-mechanical response of composites subjected to fire in order to prevent these failures. This type of modeling, including pyrolysis, is not available nowadays at some companies working on composite materials. It is therefore useful to investigate this subject.

In this work, the physics related to composites in fire are first explained. The most used thermo-mechanical models are identified. A common feature between them is the use of a two-step analysis. First, a thermal analysis is performed. It is then followed by a decoupled mechanical analysis. This work is focusing mostly on the thermal part. A thermal model developed by Henderson et al. is found to be a reference in that domain. The classical mechanical models are also briefly explained.

Using the finite element software SAMCEF, the thermal model is solved. The detailed methodology required to use correctly the software is given. Some adaptations of the formulas and the material properties are done. A methodology used to perform a short mechanical analysis is also given. The results from the thermal model, and more specifically the temperature distributions, are compared to experimental and analytical results found in the literature. They are not very conclusive in the first instance. The value of the matrix decomposition energy must be increased in order to improve the results. It is also shown that some properties must be tuned to fit the experimental curves when the material data is not precisely known.

Eventually, a short and simple mechanical analysis using elastic and advanced material laws is performed and some results are interpreted. It is nonetheless limited by the lack of knowledge about both the thermal and mechanical properties for a same composite material. Therefore, only generic results are obtained. They cannot be over-interpreted.

Acknowledgements

Contents

6 Conclusions and perspectives   82

Appendix   84

Bibliography   91

List of Figures

List of Tables

Nomenclature

Abbreviations

CFD Computational Fluid Dynamics

DSC Differential Scanning Calorimeter

EGVE E-Glass Vinyl Ester

FRP Fiber Reinforced Polymer

PMC Polymer Matrix Composite

RMF Remaining Mass Fraction

STA Simultaneous Thermo-gravimetric Analyzer

TGA Thermo-Gravimetric Analyzer

Symbols

α absorptivity

α generalized density

β thermal diffusivity

ΔA unit cross-sectional area

Δx control volume width

δ thermal conduction boundary layer

$\dot{m}$ mass flow rate

$\dot{m}''$ mass flux

γ permeability

μ dynamic viscosity

Φ constant related to the temperature range over which strength is reduced

NOMENCLATURE

ϕ porosity

ρC volumetric heat capacity

ρ density

σ Stefan-Boltzmann constant

$\sigma_{c(R)}$ residual compressive strength at high temperature

σ_{av} average compressive strength

$\sigma_{c(o)}$ compressive strength at room temperature

ε emissivity

φ_s solid material volume fraction

φ_{cr} cracks volume fraction

ζ decomposition permeability factor

A rate constant of the polymer matrix decomposition reaction

C specific heat capacity

d damage variable

E activation energy of the polymer matrix decomposition reaction

F surface load

F virgin material relative mass fraction

h specific enthalpy

H_p pyrolysis heat

h_{conv} convection coefficient

K boundary condition parameter

k thermal conductivity

K_p gas diffusion coefficient

L thickness

M polymer matrix mass

m mass

NOMENCLATURE

M_g molecular mass

n order of the polymer matrix decomposition reaction

P pressure

Q decomposition energy

q'' heat flux

R universal gas constant

R_{rc} scaling function

T temperature

t time

T_k temperature at which the compressive strength is half the strength at room temperature

u displacement

u specific internal energy

V volume

v specific volume

x through-thickness spatial variable

x' specific location in the through-thickness direction

Subscripts

$_0$ initial

$_c$ char

$_f$ final

$_g$ decomposition gases

$_p$ polymer matrix

$_r$ radiation source

$_s$ surface

$_v$ virgin

NOMENCLATURE

$_{11}$	fiber direction
$_{12}$	shear direction
$_{22}$	transverse direction
$_{\infty}$	surrounding
$_{\perp}$	through-thickness (transverse)
$_{app}$	apparent
$_{rad}$	radiation
$_{ref}$	reference

Chapter 1

Introduction

This master thesis consists in the thermo-mechanical modeling of composite materials subjected to fire. It is realized as part of an internship at the company GDTECH. In this chapter, a short summary is made about the general context and the main motivations regarding this subject. Then the objectives of the work, jointly defined with the company, are detailed. A first preview of the methodology used to achieve these objectives is presented. Eventually, the outline of this master thesis is given.

1.1   Context and motivations

Composite materials, and especially Polymer Matrix Composites (PMC), are increasingly used in engineering applications such as in aerospace or marine structures. Another common name for PMC is Fiber Reinforced Polymer (FRP). As their names suggest, PMC or FRP are composed of a polymer matrix in which are present reinforcing fibers. There exist many resin-fiber combinations used in the industry. These materials present a high strength-to-weight ratio, which is their main advantage. They allow therefore to have lightweight structural elements that comply with the mechanical properties required by the application. In the aerospace industry, for example, some fuselage and wings components are nowadays made with composite materials. They are chosen at the expense of regular isotropic materials such as aluminum for the purpose of weight and, eventually, fuel consumption reduction. PMC materials also present other advantages such as a good resistance to corrosion and fatigue. Moreover, composite materials allow for creating complex shapes which is a limitation for metal parts. It therefore requires less assembly processes. All these advantages justify the use of PMC in the aerospace and marine industries [1–3].

Although PMC are competitive materials, they are also known to have several drawbacks compared to regular isotropic materials. Among these drawbacks, mention can be made about the high cost of constituents materials and manufacturing. Composite mate-

rials also present a risk of delamination upon shocks. This often leads to the replacement of the entire component since local repairs are difficult to achieve. Another important concern about PMC is their poor fire resistance and high flammability. Indeed, since they are composed of an organic matrix, they react to fire.

PMC materials are sometimes used in environments where they are prone to be subjected to fire. In aircraft, ships or even offshore platforms, fire can develop and reach structural elements made in composite materials. The occurrence of fire leads to the matrix degradation and decomposition through a pyrolysis effect. It releases smoke, toxic fumes and generates a large amount of heat. Besides that, the resulting temperature increase leads to thermal softening. Both the polymer matrix degradation and the thermal softening alleviate the PMC's mechanical properties. This causes loaded structures to deform and eventually fail. All these fire consequences constitute a serious hazard for the affected structure, but also for the people on board [4]. It is therefore important to consider the fire properties of PMC when they are used in dangerous environments. The characterization of the thermal response and degradation as well as the decrease of the mechanical properties is crucial in order to avoid incidents.

1.2 Objectives

As explained at the beginning of this chapter, the master thesis is realized as part of an internship at the company GDTECH. The objective of this internship is to model the thermo-mechanical behavior of PMC materials subjected to fire thanks to the finite element software SAMCEF [5]. The thermo-mechanical model is decoupled which means that first a thermal analysis is performed and then the resulting temperatures are used in a mechanical model. This type of analysis has never been done at GDTECH and they are therefore not able to model these kinds of problems. The goal is thus to initiate this modeling for the company and to prove that it is feasible, especially regarding the thermal part which is really not mastered at GDTECH.

The first objective is to understand the physics behind the thermal response of composite materials exposed to fire (one-sided heating). The different processes occurring in reality have to be well understood in order to develop an accurate model.

Then, the second objective is to represent accurately the time-dependant thermal response of the composite material subjected to fire. This requires the use of a thermal model representing the physics of the problem identified in the first objective. It is aimed at predicting the matrix degradation and the internal temperature distribution in a composite sample. Note that this is the main objective because thermal models including pyrolysis have never been used at GDTECH. Therefore, they would like to focus on

this type of problems and apply it to mechanical models that they already have in their database.

The last objective is to apply the temperature distribution obtained thanks to the thermal model to a mechanical model already used by the company. It allows to show that a complete thermo-mechanical modeling can be performed with SAMCEF to simulate the temperature-dependent mechanical response of a PMC sample. The main goal is to show that a transfer of the temperature distribution from the thermal to the mechanical model can be done and to verify if the results are consistent. A complete mechanical modeling is not the objective because of time constraints and a lack of experimental data in the literature to validate the results.

1.3   Preview of the methodology

The most used models coming from the literature are first identified. They all consider a two-step analysis involving first a thermal and then a mechanical model [6, 7]. Many thermal models have been developed in the past years [6, 7]. They are more or less complex depending on the processes that they take into account. The one that is considered as a reference to predict the thermal response is a model developed by Henderson et al. [8]. It is a rather simple model but which represents nonetheless accurately the thermal behavior of composites exposed to fire. It takes into account the most important processes that are involved in the composite response to fire conditions. This model is governed by an energy equation and a continuity equation (mass conservation). It is based on the material thermal properties which are temperature-dependent but which also depend on the state of decomposition in the material. Moreover, this model presents the required boundary conditions that have to be defined.

Regarding the mechanical part, not a lot of research has been done in the literature since the objective of this master thesis is not to focus on the mechanical modeling. Some mechanical models have nonetheless been identified in the literature in order to see what is done in practice. Some simple analytical models have been found [4, 9]. They mainly consider the decrease of the strength due to temperature. They are used to calculate the time-to-failure of composite samples. There also exist very complicated models that are beyond the scope of this work [7].

In order to model the thermal response using SAMCEF, the model from Henderson et al. [8] is used as a reference (most used model in practice). The way a thermal problem is solved by the solver is identified. Then, the heat transfer and continuity equations (including pyrolysis) implemented by default in the software are compared to the one used in the reference model. They are adapted (if needed) to stick to this model. The

materials properties required by SAMCEF for this type of problem are identified. The mesh, the thermal loads and the boundary conditions are then defined. Moreover, the time integration parameters are chosen according to the problem. Experimental and analytical results for the thermal response of composites exposed to fire are used to validate the results obtained with SAMCEF for these same composites. They come from two different publications [4, 10] using the reference model developed by Henderson et al. [8]. Some materials parameters are adapted if needed based on a sensitivity analysis.

Once the thermal response is correctly represented, the resulting time-varying temperature distribution is imposed in a decoupled mechanical model. The goal is here to present a simple and rapid analysis since it is not the main objective of the work and that not a lot of time is dedicated to it. As done for the thermal part, the geometry and the mesh are created. Then, the loads and boundary conditions are chosen. Eventually, the material is defined with temperature dependent properties. Note that it was difficult to find publications about this subject giving enough information about both their thermal and mechanical properties of materials. It is therefore complicated to perform a complete valid thermo-mechanical analysis for a specific composite due to this lack of information. The temperature distribution obtained thanks to the thermal model for the material used in [4] is thus applied to another material available in the database of GDTECH, for which the mechanical properties are known.

1.4 Outline of the thesis

In Chapter 2, a review of the multi-physics models found in the literature is made. The most used models are discussed in details, including the materials definitions. The common assumptions made in practice are explained.

In Chapter 3, the methodology used in the thermal modeling using the software SAMCEF is presented. The geometry, material definitions, boundary conditions and the time integration are discussed. After the modeling of the thermal part, the modeling methodology used for the mechanical part is detailed.

In Chapter 4, the thermal model is validated based on two different publications coming from the literature. The methodology explained previously is applied and the results are discussed. Some materials parameters are tuned to adapt the numerical model.

In Chapter 5, the application of a temperature distribution in a mechanical model and the resulting mechanical response are analyzed and discussed.

In Chapter 6, the conclusions and some perspectives for further works are presented.

Chapter 2

Multi-physics models

2.1   Introduction

A lot of research has been conducted on composite materials subjected to fire since the 1990s. The first studies focused mainly on the fire properties of the PMC such as their flammability, the heat release rates and the smokes properties. Researchers also focused on the polymer composites flammability reduction [11–14].

Then, more researches have been undertaken about the structural properties of polymer matrix composites during exposition to fire. These researches aimed at analyzing and modeling the fire-under-load behavior of PMCs. Mouritz et al. [6] made a general review of the different structural response models developed for PMC materials subjected to fire. The models have been assessed thanks to experimental tests carried out to this end.

When PMC materials are exposed to fire, four different types of processes take place. These are either *thermal*, *chemical*, *physical* or *failure* processes. It is important to take them into account in order to accurately model the structural response of the exposed PMC. Before going into the details, the three first types of processes are listed in Tab. 2.1 and represented schematically in Fig. 2.1. The thermal, chemical and physical processes occur during exposure to fire of PMC materials no matter the presence or not of loading. On the contrary, the failure processes are load-dependent. They also depend on the processes presented in Tab. 2.1 which influence the mechanical properties of the material.

These four processes are not well separated from each other. An important coupling between them is present. Indeed, as it can be seen in Tab. 2.1, the thermal and chemical processes are for example really interdependent. The relation between these two types of processes and the physical processes is less straight forward but exists. All these interactions make the structural behavior of PMC difficult to model.

Fire processes		
Thermal	**Chemical**	**Physical**
Heat conduction from fire through the composite	Matrix viscous softening	Thermal strains
Heat generation (exothermic) or absorption (endothermic) from the matrix decomposition	Matrix melting	Internal pressure accumulation
Heat convection (cooling) from the hot gases and moisture vapors	Matrix decomposition	Pores creation
Heat generation from oxidation (char + fibers)	Matrix volatilisation	Matrix cracking
Heat generation from flammable volatiles' ignition	Char formation, growth and oxidation	Delamination
	fibers oxidation	fiber-matrix debonding
	Char-fibers reactions	Surface ablation

Table 2.1: Listing of the thermal, chemical and physical processes occurring in PMC exposed to fire [6]. The failure processes are not presented.

As it is explained above, the thermal, chemical and physical fire processes are coupled. This leads to a complex thermo-mechanical behavior of the composite materials when they are subjected to fire. In practice, it is really complicated to model such interactions. Therefore, most thermo-mechanical models are based on a two-step analysis [6]. First, the thermal response is computed thanks to a thermal model in order to obtain an accurate solution for the temperature distribution. Then, this temperature distribution is used in a mechanical model in which the material properties are influenced by the temperature. This leads to a simpler analysis than if all the couplings had to be taken

into account. The results obtained thanks to this kind of two-step analysis present a good agreement with the one obtained experimentally [6].

Both the thermal and the mechanical models found in the literature are discussed in the next sections. The focus is put on the thermal models since it is the most important part of this master thesis. Then a short presentation of mechanical models is made.
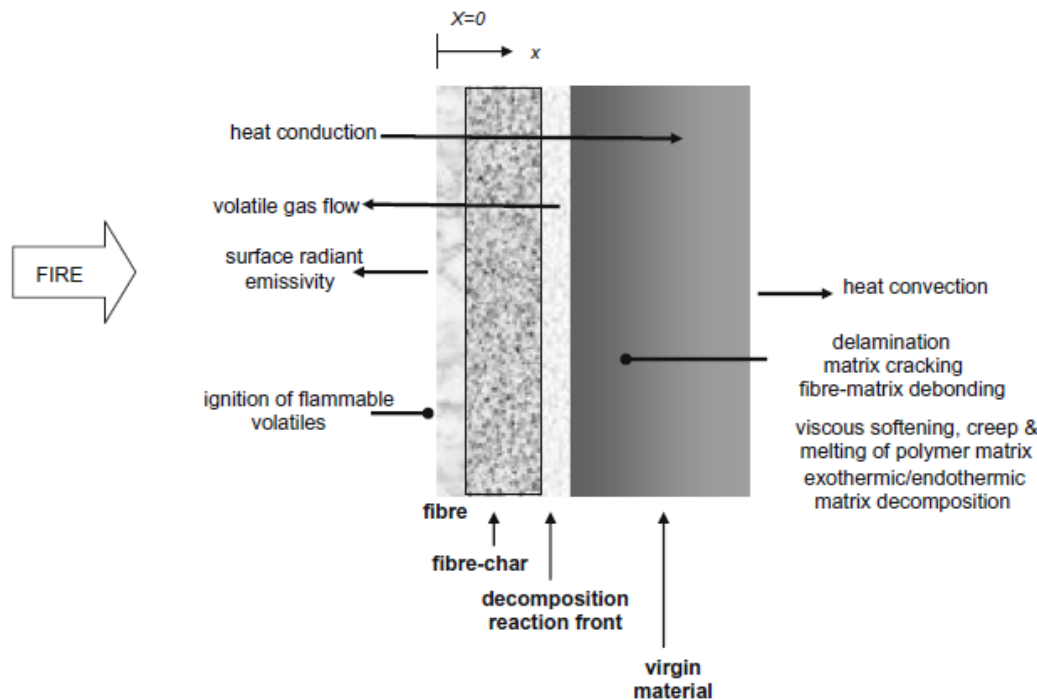
Figure 2.1: Schematic representing the different processes occurring in the through-thickness direction during fire exposure of a PMC. From Mouritz et al. [6].

2.2 Thermal models

The structural behavior of PMC materials subjected to fire has been modeled by several researchers in the past years. The first step in the modeling is about the correct representation of the thermal processes taking place in reality. The main goal is to accurately determine the temperature distribution inside the material. It also allows to characterize the decomposition state inside the material. As specified by Mouritz et al. [6], the PMC thermal modeling is therefore a crucial stage.

Multiple thermal models exist in the literature. These models are more or less complex. They take into account multiple transient processes which depend on the temperature through the material. They are either chemical or physical and are governing the PMC thermal response. These processes as well as the temperature at which they occur in the case of fiberglass composites are presented in Fig. 2.2. It is important to note that

the temperature ranges given in Fig. 2.2 may vary with the type of matrix and the fire conditions. Among all these processes, at least three are always present in the thermal models used in practice: heat conduction, matrix pyrolysis and gas flow. It is the case in the models developed by Henderson et al. [8] and Gibson et al. [15], in which only these three processes are considered. In addition to those mentioned above, other processes such as the thermal expansion/contraction and the increasing gas pressure are taken into account in different thermal models although they influence less the composites thermal response [16, 17].
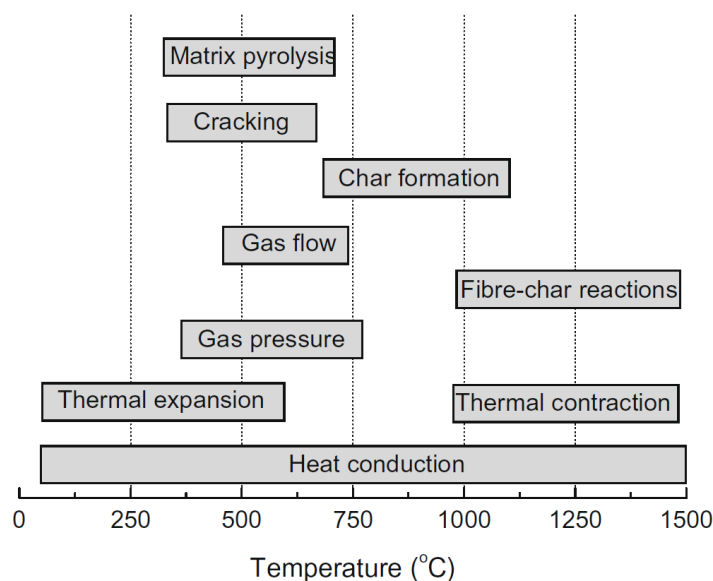
Figure 2.2: Temperature-dependent processes occurring inside fiberglass PMC laminates. From Mouritz et al. [6].

A significant majority of the developed thermal models assume one-sided heated materials. Most of them are thus one-dimensional models considering the temperature variation only in the through-thickness direction. Indeed, it is very important to know how the temperature evolves in that direction. Moreover, regarding the fire itself, it is in most cases simulated by a regulated radiant heat flux or by an imposed surface temperature [6]. The fire expansion as well as the fire-composite interactions are hence not represented. However, more sophisticated models have been developed in order to simultaneously simulate the fire dynamic behavior and its interaction with the PMC exposed surface [18–20]. These models use Computational Fluid Dynamics (CFD) techniques that allow to represent the complex heat flow coming from the flames. The CFD simulation results are then coupled with the finite element representation of the PMC material. This enables to properly model the boundary conditions variations at the fire-exposed surface. Nevertheless, as explained previously, most existing models do not take into account these fluid dynamics interactions.

2.2.1 Common assumptions

Many assumptions are made in the thermal models used in practice. However, making these assumptions do not influence much the temperatures compared to the one obtained experimentally.

First, as explained above, only three main processes are usually considered. The others that are presented in Tab. 2.1 are not taken into account in the models. These three main processes are: the heat conduction, the polymer matrix decomposition (pyrolysis) and the gas diffusion coming from this decomposition. The matrix cracking, the pressure rise, the thermal expansion/contraction and the fiber-char reactions are generally not represented in the thermal models because they influence much less the thermal response [6].

Then, it is usually assumed that there is a thermal equilibrium between the material and the gases coming from the decomposition. These gases are also considered to behave ideally and to be non-reactive [10].

Eventually, the composite material is viewed by the thermal model as being "homogeneous". This means that no distinction is made between the fibers and the matrix. Indeed, the material thermal properties are generally defined for the composite as a whole [7] (except for the matrix decomposition properties).

2.2.2 Energy equation

Many thermal models exist to simulate the thermal response of PMC materials subjected to fire. Nonetheless, the model developed by Henderson et al. [8], has been one of the most used models and is still used nowadays [21]. Therefore, this is the model that is mainly explained in this chapter. It is governed by a one-dimensional energy equation characterizing the global thermal response of the composite along its thickness. As specified previously, this model considers three processes influencing the temperature distribution through the material. These are the heat conduction, the polymer matrix decomposition (pyrolysis) and the gas diffusion coming from this decomposition. Taking these processes into account, the one-dimensional governing energy equation writes [8]:

$$\frac{\partial}{\partial t}\left(mh + m_g h_g\right) = \frac{\partial}{\partial x}\left(k_\perp \frac{\partial T}{\partial x}\right)\Delta x \Delta A - \frac{\partial}{\partial x}\left(\dot{m}_g h_g\right)\Delta x - Q_i \frac{\partial m}{\partial t}. \qquad (2.1)$$

It is a non-linear partial differential equation with a control volume formulation. The material properties depend on the temperature and on the decomposition state of the material. They are discussed in details in Section 2.2.5.

The different variables present in Eq. 2.1 are the:

- time t

- composite instantaneous mass m

- composite specific enthalpy h

- decomposition gases mass m_g

- decomposition gases specific enthalpy h_g

- through-thickness spatial variable x

- through-thickness thermal conductivity $k_\perp$

- temperature T

- control volume width Δx

- unit cross-sectional area ΔA

- decomposition gases mass flow rate $\dot{m}_g$

- decomposition energy Q_i

Another form of the energy equation is usually used in the thermal models. It is obtained by applying the mass conservation equation to Eq. 2.1. The mass conservation equation, also called continuity equation, is discussed in the next section and is written as follows [8]:

$$-\frac{\partial m}{\partial t} = \frac{\partial \dot{m}_g}{\partial x}\Delta x + \frac{\partial m_g}{\partial t}. \tag{2.2}$$

Applying this continuity equation to the energy equation given by Eq. 2.1 leads to the other form of the energy equation represented by Eq. 2.3. The detailed mathematical developments used to derive this equation are given in Appendix A.

$$(mC + m_g C_g)\frac{\partial T}{\partial t} = \frac{\partial}{\partial x}\left(k_\perp \frac{\partial T}{\partial x}\right)\Delta x \Delta A - \dot{m}_g C_g \frac{\partial T}{\partial x}\Delta x - \frac{\partial m}{\partial t}\left(Q_i + h - h_g\right), \tag{2.3}$$

where C and C_g are the composite and the decomposition gases specific heat capacities, respectively.

As said previously, the thermal equation Eq. 2.3 developed by Henderson et al. [8] is one-dimensional and non-linear. The first term on the right-hand side represents the heat conduction process which occurs in the through-thickness direction. It considers classical heat conduction and takes into account the fact that the thermal conductivity varies through the material. The value of the thermal conductivity depends on the temperature and also on the stage of the matrix decomposition. A detailed description of the thermal conductivity is made in Section 2.2.5.2.

The second term considers the heat convection due to the outflow of volatiles coming from the polymer matrix decomposition. These hot gases flow out of the material towards the heated surface through the char material. Since they are colder than the heated part, they have a convective cooling effect on the material which explains the minus sign. More information about the gas mass flow is provided in Section 2.2.3.

The last term stands for the heat generated or consumed by the polymer matrix decomposition ($i = p$) and the carbon-silica reactions ($i = c$). The carbon-silica reactions may occur between the fibers and the char region when the temperature is high enough (~ 1000°C for glass fibers). It is therefore usually not occurring and the models consider only the term Q_p. If the decomposition process is endothermic, this term is negative which characterizes a heat consumption. This is the case for most polymer matrix. In the presence of an exothermic reaction, this term would obviously be positive to characterize a heat generation. As it can be seen in this last term of Eq. 2.3, the heat generated or consumed by the polymer matrix pyrolysis depends on the decomposition reaction rate expressed by $\frac{\partial m}{\partial t}$. This term is developed in Section 2.2.5.1.

The thermal model developed by Gibson et al. [15] has been and remains also used a lot in practice. This is actually a slightly modified version of the model from Henderson et al. [8] presented above. In this case, the thermal response of the PMC material is described by the following equation:

$$\rho C \frac{\partial T}{\partial t} = \frac{\partial}{\partial x} \left(k_\perp \frac{\partial T}{\partial x} \right) - \dot{m}_g'' \frac{\partial h_g}{\partial x} - \frac{\partial \rho}{\partial t}(Q_p + h - h_g), \tag{2.4}$$

where ρ is the instantaneous composite density. Eq. 2.4 is directly obtained from Eq. 2.3 which is divided by the total volume V, assumed constant (no expansion considered). Note that the through-thickness thermal conductivity is going to be simply written k in the rest of the text.

The three terms on the right-hand side of Eq. 2.4 represent the three main fire processes presented previously, as in Eq. 2.3. Nevertheless, this thermal model from Gibson et al. [15] does not consider the reactions between the char and the fibers. Therefore, only the value of Q_p representing the polymer matrix decomposition energy is taken into account in the last term. This model is thus able to predict the thermal response of the PMC material up to temperatures below which these reactions do not occur (~ 1000°C for glass fibers). The decomposition reaction rate of the polymer matrix in terms of density can also be represented by a term $\frac{\partial \rho}{\partial t}$ based on the Arrhenius law (see Section 2.2.5.1).

It can also be noticed in Eq. 2.4 that the decomposition gases specific heat capacity C_g is not present on the left-hand side. This is because it is considered to be already

taken into account in the composite specific heat capacity C. Indeed, depending on how C is measured in practice, it sometimes already includes the contribution of the heat capacity from the gas present in the pores. In that case, the real expression for C is given by Eq. 2.5. This equation is valid under the assumption that the decomposition gases and the gas present in the pores during the property measurement (air/nitrogen) have the same specific heat capacity. This is not the case in reality but this assumption is usually considered to be valid [22].

$$C \approx \left[C + \frac{(m_g/V)}{\rho} C_g \right].$$ (2.5)

As explained previously, both thermal models described by Eq. 2.3 and Eq. 2.4 are used to estimate the time-dependant temperature distribution through PMC materials exposed to fire. Experimental studies validated the models by showing that they could accurately predict the temperature evolution at different locations in the material [4, 9]. For example, Feih et al. [9] compared experimental measurements to temperatures predicted by the model from Gibson and colleagues [15]. They used PMC laminates made of E-glass fibers (woven fabric) and vinyl ester resin with a [0/90] stacking sequence. The samples were 9 mm thick and were exposed to a constant heat flux using a conical heater (on one side). The heat flux, denoted q'', ranged from 10 kW/m² to 75 kW/m². A good correlation was observed between the predicted and measured temperatures as it can be seen in Fig. 2.3.

2.2.3 Continuity equation

The energy equation governing the thermal response of FRP exposed to fire has been described in the previous section. In order for the thermal model to be consistent, this equation requires an additional relation related to mass conservation. Indeed, when the polymer matrix is subjected to pyrolysis, it loses solid mass at a certain rate $\frac{\partial m}{\partial t}$. This process releases decomposition gases. In that case, it is thus necessary to respect the principle of mass conservation expressed by Eq. 2.6. It is called the mass continuity equation and must always be verified [8].

$$-\frac{\partial m}{\partial t} = \frac{\partial \dot{m}_g}{\partial x} \Delta x + \frac{\partial m_g}{\partial t}.$$ (2.6)

The mass loss rate $\frac{\partial m}{\partial t}$ on the left-hand side of Eq. 2.6 is computed thanks to an Arrhenius function explained in Section 2.2.5.1. The first term on the right-hand side represents the spatial variation of the gas mass flow rate $\dot{m}_g$. This gas mass flow rate can be obtained thanks to the Darcy law rewritten in Eq 2.7 [10]. The last term in Eq. 2.6 stands for the storage rate of gas mass m_g into the material. The continuity equation Eq. 2.6, combined with Eq. 2.7, allows calculating the gas mass flow rate during

(a) $q = 10 \text{ kW/m}^2$

(b) $q = 25 \text{ kW/m}^2$

(c) $q = 50 \text{ kW/m}^2$

(d) $q = 75 \text{ kW/m}^2$
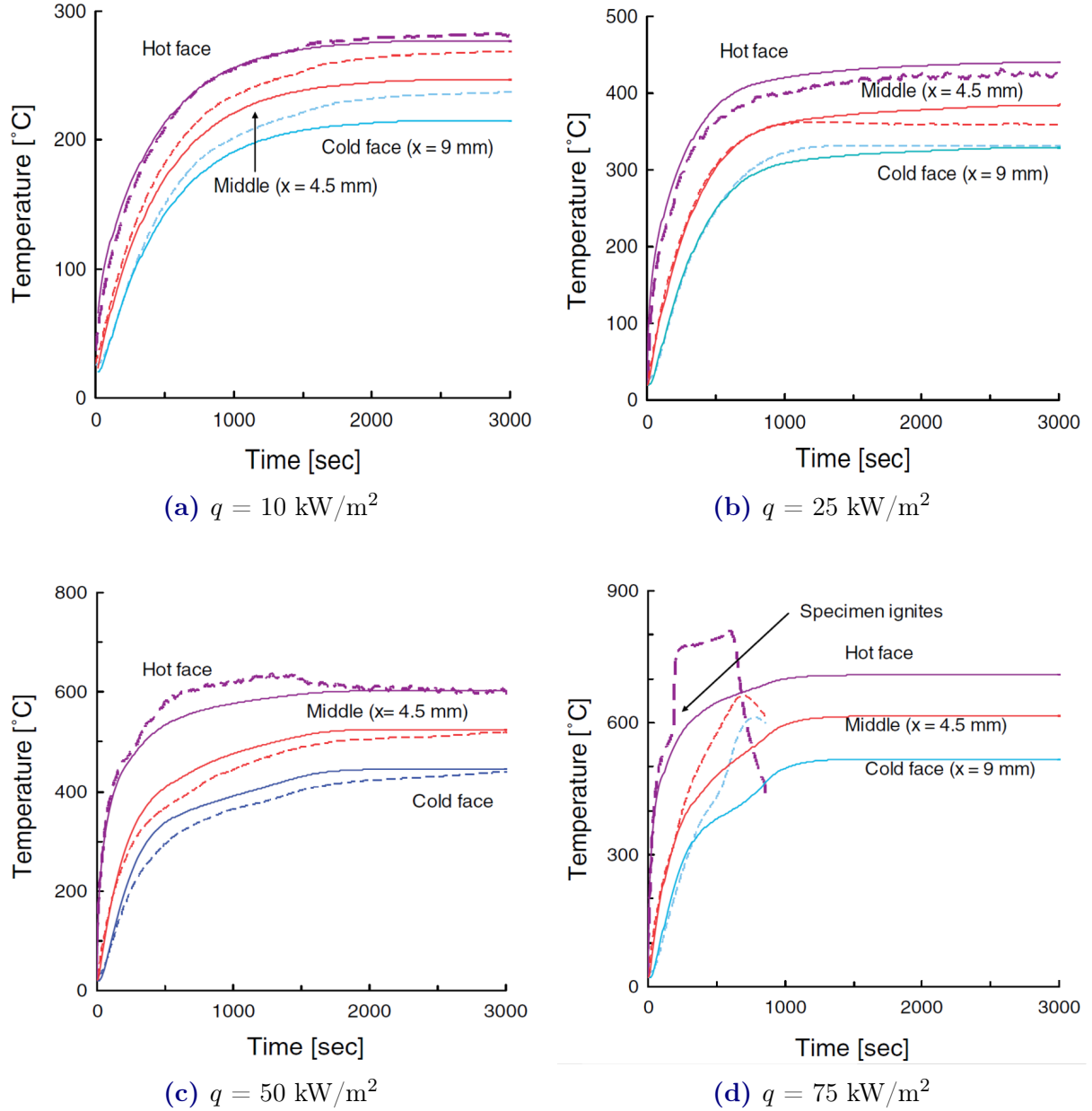
Figure 2.3: Evolution of the time-varying temperature at the hot, middle and cold
faces of a glass/vinyl ester laminate for different values of the heat flux q.
Experimental results (dashed lines) and predicted values (solid lines).
From Feih et al. [9].

decomposition.

$$\dot{m}_g = -\frac{\gamma m_g}{\mu \phi \Delta x} \frac{\partial P}{\partial x}, \tag{2.7}$$

where γ is the composite permeability, μ the decomposition gases viscosity, ϕ the composite porosity and P is the pressure. The composite permeability and porosity depend
on the material state of decomposition. These parameters are discussed later in Section 2.2.5.7. Note that the pressure can be found thanks to Eq. 2.8 [10].

$$P = \frac{\rho_g RT}{M_g} \qquad \text{with} \qquad \rho_g = \frac{m_g}{\phi \Delta x \Delta A}, \tag{2.8}$$

where ρ_g is the decomposition gases density, R the universal gas constant and M_g the decomposition gases molecular mass.

Some other thermal models, such as the one from Lattimer et al. [22], use a modified version of the continuity equation given by Eq. 2.6, which is the following:

$$-\frac{\partial \rho}{\partial t} = \frac{\partial \dot{m}_g''}{\partial x}, \tag{2.9}$$

which is based on the following assumptions:

$$V = \text{cst}, \tag{2.10}$$

$$m_g \ll m. \tag{2.11}$$

The mass conservation equation expressed by Eq. 2.9 is particularly convenient in order to compute the gas mass flux $\dot{m}_g''$. Indeed, Lattimer et al. [22] derived from it a simple expression for the gas mass flux through the material. This expression is given by Eq. 2.12. Decomposition gases are assumed to only escape the material through the face exposed to fire. Moreover, it is assumed that the material does not expand.

$$\dot{m}_g''(x', t) = \frac{\partial}{\partial t} \int_{x'}^{L} \rho \, dx, \tag{2.12}$$

where x' is a specific location in the through-thickness direction and L is the composite thickness. The density is known at any time and location in the material thanks to an Arrhenius function representing the decrease in density and described in Section 2.2.5.1. Therefore, obtaining the value of the gas mass flux is straightforward.

2.2.4 Boundary conditions

The thermal models also require appropriate boundary conditions in order to be accurate. These have to be defined for both the exposed and non-exposed side of the composite material. The existing models from different authors present identical boundary conditions definitions [6, 10, 15, 22]. The boundary conditions involve a radiative and convective component. Combined together, the radiative and convective terms represent the net surface heat flux into the material. These boundary conditions are expressed by Eq. 2.13 and 2.14, respectively for the exposed and unexposed sides [22].

$$-k \left. \frac{\partial T}{\partial x} \right|_{x=0} = \varepsilon_s \left(q''_{rad} - \sigma T_{s,0}^4 \right) + h_{conv,0} \left(T_\infty - T_{s,0} \right), \qquad (2.13)$$

$$k \left. \frac{\partial T}{\partial x} \right|_{x=L} = \varepsilon_s \sigma \left(T_\infty^4 - T_{s,L}^4 \right) + h_{conv,L} \left(T_\infty - T_{s,L} \right). \qquad (2.14)$$

with ε_s being the composite surface emissivity, σ the Stefan-Boltzmann constant, h_{conv} the convection coefficient, T_s the composite surface temperature and T_∞ the surrounding temperature (ambient). The effect of fire is represented by the radiative heat flux q''_{rad}.

Henderson et al. [10] give a more detailed expression of the boundary condition for the exposed side. It is represented by Eq. 2.15.

$$-k \left. \frac{\partial T}{\partial x} \right|_{x=0} = \sigma \varepsilon_r \alpha_s T_r^4 - \varepsilon_s \sigma T_{s,0}^4 + h_{conv,0} \left(T_\infty - T_{s,0} \right), \qquad (2.15)$$

where ε_r is the radiation source emissivity, T_r is the radiation source temperature and α_s is the composite surface absorptivity. Note that the emissivity and the absorptivity of the material usually depends on its state of decomposition. This parameter is discussed in a following section (see Section 2.2.5.6).

The material exposed surface is often assumed to be a gray surface, its absorptivity α_s and its emissivity ε_s are equal [23]. Therefore, Eq. 2.15 can be rewritten as follows:

$$-k \left. \frac{\partial T}{\partial x} \right|_{x=0} = \varepsilon_s \left(q''_{rad} - \sigma T_{s,0}^4 \right) + h_{conv,0} \left(T_\infty - T_{s,0} \right), \qquad (2.16)$$

$$\text{with} \qquad q''_{rad} = \sigma \varepsilon_r T_r^4. \qquad (2.17)$$

It can be observed that Eq. 2.16 corresponds to the boundary condition used in most models, which is given by Eq. 2.13. Slightly different boundary conditions definitions exist in the literature. For example, Yu and Zhou [24] developed a more sophisticated model to simulate a flame heat flux.

Another important boundary condition imposed in the thermal models is the surface pressure. It is usually the same for both the exposed and unexposed faces and is assumed to be the atmospheric pressure.

2.2.5 Material properties

Different thermal models have been presented in the previous section. They allow to accurately predict the temperature evolution in PMC materials exposed to fire. These models are based on thermal equations taking into account different fire processes. It was shown that the most used models considered three of these thermal processes. They are the heat conduction through the material, the heat convection from the volatile gas flow and the heat absorbed (or generated) by the polymer matrix pyrolysis. In order to obtain accurate temperature predictions, the material properties used in the thermal equations (Eq. 2.3 or Eq. 2.4) must be known. These properties are the composite density, heat capacity, thermal conductivity and enthalpy. There are also the volatile gas enthalpy, the polymer decomposition energy, the emissivity, the absorptivity, the porosity and the permeability.

The mentioned properties are temperature-dependent and they also depend on the polymer matrix decomposition state. Knowing that, it is necessary to determine their value, and this all across the expected temperature range. It must also be determined how the properties evolve due to matrix pyrolysis. There is however often a lack of information about some of these material properties because they are usually very difficult to measure accurately over the temperature range of interest. They are therefore sometimes only estimated which leads to some limitation of the models. Note that, as explained in the common assumptions (see Section 2.2.1), the composite is considered as a whole in the models. Therefore, the thermal properties are usually given for the entire composite and not for the matrix and the fibers separately (except for the matrix decomposition properties).

2.2.5.1 Density

The first material property to be addressed is the *density*, which changes over time due to the polymer matrix pyrolysis. This is thus an important property to consider in the thermal modelling of composite materials subjected to fire. Indeed, it influences the thermal response since the pyrolysis reaction requires (or releases) energy and therefore leads to heat consumption (or generation). Moreover, the matrix decomposition modifies the nature of the material from a virgin to a charred state. This transformation influences other material properties such as its thermal conductivity or heat capacity (see Sections 2.2.5.2 and 2.2.5.3).

Most thermal models use a relation based on the Arrhenius law to determine the decrease in density. It directly results from a relation representing the mass loss rate. Depending on the authors, this relation slightly differs. For example, Henderson et al. [8] use Eq. 2.18 whereas Lattimer and colleagues [22] use Eq. 2.19. Both these equations

16

are expressed in terms of the composite instantaneous mass m, initial mass m_0 and final mass m_f. Another relation, given by Eq. 2.20, is also used by some authors [4, 9, 21]. This equation is expressed in terms of the polymer matrix instantaneous mass M, initial mass M_0 and final mass M_f.

$$\frac{\partial m}{\partial t} = -m_0 \left[\frac{m - m_f}{m_0} \right]^n A \mathrm{e}^{-\frac{E}{RT}}. \tag{2.18}$$

$$\frac{\partial m}{\partial t} = -(m_0 - m_f) \left[\frac{m - m_f}{m_0 - m_f} \right]^n A \mathrm{e}^{-\frac{E}{RT}}. \tag{2.19}$$

$$\frac{\partial M}{\partial t} = -M_0 \left[\frac{M - M_f}{M_0} \right]^n A \mathrm{e}^{-\frac{E}{RT}}. \tag{2.20}$$

The variables A, n and E are respectively the rate constant, the order and the activation energy of the polymer matrix decomposition reaction. The term $m_0 - m_f$ in Eq. 2.19 is called the initial mass of active material (or pyrolysable material). It corresponds to the total mass that can be lost during the decomposition process. The term $m - m_f$ in Eq. 2.18 and Eq. 2.19 represents the instantaneous remaining mass of active material, which can still be decomposed. The term $M - M_f$ is equivalent to $m - m_f$ but in terms of the remaining mass of active polymer matrix.

In the case of a decomposition reaction involving the polymer matrix alone, the mass loss rate equations given by Eq. 2.19 and Eq. 2.20 are almost equivalent. Indeed, the following relations hold:

$$\frac{\partial m}{\partial t} = \frac{\partial M}{\partial t}, \tag{2.21}$$

$$m - m_f = M - M_f. \tag{2.22}$$

If the polymer matrix is assumed to fully decompose, Eq. 2.19 and Eq. 2.20 are equal. In that case, an additional relation holds:

$$m_0 - m_f = M_0. \tag{2.23}$$

The different expressions used to represent the mass loss rate of decomposing composites have been detailed. It allows to derive the corresponding relations in terms of density. Assuming a constant volume, the density decrease rate is easily obtained. Note that it represents exactly the same phenomenon as the mass loss rate but density is more convenient than mass regarding the material properties definition. Eq. 2.24 is obtained from Eq. 2.18, whereas Eq. 2.25 is obtained from Eq. 2.19.

$$\frac{\partial \rho}{\partial t} = -\rho_v \left[\frac{\rho - \rho_c}{\rho_v} \right]^n A \mathrm{e}^{-\frac{E}{RT}}. \tag{2.24}$$

$$\frac{\partial \rho}{\partial t} = -(\rho_v - \rho_c) \left[\frac{\rho - \rho_c}{\rho_v - \rho_c} \right]^n A \mathrm{e}^{-\frac{E}{RT}}. \tag{2.25}$$

Eq. 2.24 and Eq. 2.25 represent the decomposition reaction rate of the polymer matrix. These equations are appropriate provided that pyrolysis occurs in one single phase. As it can be noticed, the knowledge of both the virgin and fully charred composite densities, respectively ρ_v and ρ_c, is required. By definition, the virgin composite density is its initial density, before the start of the decomposition process. Regarding the charred composite, its density is obtained by combining the fibers' density (assumed constant) and the remaining density of the charred polymer matrix. As an example, Feih et al. [9] found that the remaining mass fraction (RMF) of a fully charred vinyl ester resin was around 3 %. This value was obtained by conducting a thermo-gravimetric analysis.

In addition to ρ_v and ρ_c, the matrix decomposition also depends on the decomposition reaction parameters A, E and n presented earlier. They are determined thanks to a thermo-gravimetric analyzer (TGA), which gives curves showing the evolution of the polymer RMF as a function of temperature. The optimal values for the parameters A, E and n are then found by fitting the curves on the experimental data. An example of TGA curves for a vinyl ester resin is given in Fig. 2.4. It can also be noticed in this figure that the decomposition reaction occurs at different temperatures depending on the heating rate. The higher the heating rate, the higher the temperature at which decomposition starts. It is explained by the fact that the material presents a thermal inertia.
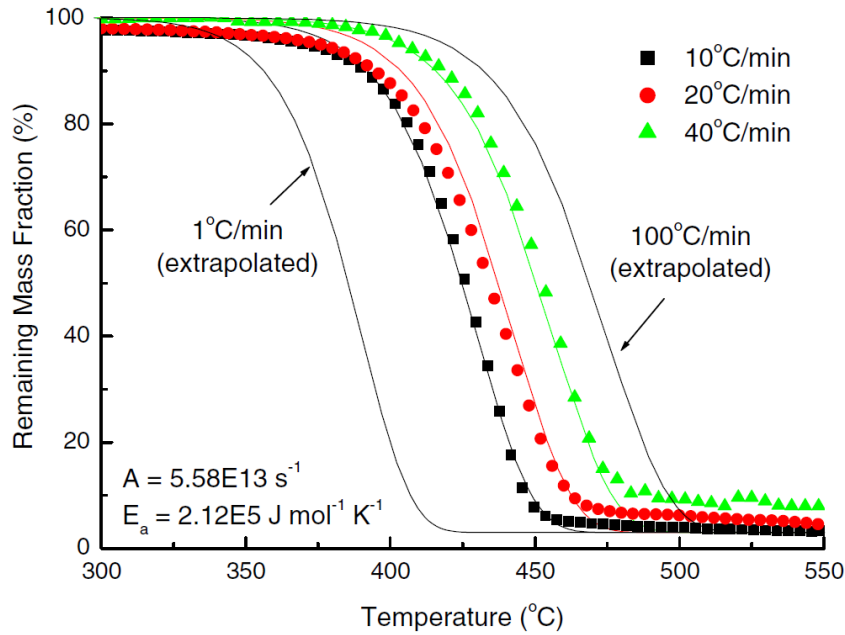
Figure 2.4: TGA curves obtained for a vinyl ester resin with different heating rates. Experimental measurements (symbols) and curve fits (solid lines). From Feih et al. [4].

The decomposition state is generally represented in the different models by a variable F called the virgin material relative mass fraction. Its value depends on the instantaneous composite mass or density and is given by the following equation (assuming constant volume):

$$F = \frac{m - m_f}{m_0 - m_f} = \frac{\rho - \rho_c}{\rho_v - \rho_c}. \tag{2.26}$$

This variable represents the proportion of virgin material that is remaining in the sample during the decomposition process. This is particularly convenient since F takes values between 1 and 0, respectively corresponding to a virgin and a fully charred state. Two limit cases can be observed:

$$\rho = \rho_v \quad \longrightarrow \quad F = 1, \tag{2.27}$$

$$\rho = \rho_c \quad \longrightarrow \quad F = 0. \tag{2.28}$$

The virgin material relative mass fraction F is used to perform interpolations between the virgin and charred material properties. This is discussed in the next sections.

2.2.5.2 Thermal conductivity

The *thermal conductivity* k quantifies the ability of the material to conduct heat. It is usually expressed in [W/mK]. The heat conduction phenomenon in a solid material is related to energy transfer between agitated atoms. In order to take place, a temperature gradient must exist in the material. In that case, thermal energy is transferred from a high energy to a low energy region (i.e. from high to low temperatures). This thermal energy transfer is called a heat flux. The basic relation linking the heat flux q'' to the temperature gradient is the following [23]:

$$q'' = -k \frac{\partial T}{\partial x}. \tag{2.29}$$

As it can be seen in Eq. 2.29, the heat flux is directly related to the temperature gradient through k. The higher the value of the thermal conductivity, the larger the heat flux. In order to obtain the positive flux going from high to low temperatures ($\frac{\partial T}{\partial x} < 0$), a minus sign is put in front of k. Regarding composite materials subjected to fire, the most important thermal conductivity to consider is the through-thickness conductivity. Indeed, the goal of the thermal analysis is to study how the temperature evolves across the material between a hot face (exposed) and a cold face.

The composite thermal conductivity is temperature-dependent. Moreover, the potential polymer matrix decomposition also influences the conductivity properties of the composite. Knowing that, the thermal conductivity of a decomposing composite can be defined by Eq. 2.30 [6].

$$k(T, \rho) = F \cdot k_v(T) + [1 - F] \cdot k_c(T), \tag{2.30}$$

where:

$$k_v(T) = k_{1(v)} + k_{2(v)}T, \tag{2.31}$$

$$k_c(T) = k_{1(c)} + k_{2(c)}T + k_{3(c)}T^2 + k_{4(c)}T^3. \tag{2.32}$$

As it can be seen in Eq. 2.30, the thermal conductivity is obtained by an interpolation between the virgin and charred material conductivities, respectively k_v and k_c. Both depend on temperature through coefficients ($k_{i(v)}$ and $k_{i(c)}$). The coefficients are usually obtained thanks to curve-fitting on experimental data, which are collected over the temperature range of interest. The interpolation between the virgin and charred conductivities depends on the virgin material relative mass fraction F. It therefore introduces the dependency on the decomposition state in the expression of k.

Henderson et al. [10] also take into account the influence of the porosity on the thermal conductivity. The expression used for thermal conductivity $k_{Henderson}$ in their model is presented in Eq. 2.33. The composite material is indeed usually porous and its porosity increases during decomposition. The resulting pores are filled with decomposition gases and lower the thermal conductivity. Therefore, the overall thermal conductivity depends on the conductivity of the solid material k and of the decomposition gases k_g, and also on the composite porosity ϕ. Note that k in Eq. 2.33 is obtained thanks to Eq. 2.30 presented earlier.

$$k_{Henderson} = \phi \cdot k_g + (1 - \phi) \cdot k. \tag{2.33}$$

The thermal conductivity of the composite material can also be influenced by damages resulting from internal degradation. For example, delamination can occur at some locations inside the material when the temperature increases. This leads to the creation of gaps and cracks that act as a barrier against conductivity. If this phenomenon is not taken into account in the thermal model, this could lead to temperature over-estimation. Luo and Desjardin [25] established another formulation for the conductivity of degrading composite. This is expressed by Eq. 2.34 where the volume fraction of cracks is considered.

$$k = (\varphi_s/k_v + \varphi_{cr}/k_{cr})^{-1}, \tag{2.34}$$

where φ_s and φ_{cr} are respectively the solid material and cracks volume fractions. k_{cr} stands for the thermal conductivity through cracks. This expression for the thermal conductivity is similar to the one given in Eq. 2.33 taking into account the porosity.

Note that the thermal conductivity of the charred material k_c is measured experimentally. Therefore, it sometimes already includes the effect of porosity or delamination [22].

2.2.5.3 Specific heat capacity

The *specific heat capacity* C of a material quantifies its capability to store thermal energy per unit mass. It is usually expressed in [J/kgK]. Multiplying C by the density ρ of the material yields the *volumetric heat capacity* ρC, expressed in [J/m³K]. It is here the ability for a precise volume of this material to store thermal energy that is quantified [23].

Similarly to the thermal conductivity, the specific heat capacity depends on temperature. Moreover, due to potential decomposition, the composite passes from a virgin state to a char state. This also influences the heat capacity property of the material. Therefore, exactly as for thermal conductivity, the specific heat capacity is defined as follows:

$$C(T, \rho) = F \cdot C_v(T) + [1 - F] \cdot C_c(T), \tag{2.35}$$

where:

$$C_v = C_{1(v)} + C_{2(v)}T, \tag{2.36}$$

$$C_c = C_{1(c)} + C_{2(c)}T. \tag{2.37}$$

Specific heat capacity for both the virgin C_v and charred material C_c has to be measured experimentally over the temperature range of interest. Based on the results, the coefficients $C_{i(v)}$ and $C_{i(c)}$ are obtained thanks to curve-fitting methods.

The governing thermal equation given by Eq. 2.3 also requires the knowledge of the decomposition gases specific heat capacity C_g. Indeed, these gases are present in the material pores or cracks and thus impact the overall heat capacity. Nonetheless, C_g is not used to express the material heat capacity in other thermal models. This is the case in the one from Gibson et al. [15] or Lattimer et al. [22] for instance. As explained in Section 2.2.2, they consider that the influence of C_g is already taken into account in the solid material heat capacity. It is valid provided that the decomposition gas and the environment gas (present in pores during the properties measurements) are assumed to have the same specific heat capacity [22]. Note that C_g is nevertheless always present in the term characterizing the convection, which comes from the gas flow through the material.

2.2.5.4 Specific enthalpy

The *specific enthalpy* of the composite material h, or the decomposition gases h_g, is a thermodynamic quantity representing the total heat content per unit mass. It is usually expressed in [J/kg]. As presented in Eq. 2.38, the specific enthalpy h includes the specific internal energy u and the product between the internal pressure P and the specific

volume v [23].

$$h = u + Pv. \tag{2.38}$$

In the models representing the thermal behavior of composite materials exposed to fire, the specific enthalpy is obtained from the specific heat capacity [6, 8, 9, 15, 22]. Indeed, the values of h and h_g, present in the thermal equations Eq. 2.3 and Eq. 2.4, are defined as follows:

$$h = \int_{T_{ref}}^{T} C dT, \tag{2.39}$$

$$h_g = \int_{T_{ref}}^{T} C_g dT, \tag{2.40}$$

where T_{ref} is the reference temperature and C is obtained thanks to Eq. 2.35.

2.2.5.5 Decomposition energy

The polymer matrix *energy of decomposition* Q_p, also called *standard heat of decomposition*, is defined by Agarwal and Lattimer as the "difference of standard heat of formations of active solid material and decomposition gas" [26]. It is usually expressed in [J/kg]. The heat of decomposition is negative if the decomposition process is endothermic. This is usually the case for polymer matrix. Argawal and Lattimer describe a detailed method in order to measure the value of Q_P. This is done thanks to a simultaneous thermogravimetric analyzer (STA). This STA simultaneously combines data from a differential scanning calorimeter (DSC) and a TGA. The DSC measures the differential energy input to the material sample and the TGA measures the mass of the sample. The standard heat of decomposition remains difficult to measure accurately. Moreover, its value is influenced by the measurement method.

The term $(Q_p + h - h_g)$ present in the thermal equation Eq. 2.4 is called the *heat of decomposition*. Another name used for this term is *heat of pyrolysis*. It represents the thermal energy absorbed (if endothermic) or delivered (if exothermic), per unit mass of volatile gases, during the decomposition process. When pyrolysis occurs, the mass loss rate $\frac{\partial m}{\partial t}$ in Eq. 2.4, initially equals to zero, becomes negative. It therefore activates the contribution of the heat of decomposition to the thermal equation. Observed from another perspective, the heat of pyrolysis modifies the composite *apparent volumetric heat capacity* ρC_{app} during decomposition. This is shown by rearranging the thermal equation given here by Eq. 2.41 [22].

$$\rho C \frac{\partial T}{\partial t} = \frac{\partial}{\partial x}\left(k\frac{\partial T}{\partial x}\right) - \dot{m}_g'' \frac{\partial h_g}{\partial x} - \frac{\partial \rho}{\partial t}(Q_p + h - h_g). \tag{2.41}$$

This expression can be modified if the change in density is rewritten as follows:

$$\frac{\partial \rho}{\partial t} = \frac{\partial \rho}{\partial T}\frac{\partial T}{\partial t}.$$
(2.42)

Eq. 2.41 therefore becomes:

$$\rho C_{app}\frac{\partial T}{\partial t} = \frac{\partial}{\partial x}\left(k\frac{\partial T}{\partial x}\right) - \dot{m}_g''\frac{\partial h_g}{\partial x},$$
(2.43)

where the apparent volumetric heat capacity is defined as:

$$\rho C_{app} = \rho C + (Q_p + h - h_g)\frac{\partial \rho}{\partial T}.$$
(2.44)

As it can be seen in Eq. 2.44, an endothermic decomposition process induces an increase of ρC_{app}. The material thus seems to have a larger heat capacity during pyrolysis. This is illustrated by the red curve in Fig. 2.5 for an E-glass vinyl ester (EGVE) sample. Note that in this figure, c_{app} and c_{sen} are respectively the composite apparent and sensible specific heat capacities. c_{sen} is seen as the actual composite specific heat capacity, neglecting the effect of decomposition. It is thus similar to the term ρC in Eq. 2.44. c_a and c_f are respectively the active material and inert filler specific heat capacities. In the case of a EGVE sample, the active material is the vinyl ester resin and the inert filler is the E-glass fibers. Inert means that the filler material is not subjected to decomposition.
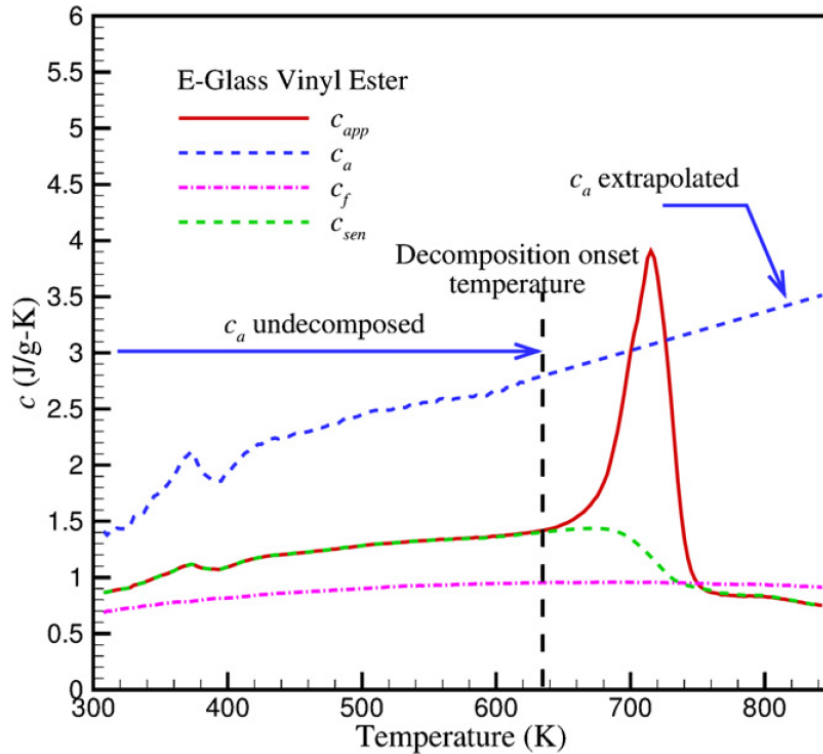
Figure 2.5: Specific heat as a function of temperature for a decomposing EGVE sample. Heating rate of 20 K/min. From Agarwal and Lattimer [26].

2.2.5.6 Emissivity and absorptivity

The composite *surface emissivity* ε_s and *surface absorptivity* α_s are used to express the radiative component of the thermal boundary conditions. For a given surface temperature, the emissivity (resp. absorptivity) corresponds to the ratio between the energy emitted (resp. absorbed) from a real surface and the energy that would be emitted (resp. absorbed) if this surface was a black-body [23]. A black-body is an idealized material being a perfect emitter (resp. absorber) which means that it emits (resp. absorbs) radiations in all frequencies and incidence. By definition, its emissivity and absorptivity are equal to 1. Both the emissivity and the absorptivity are dimensionless variables.

As explained in Section 2.2.4, the thermal models used in practice usually consider gray surfaces [8, 22]. This means that the emissivity and the absorptivity are equal. However, they can be smaller than 1. Moreover, they are usually defined dependent on the decomposition state of the material. Therefore, they are computed as follows [8]:

$$\varepsilon_s = F \cdot \varepsilon_{s,v} + (1 - F) \cdot \varepsilon_{s,c}, \tag{2.45}$$

$$\alpha_s = F \cdot \alpha_{s,v} + (1 - F) \cdot \alpha_{s,c}, \tag{2.46}$$

where $\varepsilon_{s,v}$ and $\alpha_{s,v}$ are the virgin material emissivity and absorptivity and where $\varepsilon_{s,c}$ and $\alpha_{s,c}$ are the charred material emissivity and absorptivity.

2.2.5.7 Porosity and permeability

The thermal model developed by Henderson et al. [8] requires the knowledge of the composite *porosity* ϕ and *permeability* γ. The porosity is used in the thermal conductivity definition (see Section 2.2.5.2) and in the Darcy's law for the gas mass flow (see Section 2.2.3). It is a dimensionless parameter ranging between 0 and 1 that represents the proportion of pores inside the material. The permeability is also used in the Darcy's law and is expressed in [m^2]. It indicates how easy it is for decomposition gases to flow through the material.

Both the composite porosity and permeability depend on its state of decomposition as for many other material properties. They are expressed as follows in the model from Henderson [8]:

$$\phi = F \cdot \phi_v + (1 - F) \cdot \phi_c, \tag{2.47}$$

$$\frac{\partial \gamma}{\partial t} = \zeta \frac{\gamma_0}{m_0} \frac{\partial m}{\partial t}, \tag{2.48}$$

where ϕ_v and ϕ_c are the virgin and charred material porosity, respectively. Regarding the expression for the permeability, γ_0 is the initial (virgin) permeability and ζ is a so-called decomposition permeability factor.

2.3 Mechanical and damage models

As explained earlier, the thermo-mechanical modeling of composites materials subjected to fire is very often made thanks to a two-step analysis. The first step of the analysis is the thermal modeling which is presented in details in the previous section. This thermal part is based on various assumptions that have been explained and do not consider any mechanical behavior in the composite. The second step is the mechanical modeling. A presentation of the models used in practice in order to represent the mechanical response is made in this section. However, since the mechanical part is not the main objective in this work, the presentation of the existing models is brief. Moreover, a lot of material data for high temperatures are lacking in the literature. It is therefore difficult to perform a mechanical analysis accurately in the scope of this work.

The mechanical models require the knowledge of the temperature distribution obtained thanks to a thermal model. The mechanical models can be divided into two different parts. The damage models and the mechanical models (tension, compression) as they are defined in [6].

2.3.1 Damage models

It was said earlier in Section 2.1, that multiple processes occur in the material during a fire event. These processes were given in Tab. 2.1. The damage caused to the composites materials exposed to fire are due to a combination of chemical and physical processes. There exist different types of damage [6]: matrix decomposition, pore formation, delamination and matrix cracking, fiber-matrix debonding and char formation. These are more or less important depending on the through-thickness location into the material. They are indeed present closer to the heated surface and less at the unexposed side of the composites. These damages are not taken into account in the most used thermal models (except the matrix decomposition) because they do not influence much the temperature distribution resulting from an exposition to fire. However, these damage influence much more the mechanical behavior of the composite materials when they are simultaneously submitted to loading.

The damages are very difficult to model since they depend on a lot of different parameters that must therefore be known to represent the problem [6]. Some models exist to take into account one type of damage that is important. This is the delamination cracking due to thermal expansion, pressure and matrix softening. These models (analytical or finite elements models) representing the thermal expansion or the crack growth of delaminated regions have been developed in the past years [6]. However, they require the knowledge of many temperature-dependent material properties which are difficult to measure and lacking in the literature. It is therefore difficult to use these models. Note

that the ones considering thermal expansion are also able to predict the composite behavior without loading. Indeed, the effect of the temperature alone leads to thermal strains. A schematic of this behavior is shown in Fig. 2.6. It can be seen that the asymmetry in the temperature distribution leads to a thermal moment. This is because the expansion directly depends on the temperature and is therefore also asymmetric.
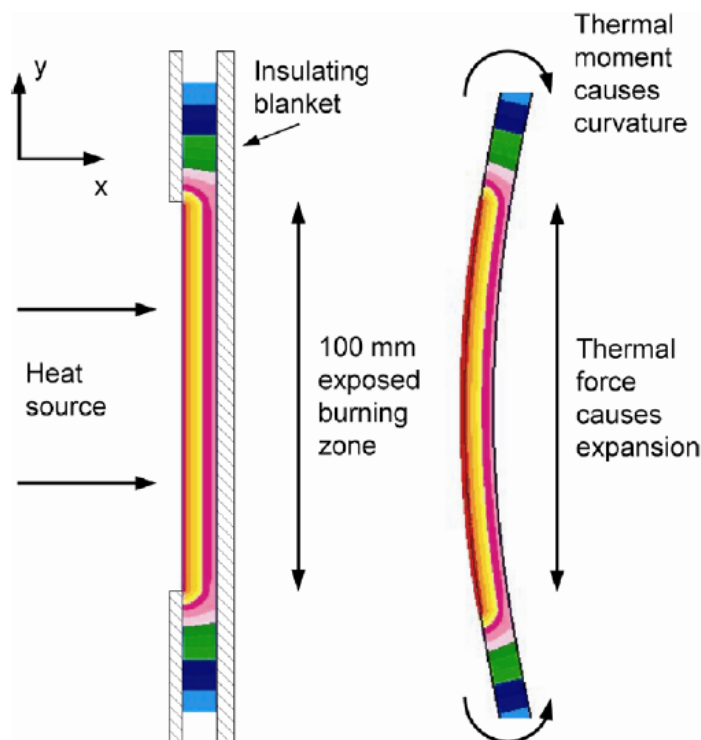
Figure 2.6: Temperature induced deformations for one-sided heating of a non-loaded composite sample [4].

The modeling of the matrix decomposition explained in Section 2.2.5.1 can also be considered as a type of damage modeling. Since this process influences much more the thermal response than the other damage processes, it is also taken into account in the thermal model. The same definition, using the Arrhenius' law, can be used in the mechanical model. It allows to take the effect of mass loss damage into account for the structural behavior modeling of the composite.

2.3.2 Mechanical models

Most researches have been made about the mechanical modeling of composites subjected to fire under compression loads. Less information is available regarding the behavior in tension. This is explained by the fact that the main effect of the temperature increase in the material is the reduction of the matrix properties. This thus influences more the composite failure in compression than in tension [9]. In order to be brief, only the compression case is presented in this section.

The common feature between the models is the use of the previously computed temperature distribution. Then, the mechanical properties are evaluated based on these temperatures. They are usually assumed to decrease in a single stage as shown in Fig. 2.7. This is mainly due to the glass transition of the polymer matrix. The compression strength and Young's modulus are the properties generally considered. They are obtained thanks to experimental measurements for the temperature range covered by the thermal analysis. The data resulting from these measurements are used to determine coefficients in empirical formulas. An empirical formula used by Feih et al. [4] for the compressive strength is given as an example in Eq. 2.49.
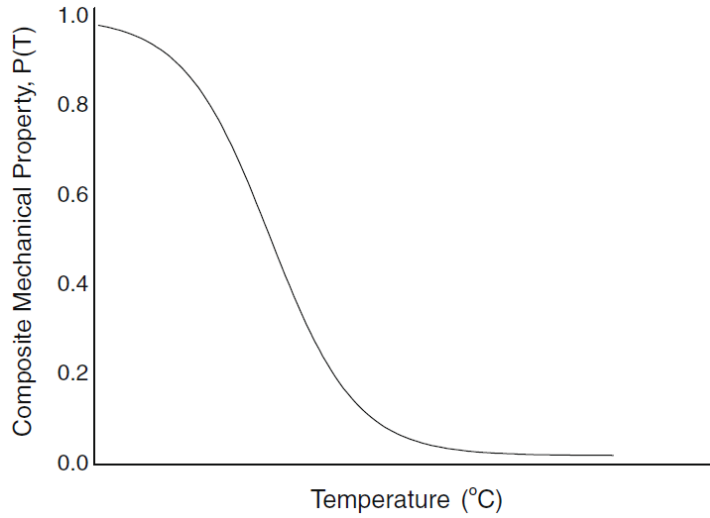
Figure 2.7: General decrease of composite mechanical properties with temperature [6].

$$\sigma_{\mathrm{c}}(T) = \left(\frac{\sigma_{c(o)} + \sigma_{c(R)}}{2} - \frac{\sigma_{c(o)} - \sigma_{c(R)}}{2} \tanh\left(\Phi\left(T - T_k\right)\right) \right) \times R_{\mathrm{rc}}(T)^n, \qquad (2.49)$$

where $\sigma_{c(o)}$ is the composite compressive strength at room temperature, $\sigma_{c(R)}$ is the residual compressive strength at high temperature. Φ is a constant related to the temperature range over which the strength is reduced. T_k is the temperature at which the compressive strength is half the strength at room temperature. R_{rc} is a scaling function that takes into account the effect of the matrix decomposition. n is an empirical value used to adjust the effect of the resin decomposition on the strength decrease.

In the most known mechanical models, there is often only the remaining compressive strength of the material that is considered [6]. Knowing the temperature evolution through the laminate, this remaining compressive strength can be calculated at different locations using the previous formula. Integrating over the thickness L leads to the average

compressive strength σ_{av} as follows (Simpson integration technique):

$$\sigma_{av} = \frac{1}{L} \int_{-L/2}^{+L/2} \sigma(x)dx = \frac{1}{L}\frac{L}{3m}\left[\sigma\left(x_0\right) + 4\sigma\left(x_1\right) + 2\sigma\left(x_2\right) + \cdots + 2\sigma\left(x_{k-2}\right) \right.$$
$$\left. +4\sigma\left(x_{k-1}\right) + \sigma\left(x_k\right)\right] \tag{2.50}$$

The failure is then assessed as follows:

- Failure when σ_{av} reaches the applied compressive stress

- Failure of all plies simultaneously (not successively)

- Failure not dependent on creep (which depends on temperature)

This method for evaluating the mechanical behavior of a composite subjected to fire is not very general. It requires a lot of experimental data in order to be used correctly. Moreover, this model does not lead to a rigorous prediction of the mechanical behavior of the material. It only leads to the evaluation of the time-to-failure from a global perspective without considering buckling. Indeed, this model is only valid for applied loads that are smaller than the buckling load [4].

Some other works have been recently published on the mechanical modeling of composites submitted to high temperatures [27–29]. They present more sophisticated models using finite element methods. However, these models are much more complicated and are beyond the scope of this master thesis, which focuses mainly on the thermal part. Further works planned at GDTECH will be related to these mechanical models using the thermal part studied in this master thesis.

Chapter 3

Modeling methodology

3.1 Introduction

The theory governing the response of composite materials subjected to fire has been described in Chapter 2. This type of problem can now be solved using SAMCEF. The software contains different modules that are attributed to different types of analysis (`Amaryllis` for thermal and `Mecano` for mechanical analysis). As for the models presented in Chapter 2, the thermo-mechanical analysis made in this work is decoupled. First, the thermal response of the composite is computed using the modeling methodology presented in the next section (see Section 3.2). No mechanical considerations are made in that part. Then, the time-dependent temperature distribution resulting from this thermal analysis is used in a mechanical model. It is possible thanks to a specific command available in SAMCEF. It is called `.IT3` and leads to a mapping of the thermal solution onto the mechanical mesh. This is explained in details further in this chapter (see Section 3.3).
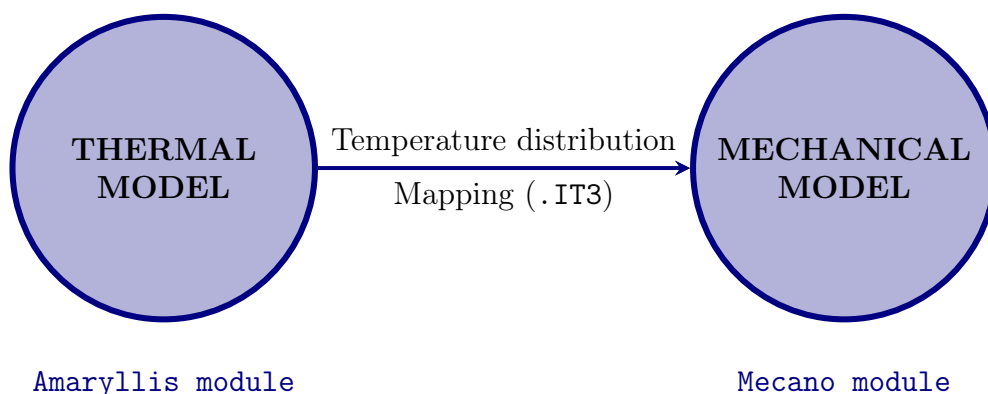
Figure 3.1: Flowchart representing the two-step thermo-mechanical analysis.

For both the thermal and the mechanical parts, the problem is defined in a so-called bank file (*.dat* file) in command language. It contains all the information listed below and required for the simulation. This file is pre-processed by a module named `Bacon`.

- geometry,

- mesh properties,

- type of problem to be solved,

- materials definition,

- loads & boundary conditions,

- time integration parameters,

- archiving parameters (not discussed here).

Once the `Bacon` module has completed the pre-process, different files are sent to the analysis module to solve the problem. These are the SAMCEF-file (*.sam* file) containing the data for computation and the database file (*.sdb* file). After the problem resolution, three important files are created by the analysis module. Two of them, the *.fac* and *.des* files, are necessary for post-processing. The other one, the results file (*.res* file), is the analysis module output containing all the warning and error messages. It also contains essential information about the iterative procedure and its convergence.

Eventually, post-processing of the simulation results is achieved through the `Bacon` module. A flowchart summarizing a general analysis in the SAMCEF software is shown in Fig. 3.2. Other files are also created during the simulation but these are not useful for the user. More information can be found in the software documentation [30].
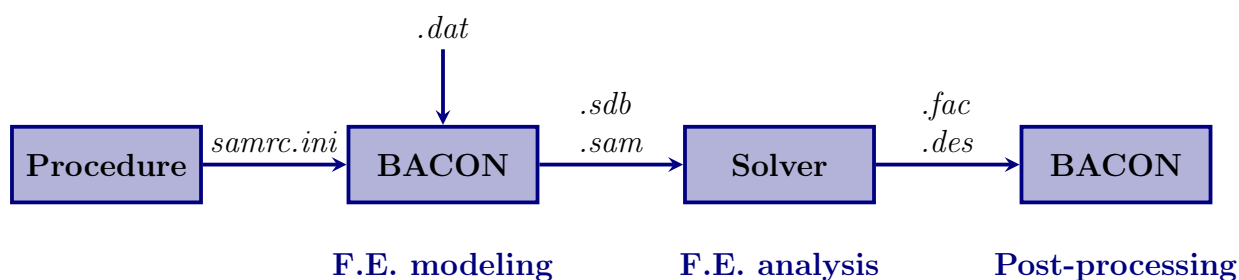
Figure 3.2: Flowchart representing the most used files and the simulation stages. Reproduced from the SAMCEF documentation [30].

3.2 Thermal model

In the case of a thermal analysis involving pyrolysis, a module called `Amaryllis` in SAMCEF is used to solve the problem. The objective in this section is to reproduce the reference model developed by Henderson et al. [8]. This model is indeed the most used for this type of problem. Therefore it has been chosen to be the one used in this work and adapted to the software. The results obtained with SAMCEF are then compared to analytical and experimental results from two different publications [4, 10].

Before performing simulations for composite materials subjected to fire, some simpler problems have been solved in order to get used to the software. This was also a good way of verifying that the solver gives accurate results before going into more complicated simulations. These small tests are not presented here since they do not bring useful information about the subject.

The next sections concern the general methodology to be used in order to represent correctly a thermal problem in SAMCEF in accordance with the theoretical model [8]. Therefore, the same assumptions than the ones in that model are made:

- modeling of the three main processes only (conduction, gas convection and matrix decomposition)

- no thermal expansion

- no damage modeling (e.g. delamination, matrix cracking)

- one-dimensional model

3.2.1 Governing equations

As explained above, the goal here is to obtain a model conformed to the Henderson model [8]. In order to do so, the default governing thermal equation used by SAMCEF must be equivalent to the one used in the theoretical model. The thermal governing equation developed by Henderson et al. is rewritten in Eq. 3.1. The solution method used to solve this governing equation is explained in another publication from the same author [10] and is based the finite volume method proposed by Patankar [31].

$$(mC + m_g C_g) \frac{\partial T}{\partial t} = \frac{\partial}{\partial x} \left(k \frac{\partial T}{\partial x} \right) \Delta x \Delta A - \dot{m}_g C_g \frac{\partial T}{\partial x} \Delta x - \frac{\partial m}{\partial t} (Q_p + h - h_g). \quad (3.1)$$

The governing equation implemented by default in SAMCEF to solve a thermal problem under the assumption of pyrolysis is:

$$\rho C \frac{\partial T}{\partial t} = \nabla (k_{ij} \nabla T) - \dot{m}_g'' \nabla h_g + \frac{\partial \rho}{\partial t} H_p. \quad (3.2)$$

Assuming constant volume V, Eq. 3.1 becomes Eq. 3.3. Moreover, considering a one-dimensional thermal analysis, Eq. 3.2 can be rewritten as Eq. 3.4.

Publication [8]

$$\frac{(mC + m_g C_g)}{V}\frac{\partial T}{\partial t} = \frac{\partial}{\partial x}\left(k\frac{\partial T}{\partial x}\right) - \dot{m}_g'' C_g \frac{\partial T}{\partial x} - \frac{\partial \rho}{\partial t}\left(Q_p + h - h_g\right), \qquad (3.3)$$

SAMCEF

$$\rho C \frac{\partial T}{\partial t} = \frac{\partial}{\partial x}\left(k\frac{\partial T}{\partial x}\right) - \dot{m}_g'' \frac{\partial h_g}{\partial x} + \frac{\partial \rho}{\partial t}H_p. \qquad (3.4)$$

Both thermal governing equations expressed by Eq. 3.3 and Eq. 3.4 are very similar. They are composed of four terms which have already been discussed in Section 2.2.2. It can nonetheless be observed that some differences are present between these equations. In order to have an exact analogy between the model from Henderson and the one in SAMCEF, some parameters have to be adapted.

Regarding the continuity equation, it must also be defined in SAMCEF as in the theoretical model. The one used in the by Henderson et al. [8] is explained in Section 2.2.3 and writes:

$$-\frac{\partial m}{\partial t} = \frac{\partial \dot{m}_g}{\partial x}\Delta x + \frac{\partial m_g}{\partial t}. \qquad (3.5)$$

A continuity equation is used by default in SAMCEF and is written as follows:

$$\nabla \dot{m}_g + \dot{\rho} = 0. \qquad (3.6)$$

The term representing the variation of gas mass storage in the material $\left(\frac{\partial m_g}{\partial t}\right)$ is not present in the continuity equation from SAMCEF. This term can be activated thanks to a specific command which is `.TMB1`. Thanks to that command the continuity equation used in SAMCEF becomes identical to the one from the reference model. Note that this continuity equation is linked to the Darcy law which is discussed later in Section 3.2.3.3.

3.2.2 Geometry and mesh

The first step in the problem definition is the geometry creation. As stated earlier, this work considers the thermal response in 1D of composites subjected to fire. Therefore, a material sample modeled in 2D is sufficient to represent the problem. It can take the form of a simple rectangle as shown in Fig. 3.3. The height of the sample does not matter. However, its length L must be equal to the thickness of the considered composite.
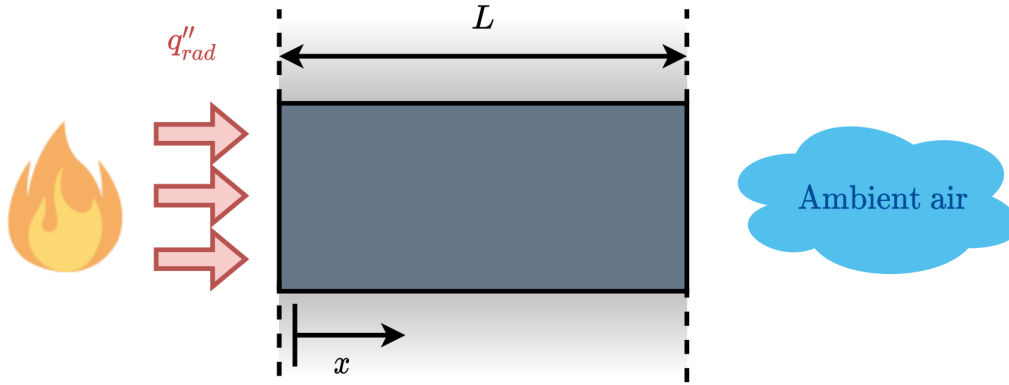
Figure 3.3: Schematic of the sample geometry used in SAMCEF and representation of the surrounding environment.

Once the geometry is created, it can be meshed. Since the problem is one-dimensional, and that the geometry is a rectangle, the mesh is rather simple. A single element along the height is sufficient. Indeed, the temperature in the material is constant perpendicular to the flux. Several elements could be used on the height but it would not improve the model. The simulation time would be longer and the results would be identical.

The mesh refinement is important in the through-thickness direction. A particular attention must be drawn about the exposed side of the sample. At this location, the transient temperature variation is expected to be large especially if the total thermal load is applied directly. In order to accurately capture the temperature gradient, the elements size Δx has to be small enough. The following condition must be ensured regarding spatial discretization [30]:

$$\Delta x \quad < \quad \delta = K\sqrt{\beta t}, \tag{3.7}$$

where:

$$\beta = \frac{k}{\rho C} \qquad \text{is the thermal diffusivity at the boundary.} \tag{3.8}$$

δ is the penetration depth, also called the thermal conduction boundary layer. K is a parameter taking values between 2 and 4 which depends on the type of boundary condition. t represents the elapsed time since the start of the thermal solicitation.

The conduction boundary layer corresponds to the area in which the total temperature variation is confined. Eq. 3.7 expresses the requirement of having at least one layer of elements inside this penetration depth in order to capture it correctly. This is illustrated in Fig. 3.4 where the total radiation heat flux is assumed to be applied brutally at the exposed face (step function).
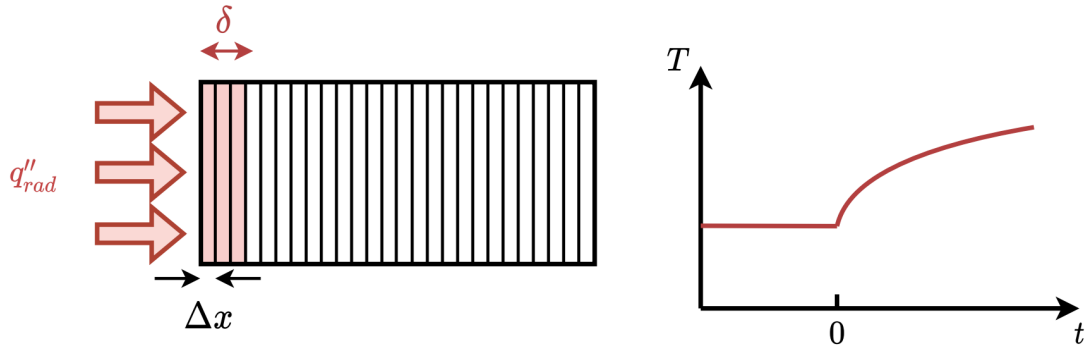
Figure 3.4: Schematic of a good spatial discretization Δx, the penetration depth δ and the imposed radiation heat flux q''_{rad} (on the left). Schematic of the resulting thermal response computed at the nodes close to the exposed face for a total thermal load q''_{rad} applied directly (on the right). Reproduced from [30].

If the condition is not respected, it leads to spatial oscillations as shown in Fig. 3.5. In that case, the nodal temperatures close to the exposed face are lower than the initial temperature during the transient phase. This is obviously not physically possible knowing that heat is transmitted at the boundary. Nevertheless, the spatial oscillations fade out after some time. Indeed, there always exists a time t after which Eq. 3.7 becomes satisfied.
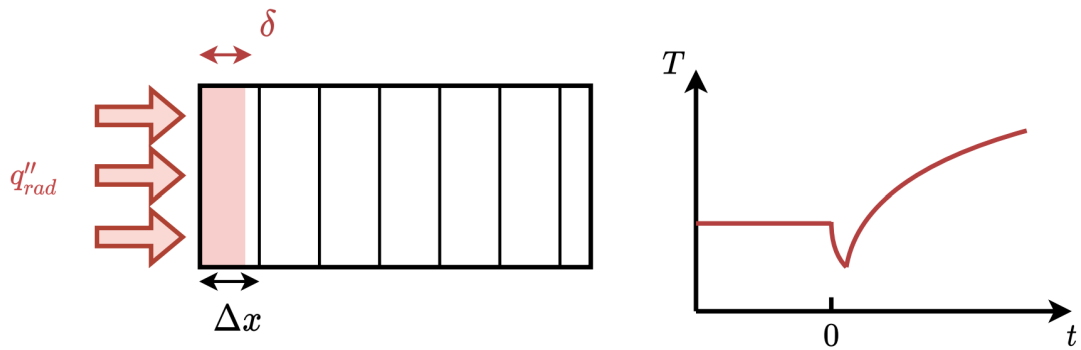
Figure 3.5: Schematic of a bad spatial discretization Δx, the penetration depth δ and the imposed radiation heat flux q''_{rad} (on the left). Schematic of the resulting thermal response computed at the nodes close to the exposed face for a total thermal load q''_{rad} applied directly (on the right). Reproduced from [30].

It can be noticed that the condition depends on the temporal discretization Δt and especially on the size of the first time step. It indeed defines the first value that t will have at the beginning of the simulation. This governs the first value of δ which is obviously the most constraining. The first time step can be increased in order to have a larger value for δ at the first iteration. It would therefore reduce the requirement about Δx. However, stability considerations restrain the value of the time step. This is explained in Section 3.2.5.

Eventually, the element type is attributed to the meshed geometry. It is automatically chosen by SAMCEF. It depends on the type of problem that is specified to the software. In this work, the elements are 2D membranes, called pyrolysis membranes. Note that a membrane thickness must be imposed but does not influence the solution. The unknowns are computed at the nodes. These are the temperature T, the pressure P and the density ρ. Fig. 3.6 shows a rectangular membrane element with the locations of the integration nodes.
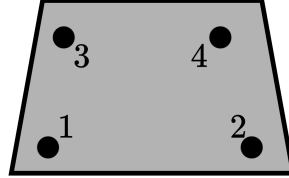
Figure 3.6: Schematic of one pyrolysis membrane used in SAMCEF (with the node locations). Reproduced from [30].

3.2.3 Material definition

When the geometry and the mesh are properly defined, the material properties can be attributed to the finite elements. In this work, these properties have to be defined in such a way that the resulting model is identical to the one developed by Henderson et al. [8]. It is assumed that all the required material properties are known. For example, in a publication from the same author [10], they mention all the properties used in their model to study the thermal response of a glass reinforced polymer.

It is first necessary to identify the parameters needed by SAMCEF for a thermal analysis with pyrolysis. The pyrolysis membrane elements require the definition of two different materials. One is the virgin and the other is the charred material. All the properties required for a thermal analysis with pyrolysis in SAMCEF are presented in Table 3.1.

Then, the solver module computes the properties of the actual material by interpolating between both virgin and charred properties. The interpolation depends on the stage of decomposition (if decomposition occurs) represented by the generalized density α given in Eq. 3.9. It is equal to 0 for the virgin state and to 1 for the fully charred state. Note that it is the opposite of the variables F presented in Section 2.2.5.2.

$$\alpha = \frac{\rho_v - \rho}{\rho_v - \rho_c} = 1 - F \tag{3.9}$$

Note that sometimes the material properties are not given in details for the composites. Therefore, it is required to slightly tune them in order to fit experimental thermal results.

Material law	Property	Virgin	Charred
Fourier law	Density ρ [kg/m³]	✓	✓
	Specific heat capacity C [J/kgK] **OR** Specific enthalpy h [J/kg]	✓	✓
	Conductivity k [W/mK]	✓	✓
Darcy law	Gas diffusion coefficient K_p [(kg.m)/(N.s)]	✓	✓
	Gas specific enthalpy h_g [J/kg]	✓	
	OR		
	Gas viscosity μ [Pa.s]	✓	
	Permeability γ [m²]	✓	
	Gas molecular mass M_g [kg/mol]	✓	
	Gas specific enthalpy h_g [J/kg]	✓	
	Porosity ϕ [-]	✓	✓
Arrhenius law	Activation energy E [J/mol]	✓	
	Rate constant A [1/s]	✓	
	Order of reaction n [-]	✓	
	Pyrolysis heat H_p [J/kg]	✓	

Table 3.1: List of the material and decomposition gas properties to be introduced in SAMCEF for a thermal analysis with pyrolysis. The symbol ✓ indicates that the property is required [30].

3.2.3.1   Volumetric heat capacity

The term on the left-hand side in the governing thermal equations represents the temporal variation of the energy stored in the material. This term depends on the volumetric heat capacity ρC. The density ρ and the specific heat capacity C have to be defined in SAMCEF for both the virgin and charred material. Knowing these parameters, the solver performs the interpolation expressed in Eq. 3.10. This leads to the value of the actual volumetric

heat capacity during decomposition.

$$\rho C = (1 - \alpha) \cdot \rho_v C_v - \alpha \cdot \rho_c C_c. \tag{3.10}$$

The volumetric heat capacity in the theoretical model is represented by Eq. 3.11. A detailed explanation about that term is given in Section 2.2.5.3.

$$\frac{(mC + m_g C_g)}{V} \tag{3.11}$$

In order to have an exact correspondence between both models, the specific heat capacities defined in SAMCEF are:

$$C_v^{\text{SAMCEF}} = \frac{\phi_v}{\rho_v} \rho_g C_g + (1 - \alpha)C_v + \alpha C_c, \tag{3.12}$$

$$C_c^{\text{SAMCEF}} = \frac{\phi_c}{\rho_c} \rho_g C_g + (1 - \alpha)C_v + \alpha C_c, \tag{3.13}$$

where the parameters on the right-hand side are assumed to be known and are temperature-dependent (except the porosity). Note that the values of C_v, C_c and C_g depend on the temperature (see Section 2.2.5.3). The mathematical developments leading to these expressions are given in Appendix B.

Unfortunately, the solver does not allow the user to define the specific heat capacities as a function of the variable α. Some tests have shown that if different values for α are imposed manually in Eq. 3.12 and 3.13, the results are not modified. This means that this dependence on α can be assumed negligible. Therefore, it is chosen to use $\alpha = 0$ (virgin material) for the virgin capacity and $\alpha = 1$ (charred material) for the charred capacity. This leads to the following definitions:

$$C_v^{\text{SAMCEF}} = \frac{\phi_v}{\rho_v} \rho_g C_g + C_v, \tag{3.14}$$

$$C_c^{\text{SAMCEF}} = \frac{\phi_c}{\rho_c} \rho_g C_g + C_c. \tag{3.15}$$

In SAMCEF, it results in a linear interpolation between C_v^{SAMCEF} and C_c^{SAMCEF} instead of a quadratic one if the dependence on α was possible. Note that the creation of a user-subroutine in the solver could allow to take into account this dependence on α. However, this is really difficult to implement and is not done in this master thesis.

3.2.3.2 Thermal conductivity

The first term on the right-hand side of the governing thermal equations represents the conductive heat flux spatial variation. This term depends on the thermal conductivity k. In SAMCEF, its value is obtained through an interpolation between the thermal conductivities defined for the virgin and the charred materials. It is expressed as follows:

$$k = (1 - \alpha) \cdot k_v - \alpha \cdot k_c. \tag{3.16}$$

The expression used for the thermal conductivity in the model developed by Henderson et al. [8] is given by Eq. 2.33 in Section 2.2.5.2 and is rewritten here:

$$k = \phi \cdot k_g + (1 - \phi) \cdot (Fk_v + [1 - F] k_c) \tag{3.17}$$

In order to correspond to the theoretical model, the virgin and charred thermal conductivities defined in SAMCEF have to be adapted. Therefore, their values are expressed as follows:

$$k_v^{\text{SAMCEF}} = k_v + k_g\phi_v - k_v \left[(1 - \alpha)\phi_v + \alpha\phi_c\right], \tag{3.18}$$

$$k_c^{\text{SAMCEF}} = k_c + k_g\phi_c - k_c \left[(1 - \alpha)\phi_v + \alpha\phi_c\right], \tag{3.19}$$

where the parameters on the right-hand side are assumed to be known and the conductivities are temperature-dependent (see Section 2.2.5.2). The mathematical developments leading to these expressions are given in Appendix C.

As for the specific heat capacities, the solver does not allow the user to define the thermal conductivities as a function of the variable α. Some tests have also shown that the terms depending on α in Eq. 3.18 and 3.19 do not influence the results. Therefore, it is also chosen to use $\alpha = 0$ for the virgin property and $\alpha = 1$ for the charred property. This leads to the following definitions:

$$k_v^{\text{SAMCEF}} = k_v + k_g\phi_v - k_v\phi_v, \tag{3.20}$$

$$k_c^{\text{SAMCEF}} = k_c + k_g\phi_c - k_c\phi_c, \tag{3.21}$$

In the same way as for the heat capacities, the creation of a user-subroutine in the solver could allow to take into account this dependence on α.

3.2.3.3 Darcy law

The second term present on the right-hand side of the thermal equations is related to the heat convection due to the decomposition gases flow. As in the model from Henderson et al. [8], the value of the gas mass flux $\dot{m}_g''$ in SAMCEF is obtained by combining the con-

tinuity equation to the Darcy law. This is explained in details in Section 2.2.3 regarding the theoretical model.

In SAMCEF, the form of the Darcy law is the following:

$$\dot{m}_g'' = -K_P \frac{\partial P}{\partial x} \qquad \text{with} \qquad K_P = \frac{\gamma M_g P}{\mu R T}, \tag{3.22}$$

where K_P is called the gas diffusion coefficient.

It can be shown that the Darcy law implemented in SAMCEF is identical to the one used in the theoretical model. This can be verified by mathematical developments that are found in Appendix D. Therefore, no adjustment is needed for the material properties required by this term.

Note that the porosity is defined as follows in SAMCEF:

$$\phi = (1 - \alpha)\phi_v + \alpha\phi_c, \tag{3.23}$$

which is the same relation as Eq. 2.47 used in the thermal model developed by Henderson et al. [8].

In SAMCEF, the permeability is calculated using the following equation:

$$\gamma = \gamma_v \frac{\phi}{\phi_v}, \tag{3.24}$$

where γ_v (or γ_0) is the virgin material permeability (initial). This definition is not exactly equivalent to the one used in the theoretical model [8] and given by Eq. 2.48. However, it is comparable. Since the permeability is said not to influence significantly the thermal response, the default definition in SAMCEF is considered to be sufficient.

3.2.3.4 Arrhenius law

The last term on the right-hand side of the thermal equations represents the heat absorption (or generation) due to the polymer matrix decomposition. In SAMCEF, it is simply represented by:

$$\frac{\partial \rho}{\partial t} H_p \tag{3.25}$$

In the model developed by Henderson [8], this term is written as follows:

$$-\frac{\partial \rho}{\partial t} \left(Q_p + h - h_g \right). \tag{3.26}$$

It depends on the density variation $\frac{\partial \rho}{\partial t}$ which is defined by an Arrhenius law. In SAMCEF, the density variation is computed as follows:

$$\frac{\partial \rho}{\partial t} = -\rho_v \left[\frac{\rho - \rho_c}{\rho_v} \right]^n A \mathrm{e}^{-\frac{E}{RT}}. \tag{3.27}$$

It can be noticed that it is exactly the same expression as Eq. 2.24 used in the theoretical model from Henderson et al. [8]. Therefore, the Arrhenius' law used by default in SAMCEF does not have to be modified. The parameters A, E and n, which are known, can be directly attributed to the virgin material.

The heat of pyrolysis is denoted by the parameter H_p in SAMCEF. In order to stick to the theoretical model, the heat of pyrolysis must be defined in the software as follows:

$$H_p = h_g - h - Q_p. \tag{3.28}$$

The value of H_p defined in SAMCEF is positive for an endothermic decomposition process.

3.2.4 Loads and boundary conditions

Once the geometry, the mesh and the materials are correctly defined, the thermal loads and the boundary conditions can be applied. The ones used in the literature have been presented in Section 2.2.4. The goal is here to reproduce the theoretical model developed by Henderson et al. [8]. It is therefore important to impose equivalent loads and boundary conditions to the model created in SAMCEF. First, the atmospheric pressure P_∞ is imposed on both sides of the sample. Then, the radiative and convective components of the flux boundary conditions have to be defined separately. Therefore, they are explained in two different sections.

It is important to mention that adiabatic boundary conditions have to be applied at the top and bottom face of the sample in the numerical model. This is because the sample only represents a slice of the actual composite exposed to a homogeneous heat flux. The one-dimensional form of the model involves that no thermal exchange is allowed at these two boundaries. Indeed, the temperature is only allowed to evolve in the through-thickness and not in the transverse direction. In SAMCEF, the adiabatic boundary condition is automatically set by default at the faces for which no other conditions are imposed.

3.2.4.1 Radiative component

Regarding the exposed face, the radiative component takes into account the flux simulating the fire. In SAMCEF, it is possible to impose a radiative flux under the following form:

$$q'' = \sigma \left(\alpha_s T_r^4 - \varepsilon_s T_s^4 \right), \tag{3.29}$$

in which α_s, ε_s and T_r have to be defined. Note that the surface emissivity and absorptivity can be defined as a function of temperature and state of decomposition.

The expression given by Eq. 3.29 is similar to the one used in the theoretical model (Eq. 2.16). Moreover, SAMCEF also assumes a gray surface by default. Only the value for the emissivity has thus to be defined. The same value is automatically attributed to the absorptivity. The radiative source temperature T_r is not usually given explicitly in the problems' data sets. Therefore, it must be defined according to Eq. 3.30 for which the value of q''_{rad} is generally imposed and thus known. A short mathematical development leading to this equation can be found in Appendix E.

$$T_r^{\text{SAMCEF}} = \sqrt[4]{\frac{q''_{rad}}{\sigma}}. \tag{3.30}$$

Regarding the unexposed face, the radiative component of the boundary condition is defined similarly. However, no fire has to be simulated on that side. The value of T_r introduced in SAMCEF is thus simply the ambient temperature $T_{\infty,L}$.

3.2.4.2 Convective component

The convective component of the boundary conditions is expressed in the same way for both the exposed and unexposed faces. In SAMCEF, the general form of the convective heat flux is:

$$q'' = h_{conv} \left(T_\infty - T_s \right), \tag{3.31}$$

in which h_{conv} and T_∞ have to be defined for both faces.

Eq. 3.31 corresponds exactly to the convective boundary condition of the theoretical model [8]. Therefore, the required parameters can be introduced as they are presented in the publication. T_∞ is the ambient temperature and is known. It was noticed that usually no indications are given about the convection coefficient h_{conv} in the literature, whether for the exposed or unexposed face. However, a coefficient for each face needs to be introduced in SAMCEF in order to take into account a convective flux. For this reason, it is decided to impose hypothetical values. They are adjusted in order to approach a satisfying solution while remaining in an acceptable range.

3.2.5 Solution method

The last step in the thermal problem implementation is the solution method definition used to perform the time integration of the governing equation. It indicates to the software how it must solve the problem. In SAMCEF, a huge amount of execution parameters exist. Most of them are set by default and are suitable for classical problems. However, they can all be modified by the user depending on the context. Since there are over 40 parameters that can be chosen, it is not possible to explain each of them in details. Only the most important ones are presented in this section.

The first important parameter that must be defined indicates the **type of analysis** required. In this work, it is a thermal transient response that needs to be computed. Therefore, it must be indicated to the software.

Then, the **imposed times** have to be chosen. These are the times in [s] at which the response must be computed at least. It means that if an automatic time stepping is chosen, the solver adjusts the intermediate steps in order to obtain a response at these specific times.

The **integration scheme** is also a very important regarding the problem resolution. In the `Amaryllis` module used in this work, the default scheme is the generalized midpoint method [30]. It is a first order implicit time integration scheme which solves the discretized thermal equation. This scheme assumes a constant variation of the temperature between two time steps. It leads to another system of non-linear equations which is then solved using a Newton iteration method. The iterative process takes place until convergence of the solution is reached.

A parameter denoted γ can be chosen to adjust the implicitness of the scheme. By default, it is set to 0.5 and it corresponds to a specific time located at the middle of two time steps. It can actually take values between 0.5 and 1 which always leads to a unconditionally stable scheme. In the case of a γ equal to 0.5, the midpoint method corresponds to a Crank-Nicholson scheme. In this work, it has been chosen to keep the value by default used for γ. Indeed, this value seems to be the best considering the trade-off between stability and convergence of the scheme. Further information about the generalized midpoint method and its associated parameter γ can be found in the software documentation [30].

Once the integration scheme is chosen, the **time step** must be defined. As recommended in SAMCEF, an automatic time step is used. It is chosen by the solver based on two different criteria. The first one is the local truncation error of the scheme. The second criteria is a measure of the non-linearity. In other terms, it is the optimum number of

iteration in the Newton method. By default, this optimum number of iteration is set to 6 for one time step. It is found to be acceptable regarding the problem considered here [30].

Four aspects have to be taken into account when choosing a time step [30]:

- a too large time step can lead to integration errors,

- a too large time step can reduce the efficiency of the scheme if the problem is non-linear (to much time required for the Newton scheme convergence),

- a too small time step can lead to very long computation times,

- a too small time step can lead to spatial oscillations.

The last aspect is directly related to the condition explained in Section 3.2.2 about the spatial discretization. Indeed, it was explained that the penetration depth δ has to be larger than the element size Δx at the loaded boundary. It was expressed by Eq. 3.7 which can be rewritten to give the following relation:

$$\Delta t \quad > \quad \frac{1}{K^2} \frac{\rho C}{k} \left(\Delta x\right)^2. \tag{3.32}$$

Eq. 3.32 shows that a minimum time step has to be respected in order to avoid the presence of spatial oscillations in the response if Δx is fixed.

3.3   Mechanical model

Once the thermal response of the composite material is known, a mechanical analysis can be performed. The temperature distributions obtained thanks to the thermal model described above are used as input data in the analysis. As explained at the beginning, the thermal modeling was the most important part of this work. Therefore, only a brief simple mechanical modeling is presented with fewer details than for the thermal part. The main objective is to prove that thermo-mechanical modeling in SAMCEF is possible and works correctly. It thus allows to show the effect of the temperature on the mechanical response of a composite exposed to fire. Note that only the temperature evolution is taken into account in the mechanical model. The decrease in density due to decomposition is not considered. It is only taken into account in the thermal model because it influences the temperature distribution but is actually not modeled physically.

The publications found in the literature do not give precise information about the mechanical properties of the materials. It is thus difficult to create an accurate model to represent their behavior. However, the main goal is here to present a mechanical model based on a thermal response and not really to study a precise material. Therefore, it has been decided to apply a temperature distributions obtained for a material (the

one used by Feih et al. [4]) to another material for which the mechanical properties are known. This is clearly not ideal since the thermal and the mechanical analysis are not conducted on the same composite. Nonetheless, the mechanical model used here could be easily adapted to a real problem provided that the thermal and mechanical properties are known for a same material. This would lead to a thermo-mechanical analysis having a real physical sense.

3.3.1 Geometry and mesh

In the same way as for the thermal model, the first step in the mechanical modeling is the geometry creation. The problem is here considered in 3D so that deformations in all directions can be analyzed. The sample is chosen to be a square laminate with the same thickness as the one used in the thermal simulation. Indeed, the temperature are transferred from the thermal to the mechanical model. Therefore, the thickness must coincide in order to represent the problem correctly. A schematic of the geometry used in the model is shown in Fig. 3.7.
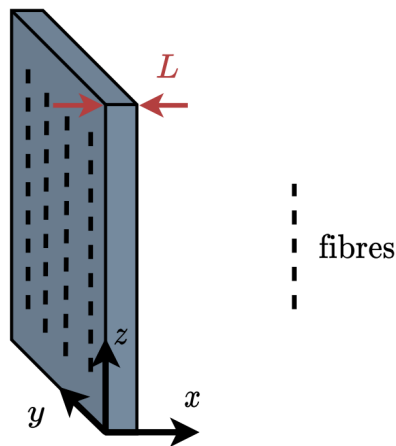
Figure 3.7: Schematic of the sample geometry used in SAMCEF.

Once the geometry is created, it needs to be meshed. The mesh depends on the number of plies present in the laminate. In the modeling of composite materials, a rule of good practice is to use one element along each ply thickness [32]. The size of the elements in the two other directions in space has to be chosen based on a convergence study as it is done usually in practice. In this work, the convergence study is not performed due to time constraint.

3.3.2 Material definition

The next step in the mechanical modeling is the material definition. Contrary to the thermal model, the composite is now defined using one material definition and not two (virgin and charred). In this work, the laminate is orthotropic and made of 9 uni-directional plies all oriented at $0°$.

Two different materials models are used successively. The first one is a ply material having elastic properties with no damage modeling and no hardening law. It allows to perform a preliminary mechanical test. The properties defined in this model are the stiffness and shear modulus, the Poisson ratios, and they are temperature-dependent. These properties allow to construct the Hooke's tensor representing the ply stress-strain relation. The laminate is constructed by the software based on the Classical Lamination Theory [33]. Note that the orthotropic thermal expansion coefficients are also taken into account in the model.

Then, another material model developed by Ladevèze [34] is used. It is based on Continuum Damage Mechanics, applied to orthotropic unidirectional PMC plies. That material can consider (see Fig. 3.8):

- Non-linear behaviors along the fibers, in tension and compression (direction "1"),

- Failure of the fibers, in tension and compression,

- Non-linear behaviors in the matrix, up to failure, in directions "2" and "12" (shear), including damage and permanent deformation.

In order to apply that material model to composites submitted to fire, it is necessary to define the evolution of its different parameters with respect to temperature. Starting from "classical" values of the model parameters for a composite material at room temperature [32], the orthotropic elastic and non-linear parameters are made dependent of the temperature, based on information found in the literature [27, 36, 37]. The evolution of the damage variable in shear (d_{12}) and of the hardening law are illustrated in Fig. 3.9.

3.3.3 Loads and boundary conditions

This section presents the load and the boundary conditions applied to the sample in order to perform a simple mechanical analysis. For the sake of simplicity, the plies are all considered to be oriented at $0°$ with respect to the vertical direction (uni-directional plies laminate). It has been chosen to show the effect of a constant compression loading on the material. The problem could be entirely modeled by having two loads on both the bottom and top side of the sample. However, thanks to symmetry, only half of the problem can be modeled. Therefore, only the top of the composite sample is subjected to
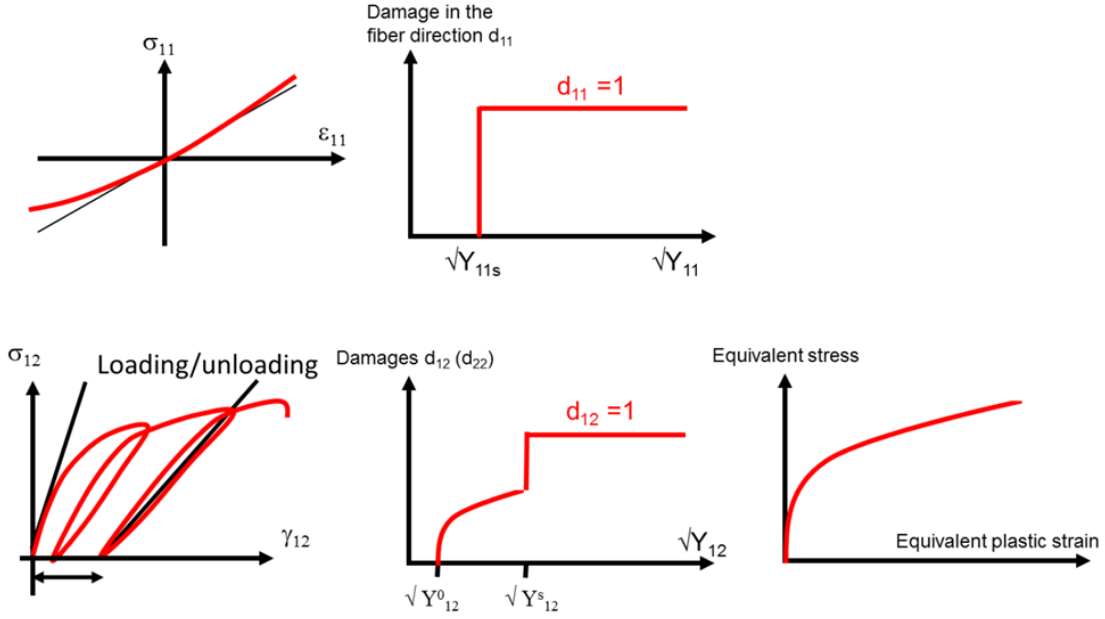
Figure 3.8: Non-linearities and damage evolution in the progressive damage model for uni-directional plies [35]. d_{11}, d_{12} and d_{22} are damage variables in fibers, shear and transverse directions of the orthotropic ply, respectively.

(a) Damage variable d_{12}.   **(b)** Hardening law.
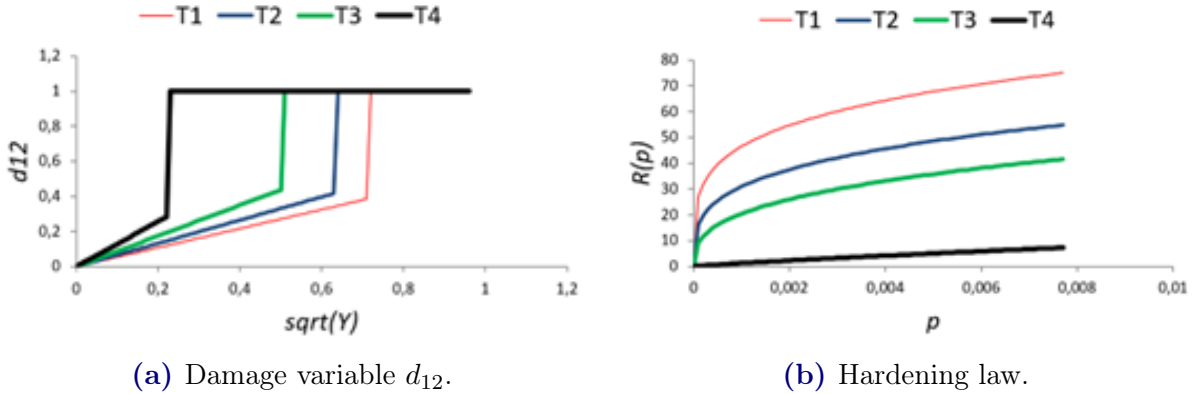
Figure 3.9: Evolution of the damage variable d_{12} and of the hardening law as a function of temperature [32].

a compressive surface load acting in the fibers' direction. This can be done provided that correct boundary conditions are defined at the symmetry plane. The load is increased linearly up to its nominal value and then kept constant during the simulation in order to avoid numerical instabilities.

Three boundary conditions are applied to the bottom face of the sample (symmetry plane). First, all the nodes are fixed in the z-direction. Indeed, this is required to represent the symmetry of the problem. Then, one corner node is blocked in the three directions. Eventually, the other corner node on the same side of the sample is fixed in two directions (x and z). The two last boundary conditions prevent the sample to

translate or rotate on the xy-plane (symmetry plane). The reason for which the bottom side cannot simply be totally clamped is that thermal expansion occurs in the problem. Therefore, the material must be allowed to expand on the symmetry plane. A schematic of the load and boundary conditions applied in the model is shown in Fig. 3.10.
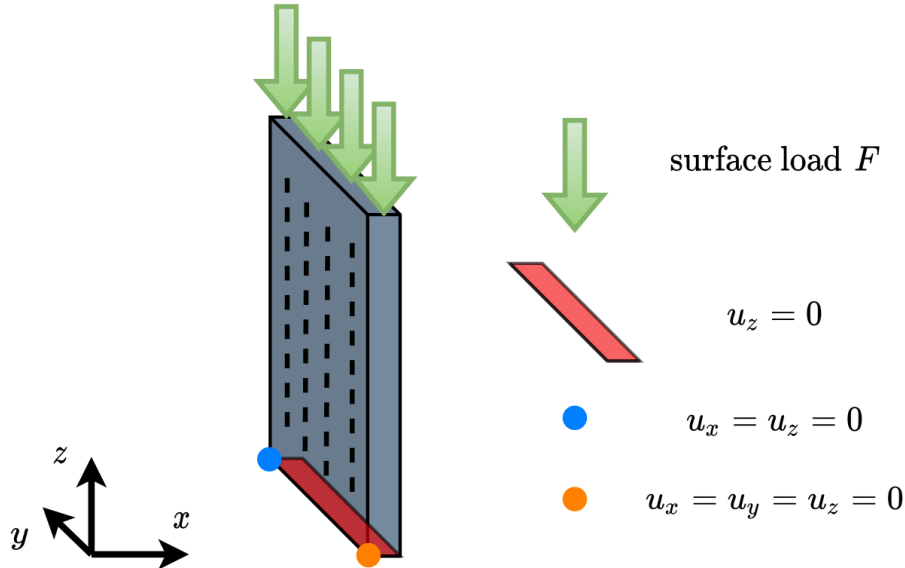
Figure 3.10: Schematic of the load and boundary conditions imposed in SAMCEF. The variable u represents a displacement.

3.3.4 Temperature distribution

The time-varying temperature distribution has also to be applied to the model in order to represent the effect of fire. As explained several times, these are obtained thanks to the thermal model. The `Mecano` module used in SAMCEF allows to apply a thermal distribution coming from an external file to the mechanical model. This is done using a specific command which performs a mapping of the temperatures from the thermal mesh toward the mechanical mesh. Indeed, in this work and also usually in practice, both meshes are not identical. They both depend on different numerical considerations. As an example, the thermal mesh requires a lot of elements in the through-thickness direction (for the reasons explained in Section 3.2.2) whereas the mechanical mesh has only one element per ply.

To illustrate the effect of high temperatures on the behavior of the sample, the choice is made to impose the temperature distribution obtained for the material from Feih [4]. Only the 50 [kW/m²] heat flux is considered. It provides a large range of temperature between the exposed and unexposed face of the sample. Note that it also leads to a total pyrolysis of the material used by Feih [4]. However, since the material used in the mechanical model is not the same material as in the thermal analysis, it is not correct to

consider that it would be entirely decomposed here. Indeed, there is actually no knowledge about the thermal response of the material used in this mechanical part. It is simply used to show that the model can correctly take into account an imposed temperature profile.

3.3.5 Solution method

The goal is not here to study the mechanical model in details but only to show that it can depend on temperatures computed in a previous stage. Since the analysis needs to be short and simple, it was decided to keep the default parameters used in SAMCEF for solving the problem.

The mechanical problem is solved by the `Mecano` module using classical finite element analysis for non-linear mechanics [38]. A static response is computed which means that inertia, friction and damping are omitted. Moreover, the time step is chosen automatically by the solver based on the evaluation of the integration error. More information about the solution method used in SAMCEF in the case of non-linear mechanics can be found in the software documentation. [30].

Chapter 4

Thermal model results

In the previous chapter, it has been explained how to correctly define in SAMCEF the reference thermal model for composite materials exposed to fire developed by Henderson et al. [8]. Once the problem is correctly set up, the simulation can be run and the results are analyzed. In order to validate the numerical model, these results are compared to experimental and analytical data presented in the literature. For the sake of completeness, it has been decided to confront the model to two independent problems dealing with composite materials subjected to fire. This allows to ensure its validity in different conditions and for different material samples.

The first problem is taken from a publication written by Henderson and colleagues [10]. It involves is a glass- and talc-filled (60.5%) composite with a phenol-formaldehyde (phenolic) resin matrix (39.5%). No information is provided about the stacking sequence but since the material is assumed to be homogeneous it has no importance. The material sample is 3 [cm] thick and is exposed to a radiant heat flux of 280 [kW/m^2] on one side.

The second material is a glass-fiber (55%) vinyl ester resin (45%) composite. The thermal response of this material under large heat flux is presented by Feih et al. [4]. In this case, the sample is 9 [mm] thick and is tested under four different heat flux (10, 25, 50 and 75 [kW/m^2]). This brings a additional validation for the numerical model. It allows to check if the results that are obtained are acceptable independently of the flux intensity for a same material.

An EXCEL sheet has been created in the frame of this work in order to allow for a semi-automatic post-processing of the results. This gives the user a tool to analyze very quickly the results without doing many manipulations. Indeed, the post-processing in SAMCEF is very exhaustive but is not easy to use.

4.1 Henderson et al.

As explained above, the numerical model used in SAMCEF is first assessed by comparing the simulation results to the one obtained experimentally and theoretically by Henderson et al. [10]. It is therefore required to model the equivalent problem in the software. This is done according to Chapter 3, which presents how to define such a problem in SAMCEF. Note that the results presented in the publication [10] are obtained thanks to the model from the same author [8], which is adapted to SAMCEF (see Chapter 3). However, they also introduced the effect of the thermal expansion in the model by using variable control volume width. This is not the case in the model used in SAMCEF and it is therefore considered as a limitation of the model.

4.1.1 Geometry and mesh

The considered composite is 3 [cm] thick. It is therefore required to have a 2D sample with the same length. Regarding its height, the sample is chosen to be 1 [cm] high but this has no effect on the solution as explained in Section 3.2.2. The mesh is usually refined at the exposed boundary and larger elsewhere. However, the computation time for a thermal analysis in SAMCEF is rather short (about 2 [min] for this problem). It is therefore useless to optimize the mesh size in order to reduce the computation time. Knowing that, it can be chosen really fine over the whole domain to ensure a converged solution. The geometry is thus uniformly meshed using 300 pyrolysis membrane elements in the through-thickness direction and 1 along its height. This leads to a Δx of 0.1 [mm].

The mesh refinement, especially close to the loaded boundary, must satisfy a specific condition in order to avoid the presence of spatial oscillations in the solution. This is explained in details in Section 3.2.2. The condition is expressed by Eq. 3.7 which is rewritten here below:

$$\Delta x \ < \ \delta = K\sqrt{\beta t}, \tag{4.1}$$

where:

$$\beta = \frac{k}{\rho C} \qquad \text{is the thermal diffusivity at the boundary.} \tag{4.2}$$

This condition can also be written differently as explained in Section 3.2.5 about the time integration method. It is expressed by:

$$\Delta t \ > \ \frac{1}{K^2}\frac{\rho C}{k}\left(\Delta x\right)^2. \tag{4.3}$$

Since it has been chosen to fix the value of Δx to 0.1 [mm], it is rather the first time step Δt that must satisfy the condition expressed by Eq. 4.3 to avoid spatial oscillations. Based on the virgin (initial) material properties given in the next section and considering $K = 2$ (most conservative), the minimum value for Δt can be calculated. It leads to the

following condition:

$$\Delta t \ > \ 0.006 \ [\text{s}]. \tag{4.4}$$

It has been decided to fix the first time step to 0.05 [s] which satisfies the condition. It assumed to be small enough to ensure convergence during this first time step. Note that, as explained previously, the time step is automatically chosen by the solver and adapted in case the solution does not converge. The absence of spatial oscillations is verified in the results section (Section 4.1.4).

4.1.2 Material properties

The material used here is a glass- and talc-filled (60.5%) composite with a phenol-formaldehyde (phenolic) resin matrix (39.5%). Its properties required by the model are given in the publication and rewritten in Tab 4.1. Moreover, the properties of the decomposition gases are given in Tab. 4.2.

	Virgin	Charred
Density ρ [kg/m^3]	1810	1440
Conductivity k [W/mK]	$0.804 + 2.8 \cdot 10^{-4} \times T$	$0.9546 + 8.42 \cdot 10^{-4} \times T$ $... - 4.07 \cdot 10^{-6} \times T^2$ $... + 5.32 \cdot 10^{-9} \times T^3$
Specific heat C [J/kgK]	$1088.57 + 1.09 \times T$	$879.23 + 1.02 \times T$
Porosity ϕ [-]	0.113	0.274
Permeability γ [m^2]	$2.6 \cdot 10^{-18}$	$1.14 \cdot 10^{-16}$
Emissivity ε_s [-]	0.6	0.9
Absorptivity α_s [-]	0.6	0.9
Decomposition parameters	$\mathbf{0 < \alpha < 0.44}$	$\mathbf{0.44 < \alpha < 1}$
Activation energy E [J/mol]	$2.6 \cdot 10^5$	
Rate constant A [1/s]	$1.98 \cdot 10^{29}$ (A_1)	$8.17 \cdot 10^{18}$ (A_2)
Order of reaction n [-]	17.33 (n_1)	6.3 (n_2)
Decomposition heat Q_p [J/kg]	-234304	

Table 4.1: Material properties given in the publication from Henderson et al. [10] and used in SAMCEF. The temperature T must be defined in [°C].

As it can be noticed in Tab. 4.1, there are two different values for the A and n parameters used for the Arrhenius' law. Both parameters depend on the state of decomposition

Thermal conductivity k_g [W/mK]	$2.99 \cdot 10^{-2} + 1.4 \cdot 10^{-4} \times T$
Specific heat C_g [J/kgK]	$2386.48 + 1.05 \times T$
Viscosity μ [Pa.s]	$1.48 \cdot 10^{-5} + 2.5 \cdot 10^{-8} \times T$
Molecular mass M_g [kg/mol]	0.01835

Table 4.2: Decomposition gases properties given in the publication from Henderson et al. [10] and used in SAMCEF. The temperature T must be defined in [°C].

of the material. Therefore, this has to be represented in the model. However, after several attempts, it was found that the definition of an Arrhenius law having its parameters changing with the decomposition state was not achievable. In order to be as close as possible to the real material, a trade-off between both values of A and n had to be found.

4.1.3 Boundary conditions

Regarding the boundary conditions, the value of the ambient temperature and the radiant heat flux simulating the fire are given. The radiative component of the boundary conditions depends on the material emissivity which is also given in the material properties. As it is usually the case, no information is provided about the convection coefficient h_{conv}. It could be explained by the fact that it is difficult to measure and therefore not possible to mention its value. A first approximation of 3 [W/m²K] for the convection coefficient is thus made in the first instance. This parameter is then adjusted if needed to better fit the results. The boundary conditions are summarized in Tab. 4.3.

As explained in the methodology, it is necessary to convert the imposed flux q''_{rad} into a radiation source temperature T_r. This is done thanks to Eq. 3.30. The radiation source temperature is in this case 1490.28 [K].

Initial (ambient) temperature T_∞ [K]	297.15
Initial (ambient) pressure P_∞ [Pa]	101325
Radiant heat flux q''_{rad} [kW/m²]	280
Convection coefficient h_{conv} [W/m²K]	3 (unknown)

Table 4.3: Initial and boundary conditions given in the publication from Henderson et al. [10] and used in SAMCEF.

4.1.4 Results and discussion

In their publication, Henderson et al. [10] give the time evolution of the temperature at different locations in the material. In order to validate the model used in SAMCEF, the computed temperatures are compared to the one coming from this publication. Note that the temperatures are computed in [K] but are presented here in [°C].

A first simulation is run with the parameters given in Tab. 4.1 for the material and in Tab. 4.3 for the boundary conditions. It is decided to use the values A_1 and n_1 for the Arrhenius' law in the first instance. In order to see how these two parameters influence the solution, it is interesting to analyze the mass loss in the material. This can be done thanks to a graph showing the remaining mass fraction depending on the depth and the time. The temperature profiles obtained with SAMCEF are shown in Fig. 4.1. As it can be observed in this figure, the results are not fitting well the one coming from the publication. The graph giving the evolution of the RMF is given in Fig. 4.2. The different curves resulting from the simulation are not conclusive.

Regarding this first simulation, it is important to verify that no spatial oscillations are present in the solution. As explained previously in Section 4.1.1, the value for Δx is 0.1 [mm]. The first time step is fixed to 0.05 [s] in order to satisfy the condition expressed by Eq. 4.3 and no spatial oscillations should be observed in the results. As shown in Fig. 4.7, there are indeed no spatial oscillations in the solution at the beginning of the simulation. There is not a temperature below the initial one (24 [°C]) close to the boundary. Note that a test has been made to see what value the solver automatically chooses for the first time step. It was larger than 0.05 [s] which means that the first Δt fixed was not too large in order to ensure convergence.

Another simulation is performed for which only the parameters of the Arrhenius' law are modified. There are chosen to be A_2 and n_2 in this case. The resulting temperature profiles and RMF evolution are shown respectively in Fig. 4.3 and 4.4. It can be seen that the change of the Arrhenius parameters does not have a significant impact on the temperature profiles. However, as expected, it influences a lot the material decomposition since the curves in Fig. 4.4 are really different from the ones in Fig. 4.2. This brings an interrogation about the model. Indeed, according to the governing thermal equation, the change in mass should affect the temperature inside the material. However, this is not the case here and this was not expected.

Therefore, it is interesting to see how the solution is changed if the influence of the mass change is increased in the thermal equation. This can be done by increasing the value of the decomposition heat Q_p. It thus results in a larger heat of pyrolysis H_p in SAMCEF which means that more energy is absorbed by the resin decomposition. Several

tests have been conducted and it was found that the optimal value for Q_p is -4×10^6 [J/kg]. Q_p seems not well interpreted by the solver. This parameter must thus be modified in SAMCEF to calibrate the numerical model. This is sometimes done in different engineering domains for some parameters used in numerical models. In this problem, the optimal value for Q_p is 17 times larger than the original one given in the publication. Unfortunately, no explanation has been found to justify such a difference. The results can even be slightly improved by adjusting the convection coefficient to 7 [W/m^{2}K]. Moreover, the Arrhenius parameters A and n have been averaged in order to have a reasonable trade-off between the two different laws existing for this material. The optimal value for n was found to be 10 [-] and the one for A is 1.27×10^{24} [1/s] (obtained thanks to a geometric mean between A_1 and A_2). The temperature profiles and the RMF curves obtained after these changes in the numerical model are respectively shown in Fig. 4.5 and Fig. 4.6. Many simulations have been performed in order to optimize the model and to get these results.

It can be seen in Fig. 4.5 that the increase of the decomposition heat influences significantly the internal temperatures as expected (at 0.5 and 1 [cm]). These temperatures are indeed lower. It comes from the fact that some thermal energy is absorbed by the resin decomposition and is therefore not transmitted further in the material. Furthermore, Fig. 4.6 shows that the parameters A and n are indeed leading to a fairly good approximation of the RMF at different times. It can also be noticed in this same figure that most of the mass loss between 0 and 0.5 [cm] occurs during the first 200 [s] after the solicitation. Regarding the mass loss between 0.5 and 1 [cm], it mainly takes places between 200 and 400 [s]. This feature is reflected in the temperature profiles given in Fig. 4.5 but in a very subtle manner. Indeed, the temperature curve for 0.5 [cm] seems to be slightly flattened between 50 and 200 [s]. The same observation can be made for the 1 [cm] curve between 200 and 450 [s]. It represents the fact that, when decomposition occurs between two different locations in the material, the temperature increase behind this decomposition zone is slowed down.

A last comment has to be made about the differences between the publication and the computed temperature profiles at 0.5 and 1 [cm] after respectively 200 and 300 [s] in Fig. 4.5. This could be explained by the fact that the resin decomposition is not perfectly modeled because of the limitation on the parameters A and n. Another reason could be the thermal expansion not taken into account in SAMCEF whereas it is considered in [10]. In this model the volume is indeed assumed to remain constant. Moreover, this assumption is used to adapt the material properties coming from the literature to the form required in SAMCEF, in order to obtain a similar model (see Chapter 3). This could also lead to discrepancies between the results coming from the publication and the one that are computed
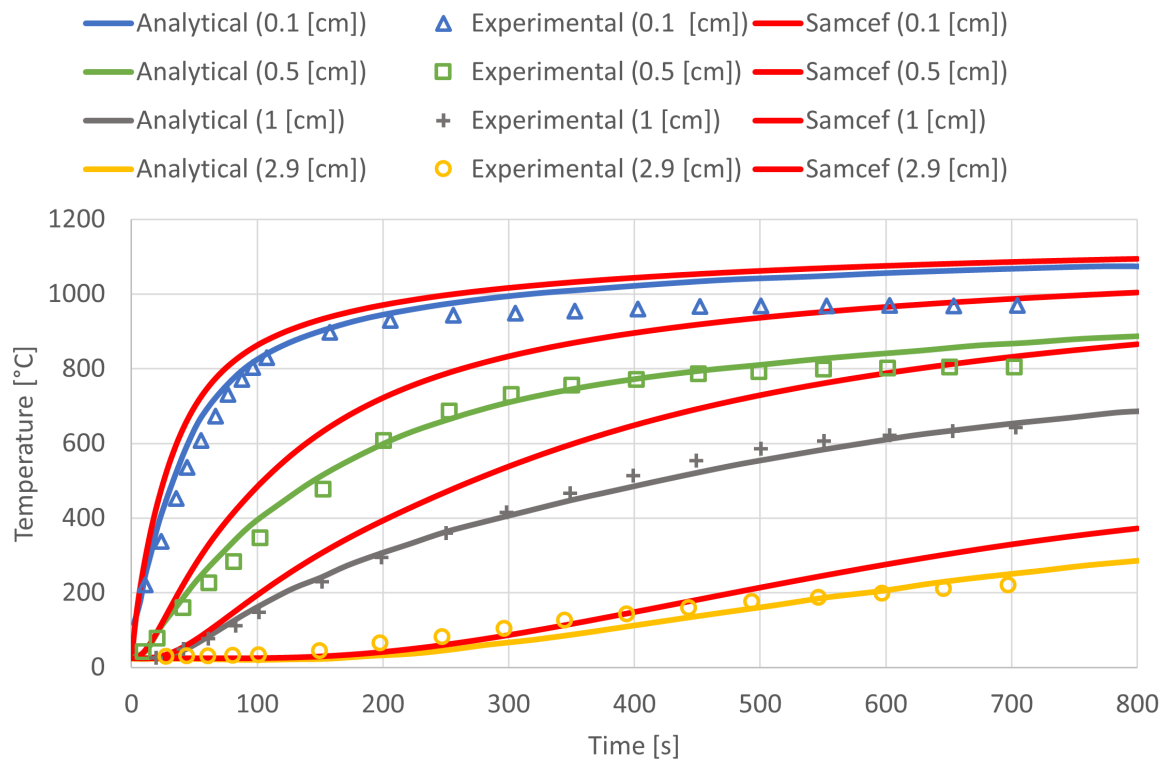
Figure 4.1: Time evolution of the temperature at different depths into the sample (0.1, 0.5, 1 and 2.9 [cm]) given in the publication [10] (analytical and experimental) and obtained with SAMCEF (with A_1 and n_1).
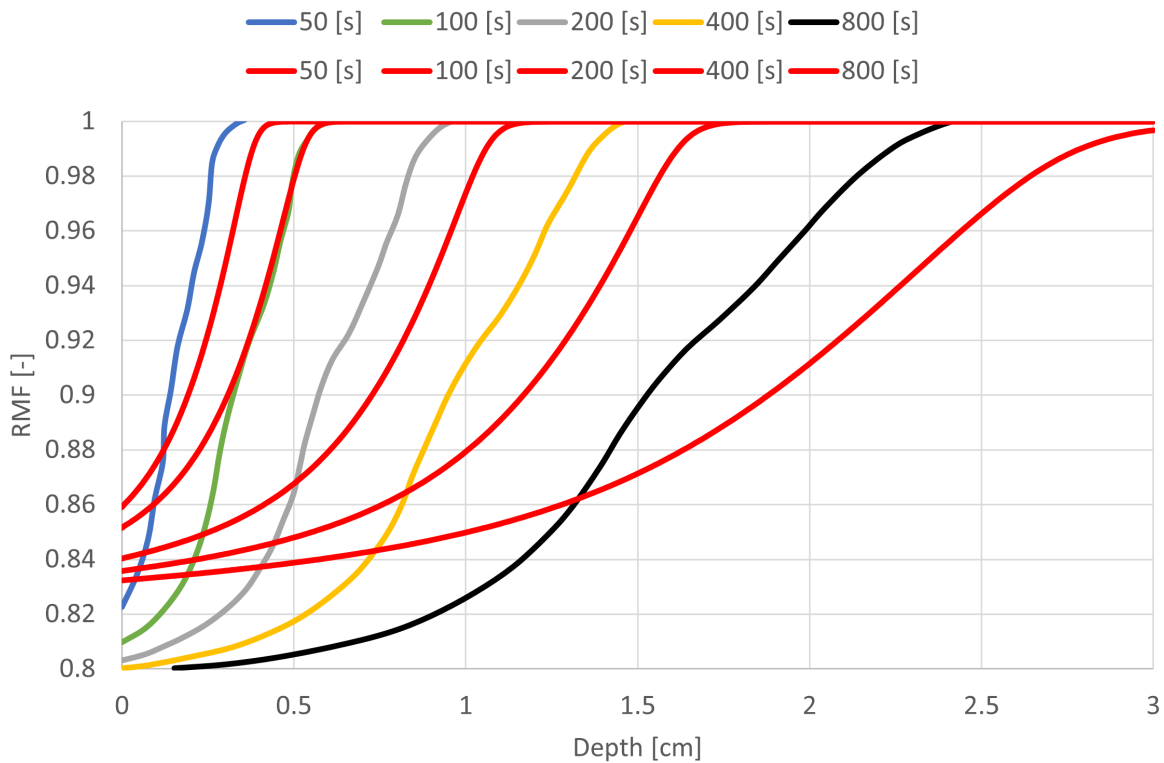
Figure 4.2: Variation of the Remaining Mass Fraction (RMF) as a function of depth for different times during the simulation given in the publication [10] (in colors) and obtained with SAMCEF (in red with A_1 and n_1).
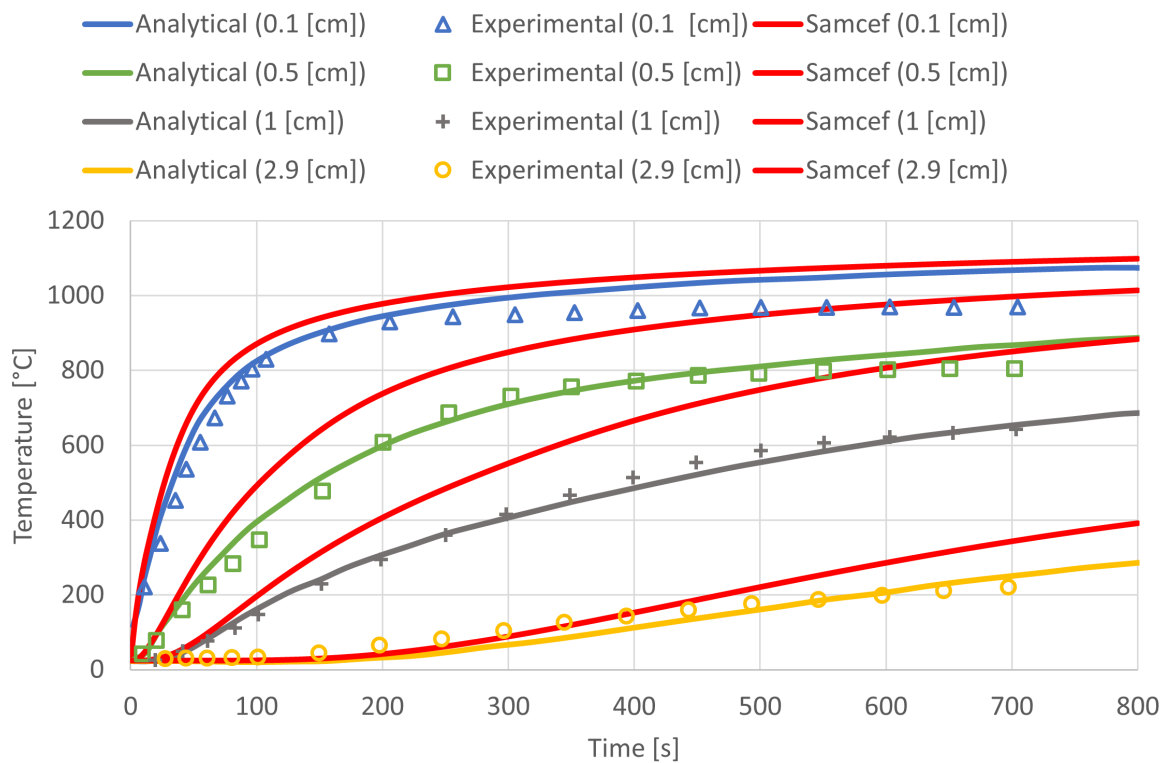
Figure 4.3: Time evolution of the temperature at different depths into the sample (0.1, 0.5, 1 and 2.9 [cm]) given in the publication [10] (analytical and experimental) and obtained with SAMCEF (with A_2 and n_2).
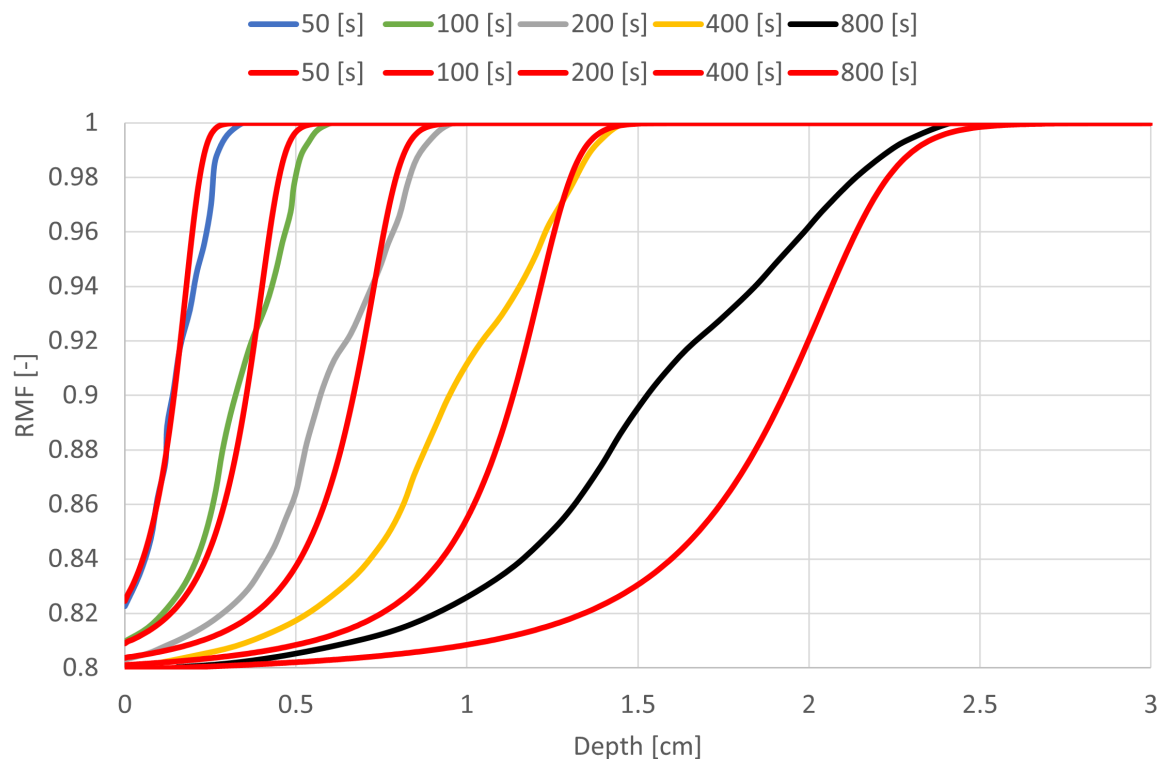
Figure 4.4: Variation of the Remaining Mass Fraction (RMF) as a function of depth for different times during the simulation given in the publication [10] (in colors) and obtained with SAMCEF (in red with A_2 and n_2).
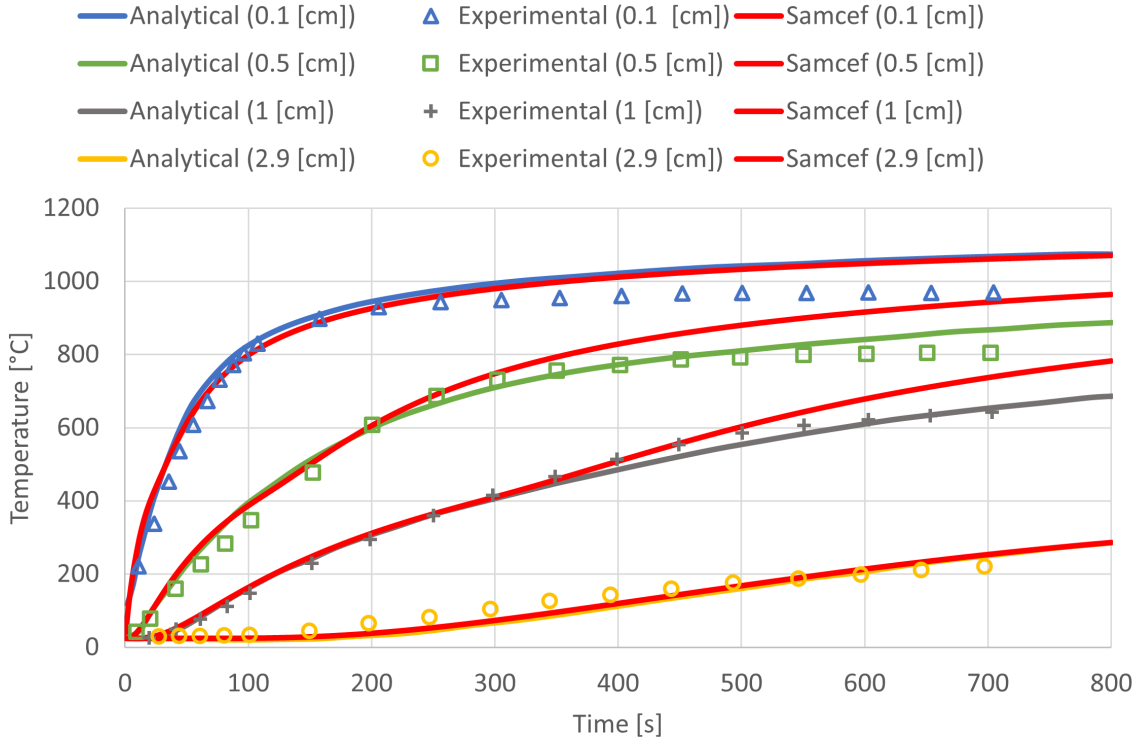
Figure 4.5: Time evolution of the temperature at different depths into the sample (0.1, 0.5, 1 and 2.9 [cm]) given in the publication [10] (analytical and experimental) and obtained with SAMCEF (with $A = 1.27 \times 10^{24}$ [1/s], $n = 10$ [-], $Q_p = -4 \times 10^6$ [J/kg] and $h_{conv} = 7$ [W/m^{2}K]).
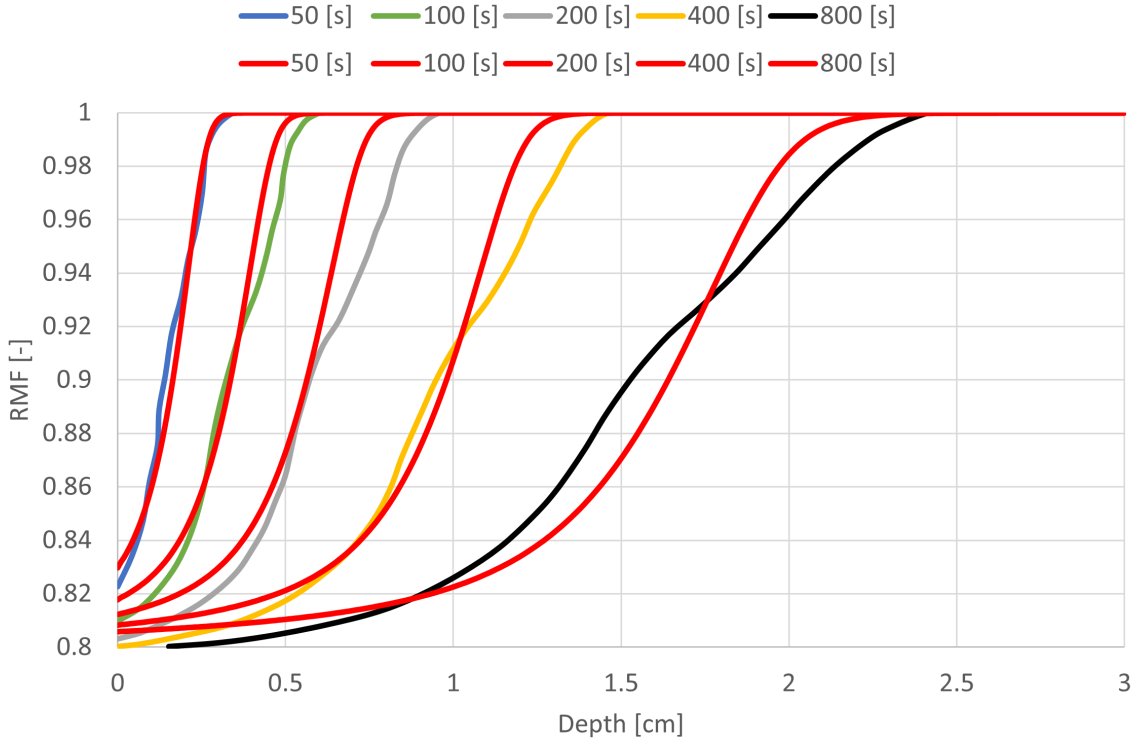
Figure 4.6: Variation of the Remaining Mass Fraction (RMF) as a function of depth for different times during the simulation given in the publication [10] (in colors) and obtained with SAMCEF (in red with $A = 1.27 \times 10^{24}$ [1/s], $n = 10$ [-], $Q_p = -4 \times 10^6$ [J/kg] and $h_{conv} = 7$ [W/m^{2}K]).

57
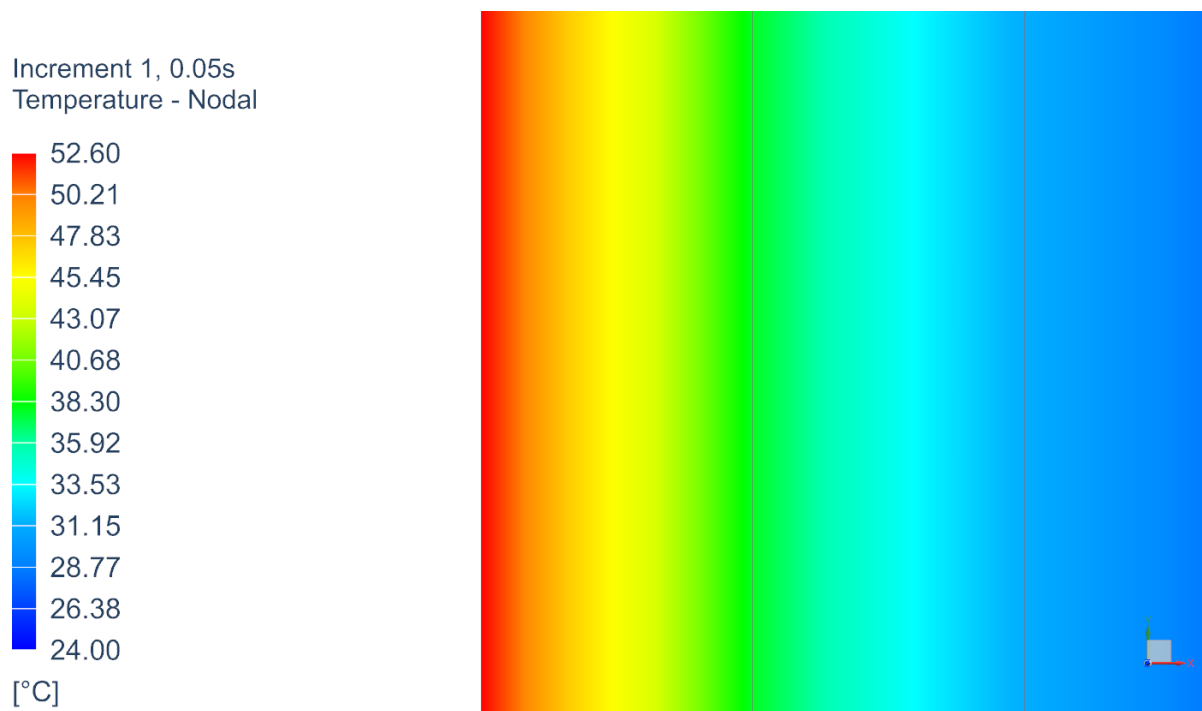
Figure 4.7: Temperature distribution through the thickness of the sample close to the exposed face after the first time step Δt of 0.05 [s]. Results obtained for the material from Henderson et al. [10] thanks to SAMCEF.

4.2 Feih et al.

The second publication used to validate the numerical model used in SAMCEF is a publication from Feih et al. [4]. They present experimental and analytical results for a glass-vinyl ester composite submitted to 4 different heat flux. The results from their publication can therefore be used as a comparison with the one obtained thanks to SAMCEF for the same problem. This is done similarly than in the previous section. The fact that 4 heat flux are considered is very interesting. As explained briefly earlier, it allows to check if the model is accurate no matter the thermal loading conditions and no matter the level of pyrolysis. Note that they used the model from Henderson et al. [8] to obtain their analytical results. However, they do not give indications about the method used to solve the governing equation.

4.2.1 Geometry and mesh

The geometry and mesh definition is done similarly to what is done regarding the first validation (see Section 4.1.1). The composite studied in the publication [4] is 9 [mm] thick. The sample needs therefore to be of the same length. Regarding the mesh, it has been chosen to use 90 elements along the thickness. This leads to a value for Δx of 0.1 [mm] as for the previous model validation.

The condition to avoid the presence of spatial oscillations in the solution expressed by Eq. 3.32 must be satisfied. Exactly as what is done for the previous validation, a minimum value for the first Δt has been calculated based on material properties of the virgin (initial) material given in the next section. The conditions on the first time step writes:

$$\Delta t \; > \; 0.01 \; [\text{s}]. \tag{4.5}$$

It has again been decided to fix the first time step to 0.05 [s] which satisfies the condition. It assumed to be small enough to ensure convergence during this first time step. Note that, as explained previously, the time step is automatically chosen by the solver and adapted in case the solution does not converge. The absence of spatial oscillations is verified in the results section (Section 4.2.4).

4.2.2 Material properties

In this problem, the material is an E-glass-vinyl ester composite made of 55% of fibers and 45% of matrix. Its properties are given by the authors and are rewritten in Tab. 4.4. The only property given for the decomposition gases is their specific heat capacity C_g which is 2386.5 [J/kgK].

	Virgin	Charred
Density ρ [kg/m³]	1921	1423.4
Conductivity k [W/mK]	0.43	1.09
Specific heat C [J/kgK]	(see Fig. 4.8)	760
Emissivity ε_s [-]	1 (unknown)	1 (unknown)
Decomposition parameters		
Activation energy E [J/mol]	$2.12 \cdot 10^5$	
Rate constant A [1/s]	$5.58 \cdot 10^{13}$	
Order of reaction n [-]	1	
Decomposition heat Q_p [J/kg]	-378800	

Table 4.4: Material properties given in the publication from Feih et al. [4] and used in SAMCEF.
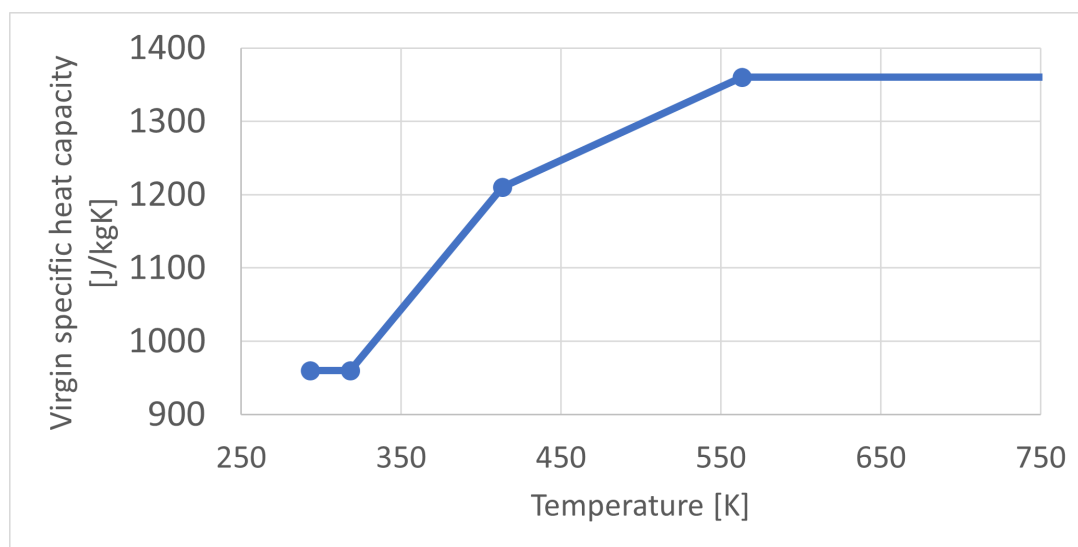
Figure 4.8: Evolution of the specific heat capacity C as a function of temperature for the virgin composite material (E-glass-vinyl ester composite) given in the publication from Feih et al. [4] and used in SAMCEF.

As it can be seen in Tab. 4.4, the material data given in the publication are rather poor compared to what was given for the other material in Section 4.1. Moreover, the authors do not mention the properties in terms of the virgin and charred state as in the previous publication. As mentioned earlier, analytical results about the temperature

evolution in the material are presented in the paper. However, nothing is said about how they obtained these results except that the classical governing thermal equation is used. Eventually, the authors indicate that the properties may evolve with temperature but no details about how they evolve are given. For all these reasons, it is difficult to accurately represent the material in SAMCEF. In the next paragraph it is explained how the properties have been defined in the software.

It has been chosen to make the assumption that the virgin material properties are the one given in terms of the "glass-vinyl ester". Regarding the charred material properties, they are considered to be the one of the glass fibers alone. This is a strong assumption since in reality the fibers are not going to be left alone in the charred material. More-over, they are not necessarily in contact with each other everywhere in the composite. However, it is mentioned that the remaining mass fraction of the resin is 3% after de-composition. Therefore, considering that the charred material properties are the ones of the fibers could be sufficient. This has to be discussed based on the results.

Eventually, it can be noticed that no information about the porosity, the permeabil-ity and the decomposition gas viscosity are given. For this reason, it is not possible to represent accurately the Darcy law in the model. The gas mass flux is therefore assumed to be exactly equal to the mass loss rate due to decomposition. Moreover, it is assumed that the gas directly leaves the material towards the heated surface. Therefore, no gas storage in the material is considered by SAMCEF in this case.

Many assumptions are made about the material properties in the software due to the lack of knowledge about them. It will probably be necessary to adapt the material properties in order to fit the curves coming from the publication. If the curves obtained for the four different heating conditions can be fitted simultaneously, the model will be assumed to be valid.

4.2.3 Boundary conditions

Regarding the boundary conditions, the ambient temperature and pressure are given in the publication. Once again, the convection coefficient is not known. Therefore, a first guess of 3 [W/m²K] is made for it and is going to be adjusted if it is needed. The boundary conditions are summarized in Tab. 4.5. As done previously, the 4 radiant heat flux that are imposed to the material sample have to be converted in a radiation temperature T_r. This conversion is based on Eq. 3.30 and the resulting values for T_r are presented in Tab. 4.6.

Initial (ambient) temperature T_∞ [K]	293.15
Initial (ambient) pressure P_∞ [Pa]	101325
Radiant heat flux q''_{rad} [kW/m^2]	10, 25, 50 and 75
Convection coefficient h_{conv} [W/m^{2}K]	3

Table 4.5: Initial and boundary conditions given in the publication from Feih et al. [4] and used in SAMCEF.

Radiant heat flux q''_{rad} [kW/m^2]	10	25	50	75
Radiation temperature T_r [K]	648.04	814.87	969.05	1072.43

Table 4.6: Radiation heat fluxes q''_{rad} imposed on the material sample (from Feih et al. [4]) and their corresponding radiation temperature T_r used in SAMCEF.

4.2.4 Results and discussion

First, the TGA curves for the vinyl ester resin can be reproduced using SAMCEF. It allows to verify that the parameters A, E and n given in the publication are correct and well interpreted in the software. If this is not the case, they have to be adapted to fit the curves from the publication. The TGA curves are obtained in practice by imposing a temperature to a tiny material sample. This sample loses mass and this is quantified by the TGA instrument. It is therefore modeled in SAMCEF by imposing a temperature to one single finite element having the vinyl ester properties. The resulting mass loss directly comes from the Arrhenius' law implemented in the software. No effects of conduction or heat capacity are taken into account, only the decrease in density due to the imposed temperature is simulated. Therefore, only the definition of the initial and final density and of the parameters A, E and n has an importance in the simulation. Indeed, these are the only parameters required by the Arrhenius' law.

The TGA curves can be obtained for different heating rates as in the publication. This allows to highlight the dependency of the decomposition process on these heating rates. The results coming from SAMCEF using the default parameters given in the paper are shown in Fig. 4.9. As it can be seen, these parameters lead to a sufficiently good correlation. Therefore, they are kept unchanged for the rest of the model validation.
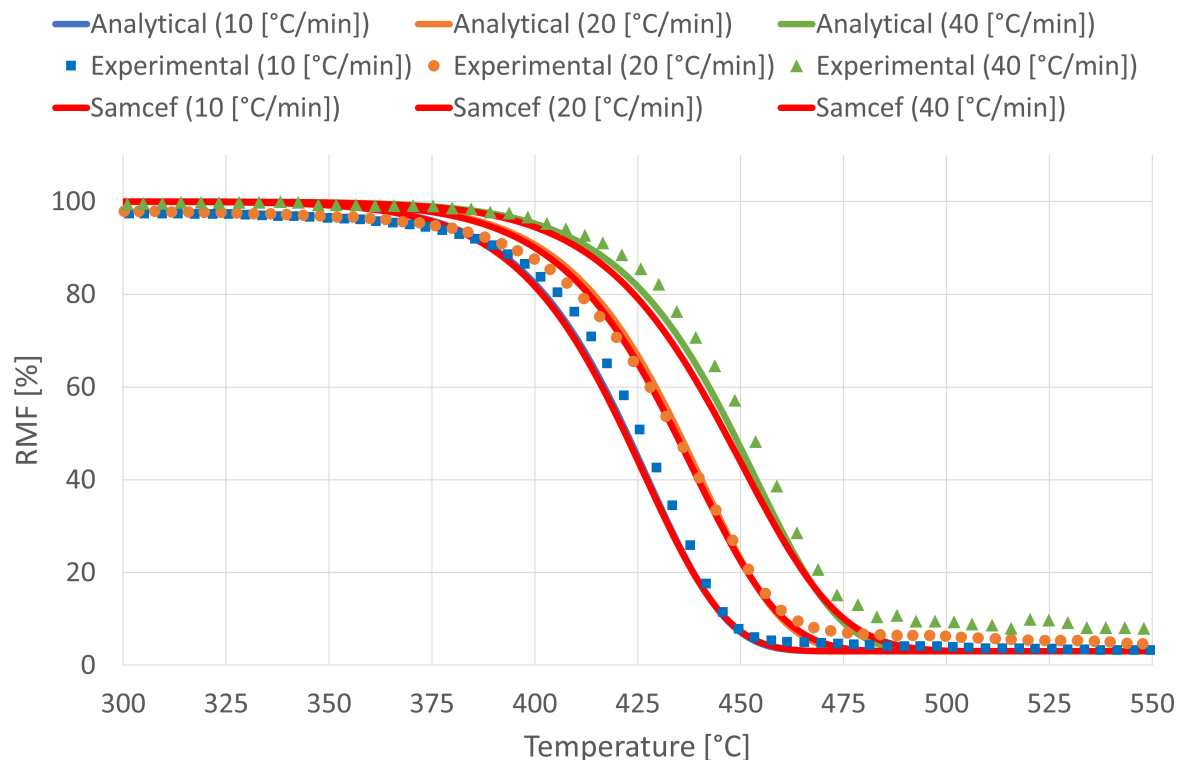
Figure 4.9: Variation of the Remaining Mass Fraction (RMF) of the vinyl ester resin as a function of temperature for different heating rates (10, 20 and 40 [°C/min]). Curves given in the publication [4] (analytical and experimental) and obtained thanks to the Arrhenius law implemented in SAMCEF. The experimental results are found by performing a TGA.

Now that the Arrhenius' law and the related parameters A, E and n have been validated thanks to the TGA curves, the temperature profiles can be computed and compared to the one given in the publication. The first results are obtained with the properties from the paper given in Tab. 4.4. They are shown in Fig. 4.10 for the different radiant heat flux. It can be seen that the temperature profiles obtained with SAMCEF do not fit well with the one coming from the publication. This is especially the case for the larger heat flux.

It was shown in the previous model validation (see Section 4.1.4) that an increase of the decomposition heat Q_p in the model leads to an improvement of the temperature profiles. Therefore, it has been decided to do the same in this case. A new value of -2×10^6 [J/kg] for Q_p has been introduced in the model. This is 5 times larger than the initial value. The resulting temperature profiles illustrated in Fig. 4.11 show that this modification improves the model. Indeed, the results for the larger heating rates are closer to the reference ones. As for the previous publication, this means that the value of Q_p has to be increased in SAMCEF in order to correctly take into account the heat absorption due to the material pyrolysis. Since some heat is absorbed, the temperature

(a) $q''_{rad} = 10$ [kW/m²]

(b) $q''_{rad} = 25$ [kW/m²]

(c) $q''_{rad} = 50$ [kW/m²]

(d) $q''_{rad} = 75$ [kW/m²]

Figure 4.10: Time evolution of the temperature at different depths into the sample (0, 4.5 and 9 [mm]) given in the publication [4] (solid curves for analytical and dotted curves for experimental results) and obtained with SAMCEF (red curves). Properties given in Tab. 4.4 used in SAMCEF.

further in the composite increases slower than if no heat was absorbed. The improvement of the results is very significant for the 50 and 75 [kW/m²] flux but less for the 10 and 25 [kW/m²]. This is explained by the fact that for the two lower heat flux, either no pyrolysis occurs (with 10 [kW/m²]), either it occurs but partially (with 25 [kW/m²]). Indeed, the TGA curves in Fig. 4.9 show that under 350 [°C], no decomposition occurs

whatever the imposed heating rate. For 10 and 25 [kW/m²], the temperatures do not go over 350 [°C] or just in a part of the sample. Therefore, since the parameter Q_p influences the temperature only when decomposition occurs, it is normal that a modification of its value does not impact materials in which low or no decomposition is present.

(a) $q''_{rad} = 10$ [kW/m²]

(b) $q''_{rad} = 25$ [kW/m²]

(c) $q''_{rad} = 50$ [kW/m²]

(d) $q''_{rad} = 75$ [kW/m²]

Figure 4.11: Time evolution of the temperature at different depths into the sample (0, 4.5 and 9 [mm]) given in the publication [4] (solid curves for analytical and dotted curves for experimental results) and obtained with SAMCEF (red curves). Properties given in Tab. 4.4 used in SAMCEF (with $Q_p = -2 \times 10^6$ [J/kg]).

The model can be further improved by tuning other material properties. First, the modification of the virgin properties is studied. In order to do that, it is decided to focus on the temperature profiles for the two lower heat flux (10 and 25 [kW/m²]). Indeed, since no pyrolysis occurs in these cases or just partially, the virgin material properties dominate the thermal response. The focus is first put on the specific heat capacity. An increase of the heat capacity should reduce the rate at which the temperature increases in the material. This is indeed what is required to improve the results as it can be observed in Fig. 4.11a and 4.11b. After testing different values, an increase of the virgin material heat capacity by 30% is found to be optimal. The temperature profiles obtained with this modification are shown in Fig. 4.12. As expected, the temperature increases at a slower rate in the material. No well-founded explanation for this need of increasing the heat capacity has been found but it improves the model.

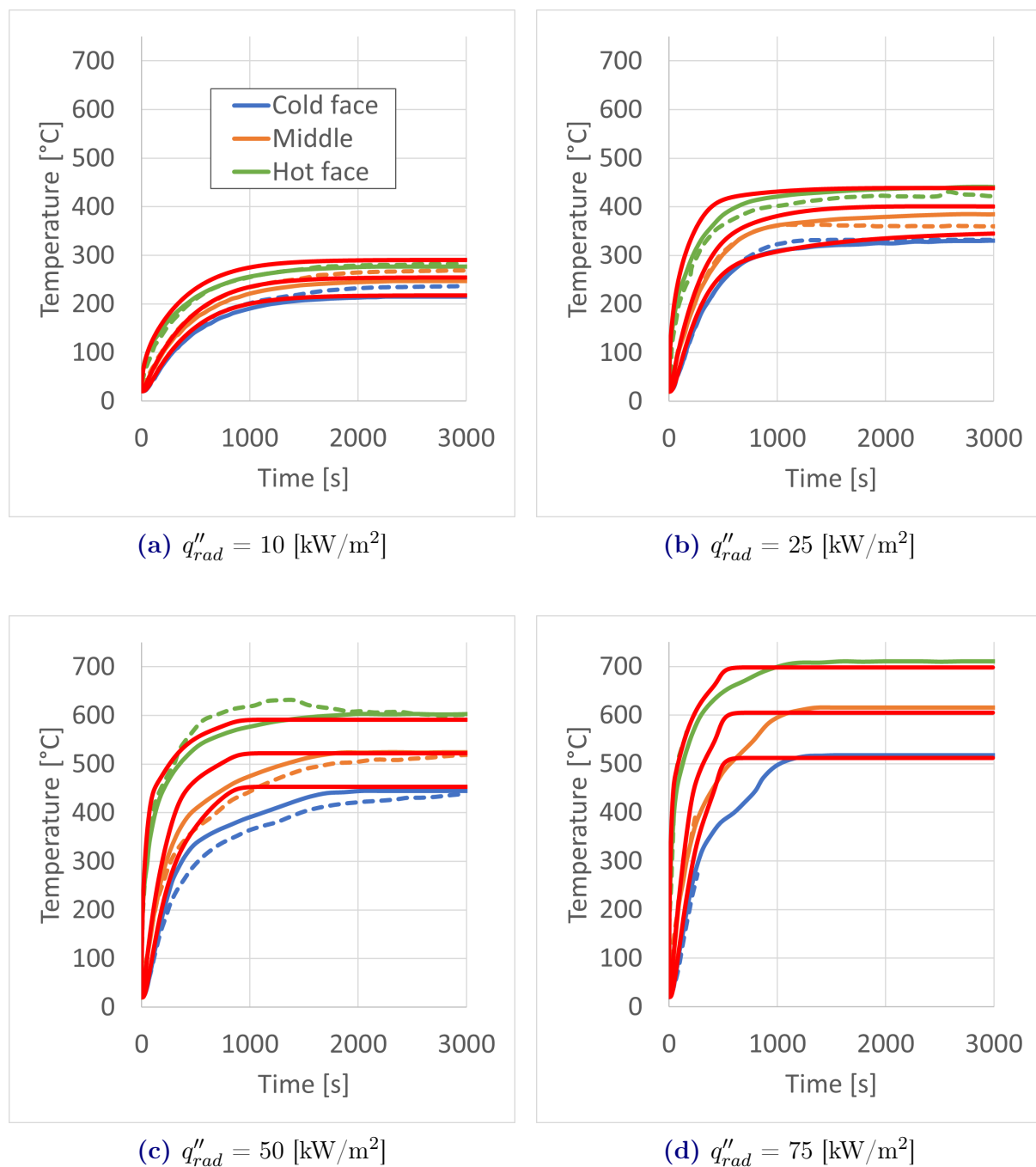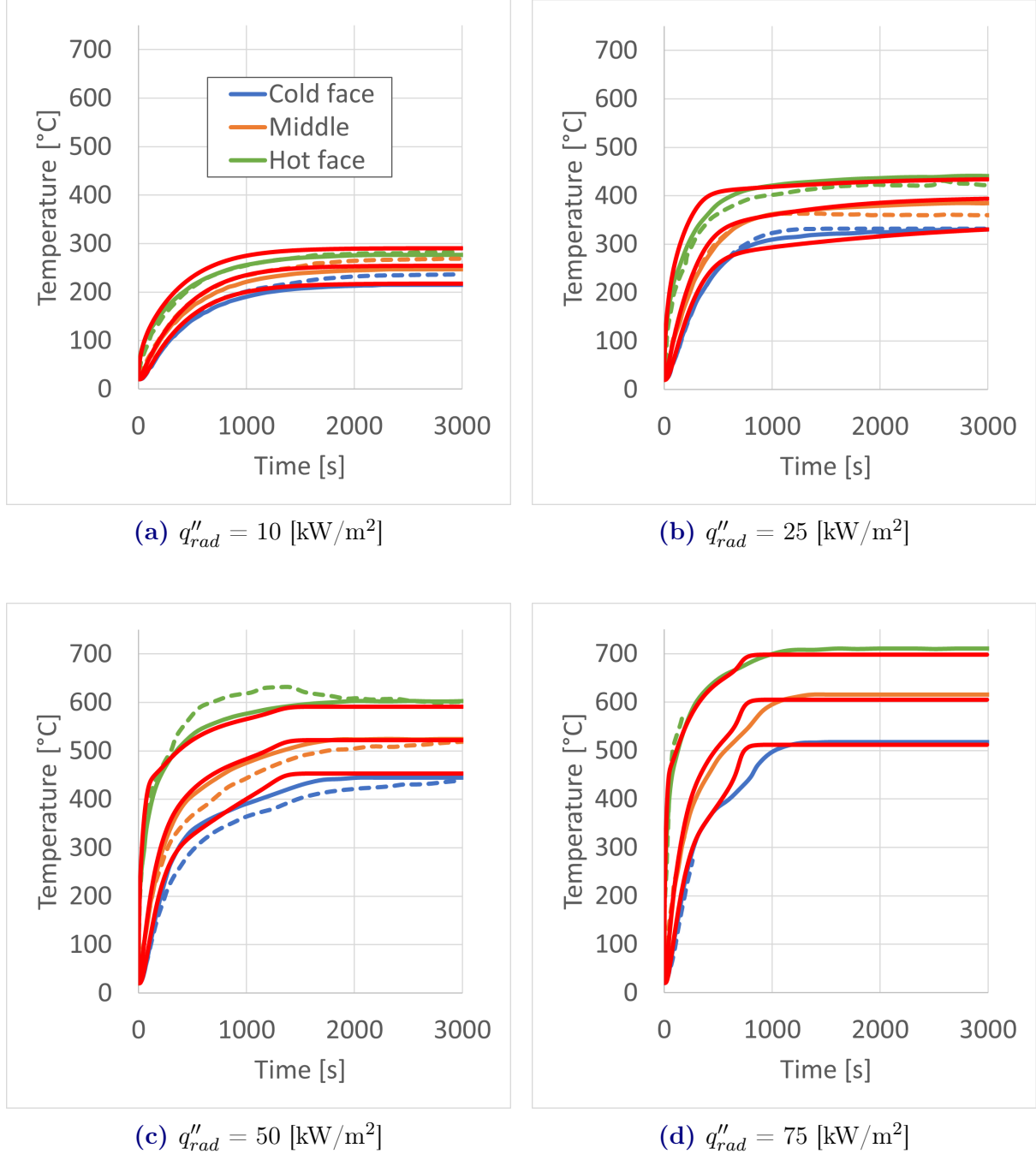(a) $q''_{rad} = 10$ [kW/m²]

(b) $q''_{rad} = 25$ [kW/m²]

Figure 4.12: Time evolution of the temperature at different depths into the sample (0, 4.5 and 9 [mm]) given in the publication [4] (solid curves for analytical and dotted curves for experimental results) and obtained with SAMCEF (red curves). Properties given in Tab. 4.4 used in SAMCEF (with $Q_p = -2 \times 10^6$ [J/kg] and $C_v + 30\%$).

Then, it is interesting to look at the thermal conductivity of the virgin material. The temperature profiles given in Fig. 4.12 show that the curves for different locations in the material should be closer to each other in the virgin state. For the 25 [kW/m²] heat flux, it is only true between the middle and the unexposed face temperatures. This makes sense because only this part of the material remains in the virgin state whereas the part between the exposed face and the middle is partially charred. It means that the conductivity of the virgin material needs to be increased. This should indeed lead to a better heat transfer and thus bring the temperatures closer to each other. Thanks to

several simulations, an increase of the virgin conductivity by 30% appears to be optimal. The resulting temperature profiles are shown in Fig. 4.13. As expected, they are slightly better than the previous ones. The need of increasing the value of the conductivity to improve the model could be explained by the fact that the material conductivity should be temperature-dependent. However, it is not the case here. Therefore, increasing its constant value allows to artificially take that behavior into account. Note that an even better improvement could be to define the conductivity by a polynomial depending on the temperature. However, this would require a lot of work in order to find the best for only a slight improvement of the results.

(a) $q''_{rad} = 10$ [kW/m^2]
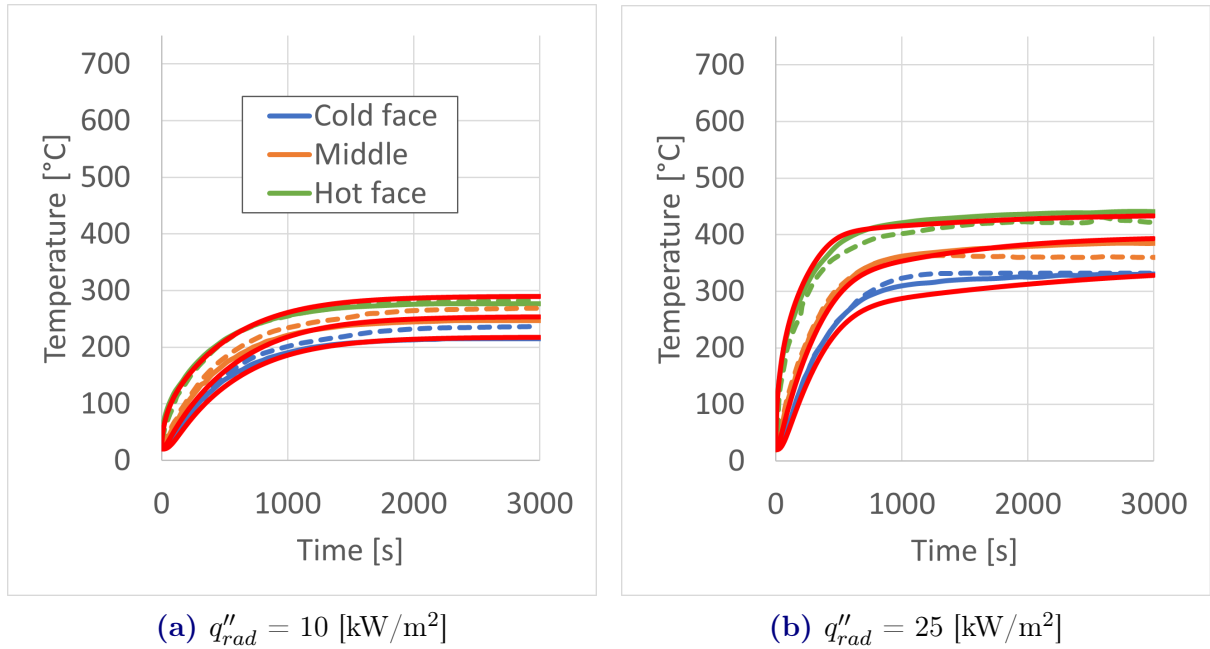
(b) $q''_{rad} = 25$ [kW/m^2]

Figure 4.13: Time evolution of the temperature at different depths into the sample (0, 4.5 and 9 [mm]) given in the publication [4] (solid curves for analytical and dotted curves for experimental results) and obtained with SAMCEF (red curves). Properties given in Tab. 4.4 used in SAMCEF (with $Q_p = -2 \times 10^6$ [J/kg], C_v+30% and k_v+30%).

The material properties for the virgin state seem to be well defined. It is now interesting to further improve the results regarding the material in its charred state. In that case, the properties adjustment is done according to the temperature profiles for the two larger heat flux (50 and 75 [kW/m^2]). Indeed, these flux induce a complete matrix decomposition and the temperature are thus highly influenced by the charred material properties. First, the thermal conductivity can be tuned. As it can be seen in Fig. 4.11c and 4.11d, there are some bumps in the profiles obtained with SAMCEF respectively at around 1200 [s] and 800 [s]. They appear at temperatures at which decomposition occurs and therefore when the conductivity becomes the one of the charred material. If the charred state conductivity is reduced, these bumps should be flattened out. When the value for the charred conductivity is reduced by 20%, the results become better as

expected. The temperature profiles that are obtained are shown in Fig. 4.14. For both flux, the bumps have indeed disappeared. The need for a reduction of the charred state conductivity can be explained by the fact that it was considered to be equal to the fibers conductivity. However, this is not true in reality because the charred composite is not full of fibers in contact with each other and thus cannot have the exact same conductivity. The little remaining mass of resin (3%) also plays a role in the overall conductivity and might therefore lead to a smaller value than expected.

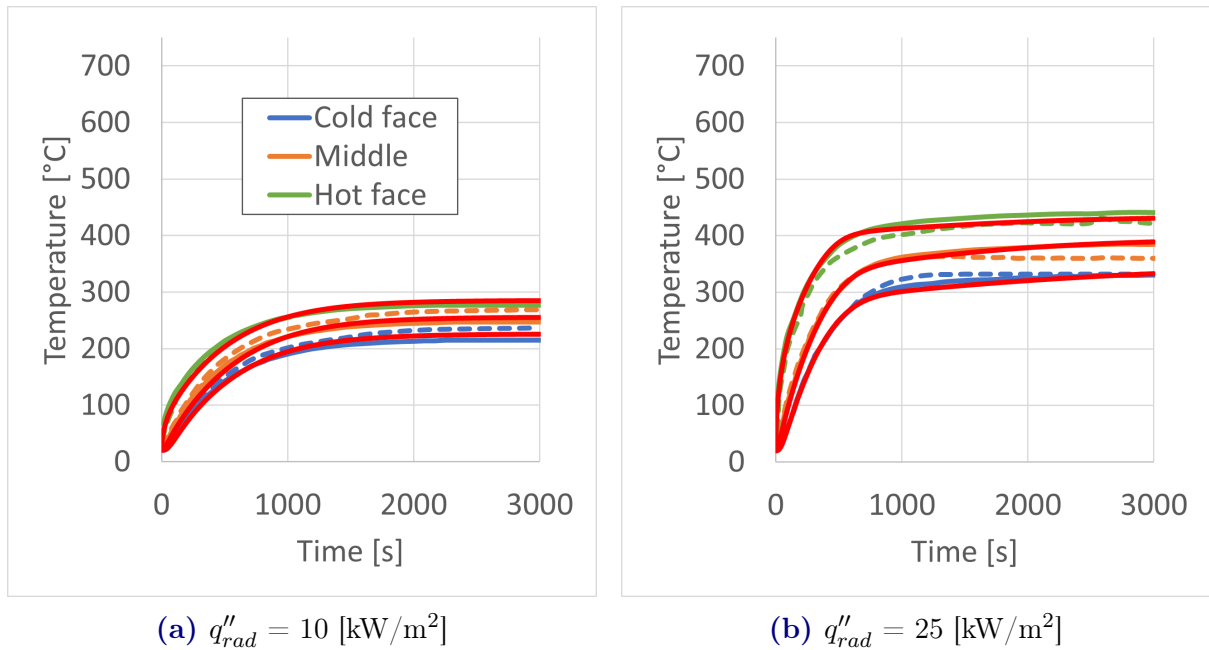**(a)** $q''_{rad} = 50$ [kW/m^2]   **(b)** $q''_{rad} = 75$ [kW/m^2]

Figure 4.14: Time evolution of the temperature at different depths into the sample (0, 4.5 and 9 [mm]) given in the publication [4] (solid curves for analytical and dotted curves for experimental results) and obtained with SAMCEF (red curves). Properties given in Tab. 4.4 used in SAMCEF (with $Q_p = -2 \times 10^6$ [J/kg], C_v+30%, k_v+30% and k_c-20%).

A last modification leading to even better results can be obtained by increasing the specific heat capacity of the charred state by 30%. It flattens out the little remaining bumps in the temperature profiles for the 75 [kW/m^2] heat flux. This effect is expected since it reduces the rate at which the temperature increases in the charred material. The reason for changing this property can be justified by the fact that the capacity was considered to be the one of the glass fibers which is not exactly the case in reality.

The temperature profiles obtained for each heat flux and taking into account all the properties modifications are shown in Fig. 4.15. The curves obtained thanks to SAMCEF are now fitting quite well the one coming from the publication. Moreover, it can be observed that the thermal behavior for this composite material is correctly represented for the four heat fluxes and thus for different decomposition cases.

(a) $q''_{rad} = 10$ [kW/m^2]

(b) $q''_{rad} = 25$ [kW/m^2]

(c) $q''_{rad} = 50$ [kW/m^2]

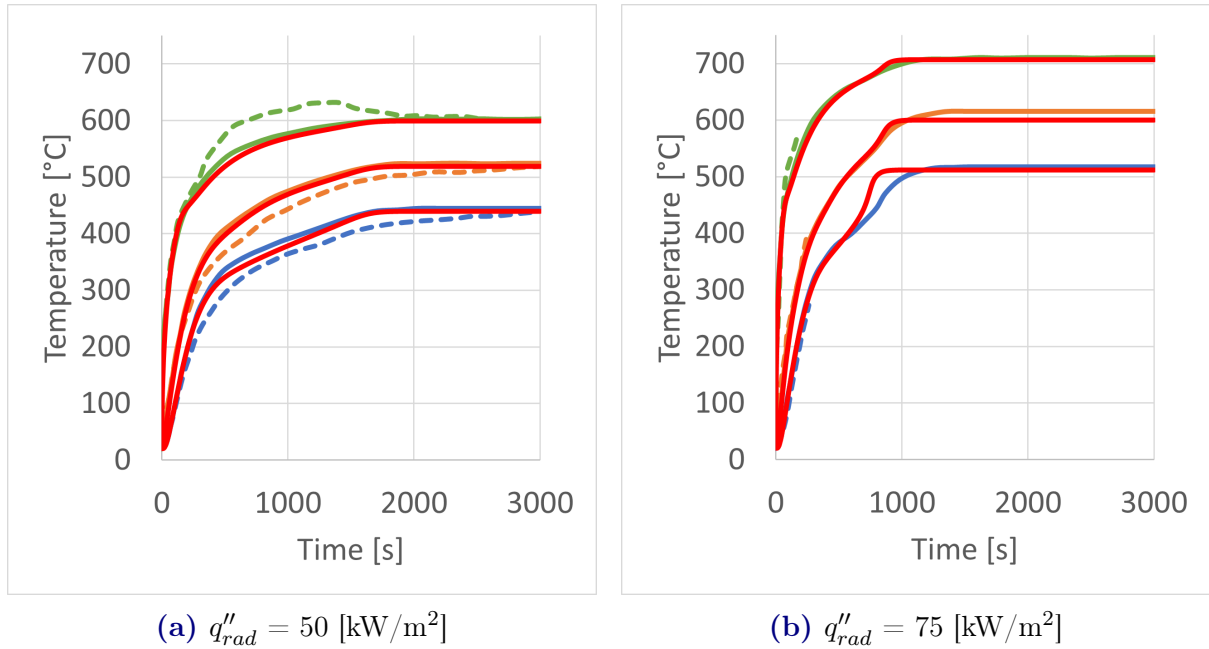**(d)** $q''_{rad} = 75$ [kW/m^2]
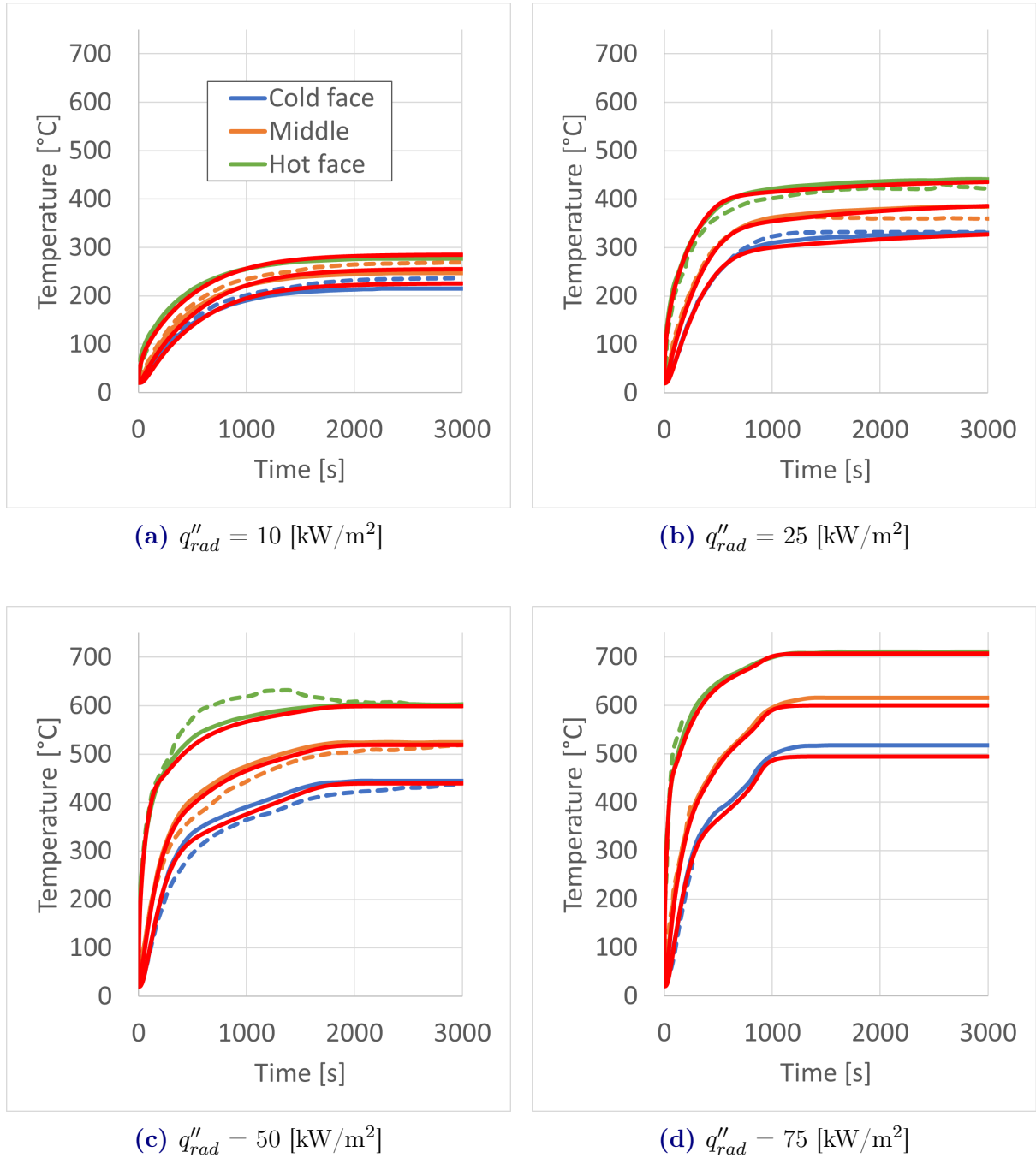
Figure 4.15: Time evolution of the temperature at different depths into the sample (0, 4.5 and 9 [mm]) given in the publication [4] (solid curves for analytical and dotted curves for experimental results) and obtained with SAMCEF (red curves). Properties given in Tab. 4.4 used in SAMCEF (with $Q_p = -2 \times 10^6$ [J/kg], $C_v+30\%$, $k_v+30\%$, k_c-20% and $C_c+30\%$).

Regarding this last simulation, it is important to verify that no spatial oscillations are present in the solution. As explained previously in Section 4.2.1, the value for Δx is 0.1 [mm]. The first time step is fixed to 0.05 [s] in order to satisfy the condition expressed

by Eq. 3.32 and no spatial oscillations should be observed in the results. As shown in Fig. 4.16, there are indeed no spatial oscillations in the solution at the beginning of the simulation for the 50 [kW/m^2] heat flux. There is not a temperature below the initial one (20 [°C]) close to the boundary. The value of the heat flux does not influence the condition to be satisfied. Therefore, this conditions does not have to be verified for the three other heat fluxes. Note that a test has been made to see what value the solver automatically chooses for the first time step. It was larger than 0.05 [s] which means that the first Δt fixed was not too large in order to ensure convergence.
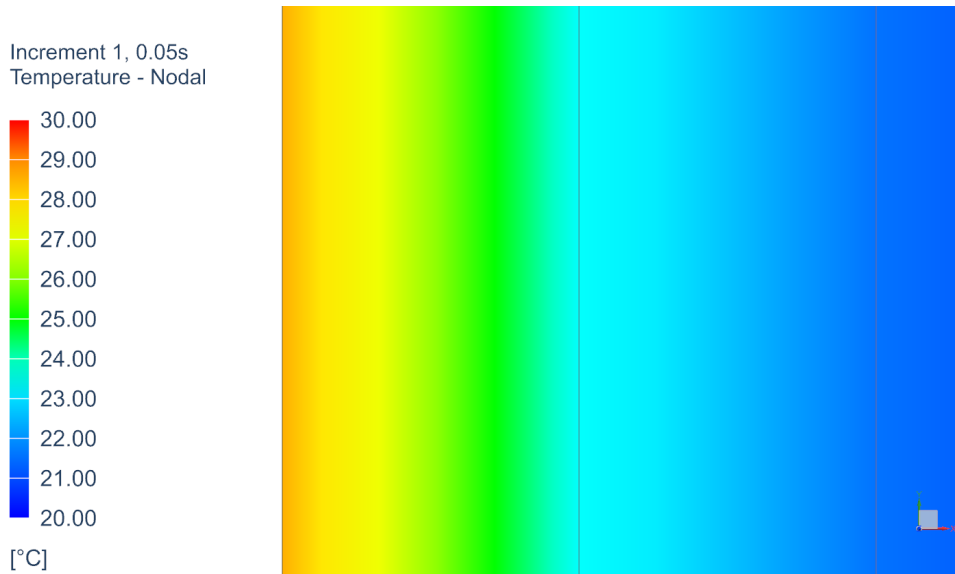
Figure 4.16: Temperature distribution through the thickness of the sample close to the exposed face after the first time step Δt of 0.05 [s]. Results obtained with SAMCEF for the material (with corrected values) from Feih et al. [4] and for the 50 [kW/m^2] heat flux.

An additional control of the model is made by analyzing how evolves the remaining mass fraction in the material for the different heat flux. This can be verified in two ways. The first way is to directly analyze the nodal density along the material and integrate it over the thickness. The total mass of the sample is then obtained and is divided by the initial mass. This leads to the fraction of mass remaining in the sample. Another way to compute the RMF is based on Eq. 2.12. Indeed, the decomposition gases mass flux can be integrated over the time and this directly gives how much mass has left the sample. Therefore, to find the RMF at a specific time is straightforward. A graph showing the evolution of the RMF obtained with SAMCEF using these two techniques and the curves from the paper is given in Fig. 4.17. As it can be observed, both methods give the same results which is expected. Indeed, this correlation is enforced by the mass continuity equation. Furthermore, these curves are fairly close to the one from the publication which proves that the model is valid for each heat flux. Note that no curve is shown for the 10 [kW/m^2] heat flux since no decomposition occurs in that case.
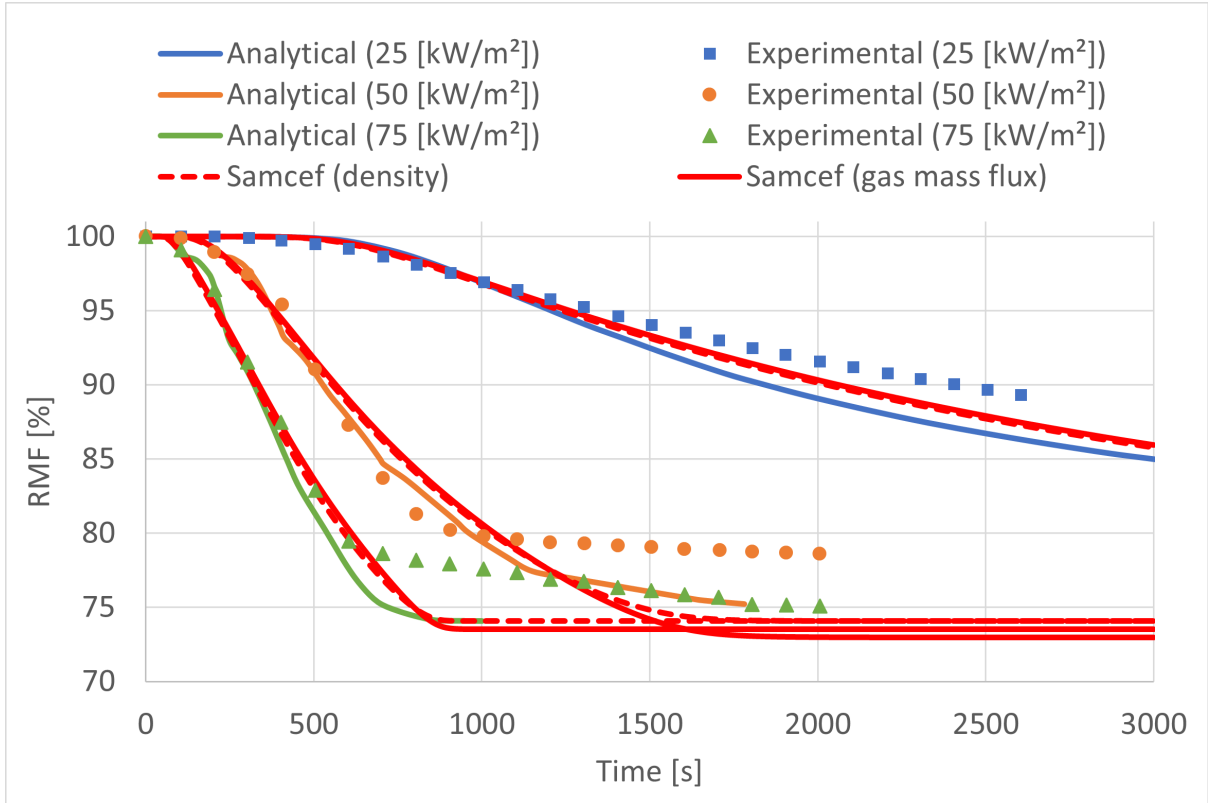
Figure 4.17: Time evolution of the Remaining Mass Fraction (RMF) of the E-glass-vinyl ester composite as a function of temperature for the different values of q''_{rad} (25, 50 and 75 [kW/m²]). Curves given in the publication [4] (analytical and experimental) and obtained with SAMCEF based on the nodal densities or on the gas mass flux (with the corrected values of the material properties).

4.3 General comments

Thanks to two different papers, the thermal results obtained with SAMCEF have been analyzed. Some general comments have to be made about this thermal analysis.

First, it must be reminded that some physical processes are not taken into account in the model such as delamination for example. Moreover, the model does not take into account the thermal expansion effect. This can explain some discrepancies with the experimental results. Perspectives for the model improvement are given in Section 6.

Then, since the material properties are difficult to measure in reality, they might be incorrect. In the case of the paper from Feih et al. [4], the informations about the material properties are even very poor. In such a situation, it was shown that the properties had to be modified in order to obtain a valid model.

A common observation is that the value of the decomposition energy Q_p must be increased a lot in order to obtain the same results as in the literature. This was not expected and it seems to indicate that this parameter is not well interpreted by the solver. Thanks to the results from Feih et al. [4], it is shown that once Q_p is tuned correctly the results are better no matter the level of decomposition. The differences between the analytical results and the ones obtained with SAMCEF could also be due to a difference in the solution methods used to solve the equations. Therefore, this should be investigated in further works in order to identify if these solution methods influence the results significantly.

Eventually, the numerical model works correctly for samples having two very different thicknesses. The first one being 3 [cm] thick and the second one 9 [mm] thick. This tends to demonstrate that the model is valid and therefore works for different samples.

Chapter 5

Mechanical model results

Based on the temperature distribution obtained thanks to the thermal model, the mechanical response of the material can be studied. The mechanical model is only presented to highlight the fact that the response of a composite sample can depend on a previously computed thermal response. The methodology dedicated to the mechanical model is presented in Section 3.3. It is important to recall that the material used in this part is not the same as the one for which the temperatures are calculated. Therefore, the results are not physically correct. This is unfortunately due to the lack of knowledge about the materials used in the literature. Moreover, since the mechanical model analysis had to be realized in a short amount of time, a mesh convergence study could not be realized. The mesh used in this part is rather coarse and it influences the results. However, as explained above, the results do not have a real physical sense due to the fact that the material used does not correspond to the one from the thermal analysis.

The results are obtained for the composite sample presented in the methodology (see Section 3.3). The general information about the material behavior and properties are also given in the methodology. The temperature imposed to this sample are coming from the thermal model used for another material, which is the one presented by Feih [4] (see Section 4.2).

The laminate used for the simulations is composed of 9 uni-directional plies all oriented at $0°$. The plies are considered to be 1 [mm] thick which leads to a total thickness of 9 [mm] for the laminate. This corresponds to the thickness of the sample used in the thermal analysis. Moreover, the sample is a 100×100 [mm] square. The schematic representing the problem is presented in Section 3.3.3 and shown again here in Fig. 5.1.
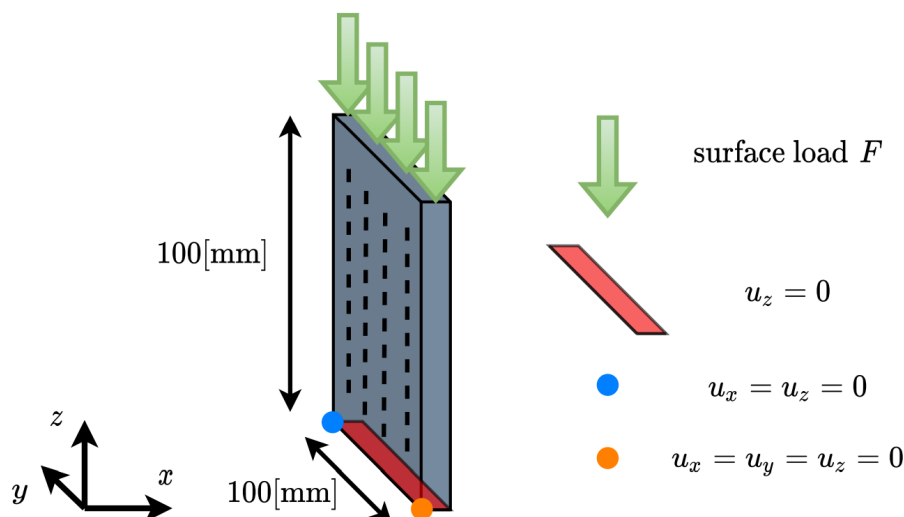
Figure 5.1: Schematic of the sample geometry used in SAMCEF with the imposed load and boundary conditions. The variable u represents a displacement.

5.1 Temperature representation

Before performing any mechanical analysis, it is important to check that the temperature distribution is correctly applied to the model. As explained previously, it has been decided to apply the time-varying temperatures coming from the material used by Feih [4] and exposed to a heat flux of 50 [kW/m²]. This temperature distribution is obtained thanks to the thermal model and is shown in Fig. 4.15c. This distribution is applied to the mechanical model thanks to a dedicated command available in SAMCEF. Once the thermal solution is mapped onto the mechanical mesh, it is possible to check that the problem is correctly represented. Fig. 5.2 shows the temperature distribution in the material for different times. The temperatures correspond exactly to the profile given in Fig. 4.15c. As expected, there is only a variation in the through-thickness direction. This comes from the fact that the thermal model is a 1D model. Note that the temperatures for the material from Feih are known up to 3000 [s]. However, since they become stationary after about 2000 [s], the mechanical simulations are stopped at that time.

(a) $t = 100$ [s].

(b) $t = 500$ [s].

(c) $t = 1000$ [s].

(d) $t = 2000$ [s].
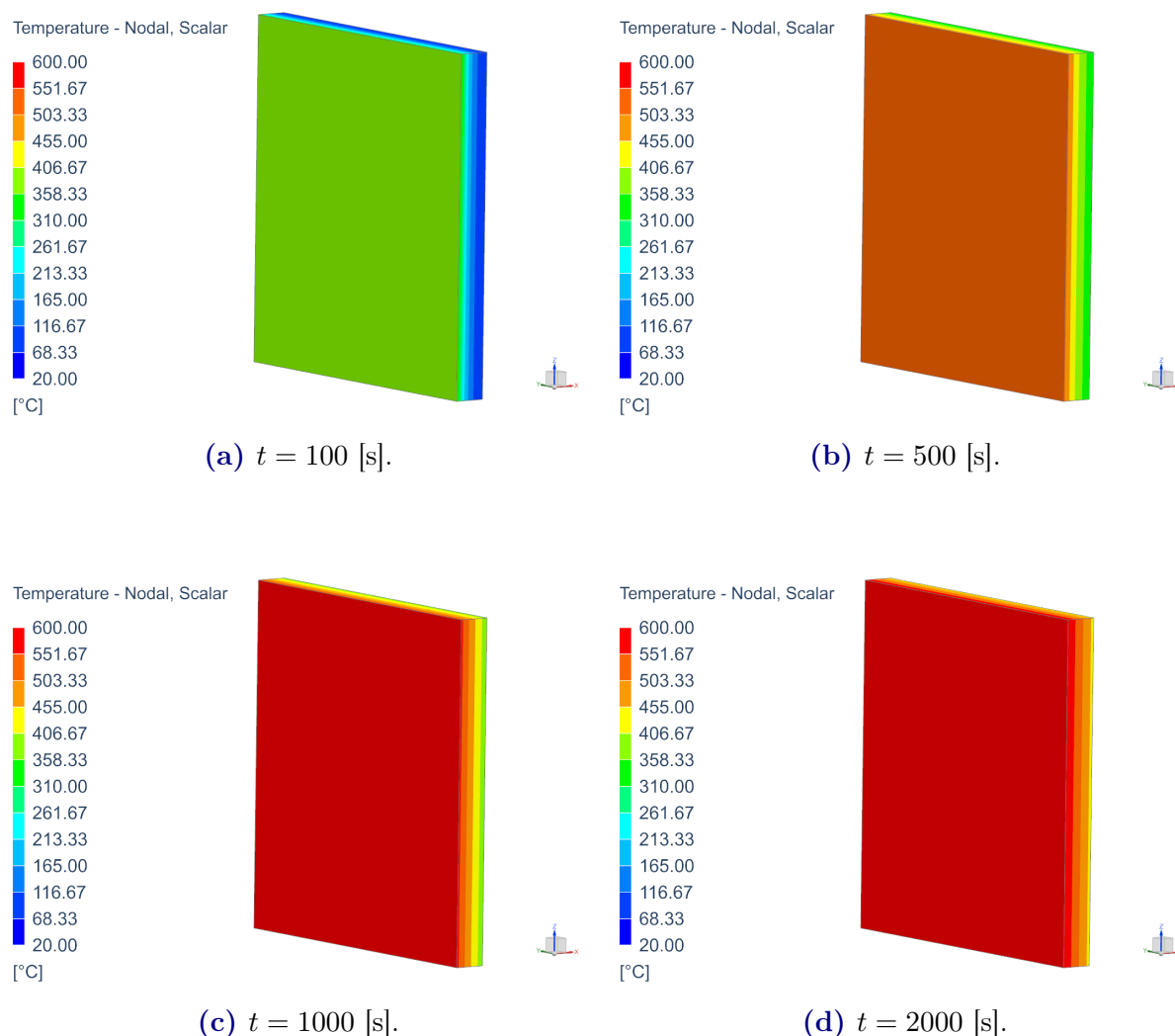
Figure 5.2: Temperature distribution imposed to the sample in SAMCEF at different times t during the simulation.

5.2 Elastic material model

As explained in the methodology, a first analysis is made using a laminate with elastic behavior. Therefore, no damage or hardening modeling is present.

Before performing the mechanical analysis with an applied load, it is interesting to observe the effect of the temperature alone. Due to the thermal expansion of the material, sample deformations are indeed appearing. Fig. 5.3 shows the deformations in the x-direction at different times of the simulation. As it can be seen in these figures, the fact that the temperature is different in the through-thickness direction leads to thermal moments. Indeed, a higher temperature at the exposed face involves a greater expansion on that side. The sample is therefore not expanding homogeneously and a curved shape is formed. Moreover, the deformation is not the same in all the directions. This is due

to the fact that the coefficient of thermal expansion in the transverse direction is larger than in the fiber direction. This explains why the thermal moment is mainly around the z-axis and almost not around the y-axis.

Another interesting observation can be made about Fig. 5.3. It can be noticed that the deformation in the x-direction reaches a maximum value at 160 [s] and then it decreases until the end of the simulation (2000 [s]). This is because the temperature difference between the exposed and unexposed faces is maximum at 160 [s]. Then, as the heat goes through the material, this difference decreases. Since the thermal expansion is directly proportional to the temperature, it leads to a reduction of the thermal moment (the sample is less curved).

(a) $t = 10$ [s].

(b) $t = 160$ [s] (maximum value).
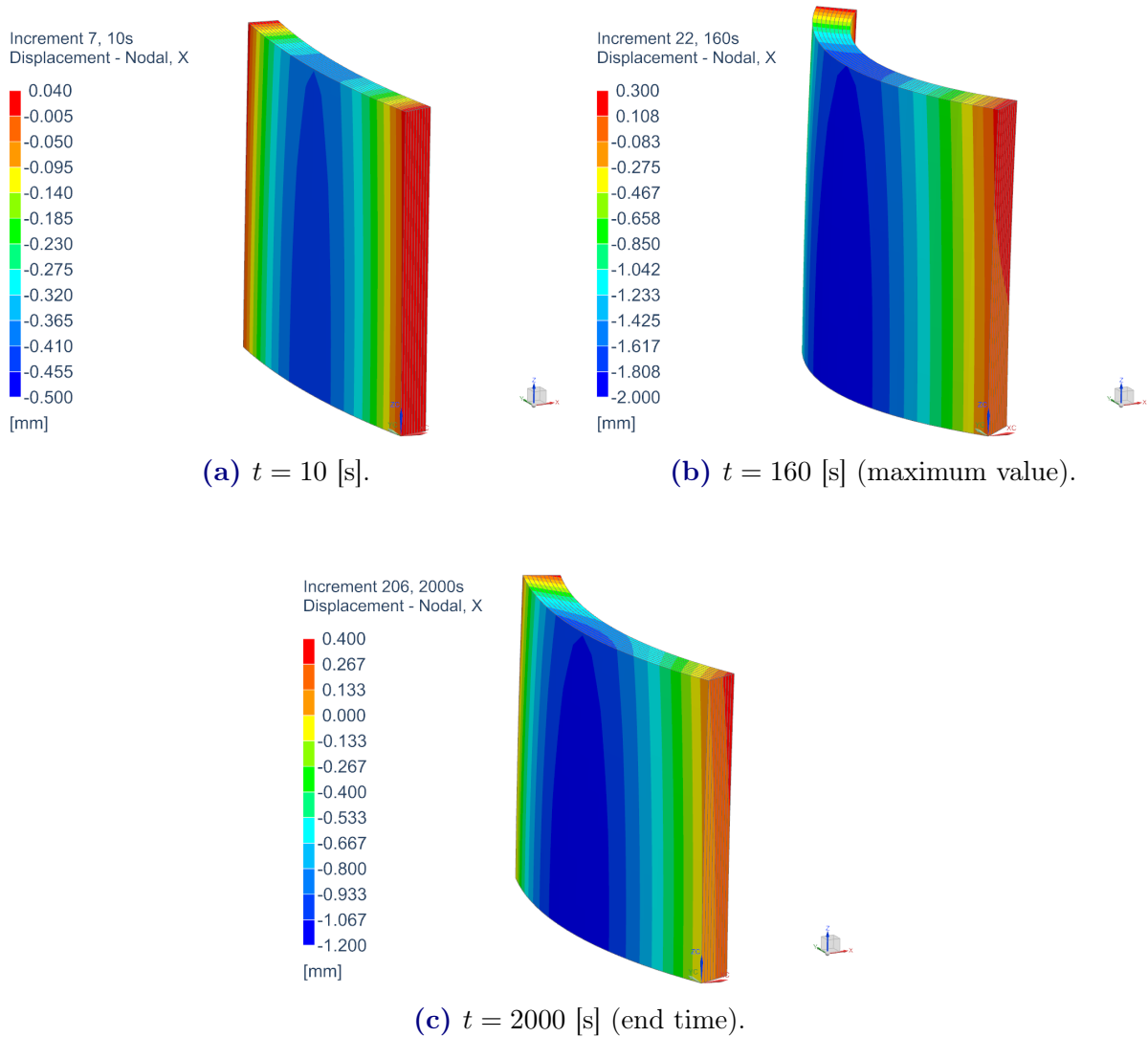

(c) $t = 2000$ [s] (end time).

Figure 5.3: Deformation of the composite sample in the x-direction at different times t during the simulation obtained with SAMCEF (without any load). The apparent shape is scaled up by a factor 10 compared to the real shape.

Fig. 5.4a shows the deformations in the y-direction at the end of the simulation. As it can be seen, the sample expands a lot in that direction (more than 3 [mm] at 2000 [s]). This is expected since it is the transverse direction, along which the thermal expansion coefficient is larger. Fig. 5.4b shows that the deformation along the z-direction is very small (maximum of 0.09 [mm] at 2000 [s]). This is due to the low thermal expansion coefficient in the fibers' direction. Note that the expansion, and thus the deformation, in the y and z directions is constantly increasing with time (provided that the temperature increases).

(a) y-direction.
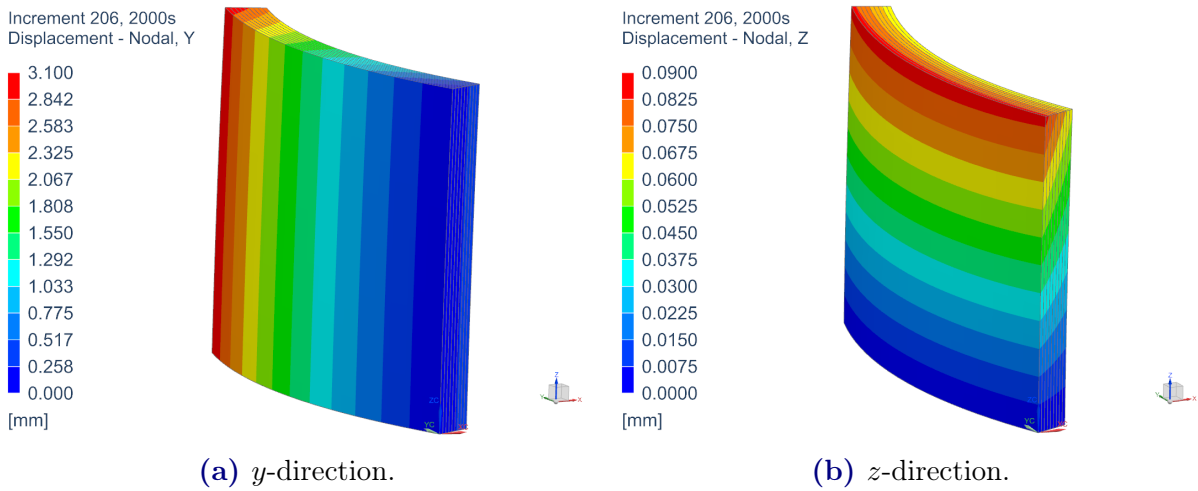
(b) z-direction.

Figure 5.4: Deformation of the composite sample in the y and z directions at time $t = 2000$ [s] obtained with Samcef (without any load). The apparent shape is scaled up by a factor 10 compared to the real shape.

Now that the influence of the thermal expansion has been discussed, a constant compression load of 10 [MPa] can be applied at the top of the sample. As it can be seen in Fig. 5.5, the sample is rapidly subjected to buckling. It collapses after about 65 [s] as shown in Fig. 5.6. This is explained by the fact that the compressive stiffness modulus in the fibers direction depends on the temperature. The evolution of the stiffness modulus with temperature is shown in Fig. 5.7. Its values have been chosen artificially in order to simulate a loss in stiffness with temperature which exist for real materials. These are not actual values of an existing material. The objective is only to show that the change in stiffness linked to temperature leads to buckling. Since the temperature is higher at the exposed face than at the unexposed one, the stiffness modulus varies along the thickness. It is smaller at the exposed face which leads to buckling towards that side. Note that at 65 [s], the temperature is around 325 [°C] at the exposed face and around 107 [°C] at the middle of the sample. According to Fig. 5.7, the stiffness modulus at that time has become very low in the first half of the sample (in the thickness direction).

The presence of the automatic time step can be observed in Fig. 5.6. Indeed, each point corresponds to a time at which the response is computed. More of these points are present at the beginning and at the end of the simulation. As explained in the methodology, this time step is chosen based on the integration error which must be lower than a fixed value. Regarding the beginning of the simulation, a small time step is required because the non-linearity of the problem is not known. Therefore, a small initial time step maximizes the chances to convergence at the first time step. Then, approaching the collapse event, the time steps are starting to be reduced. It is due to the fact that the problem does not converge anymore and that the solver is searching for a solution by slightly varying the time.
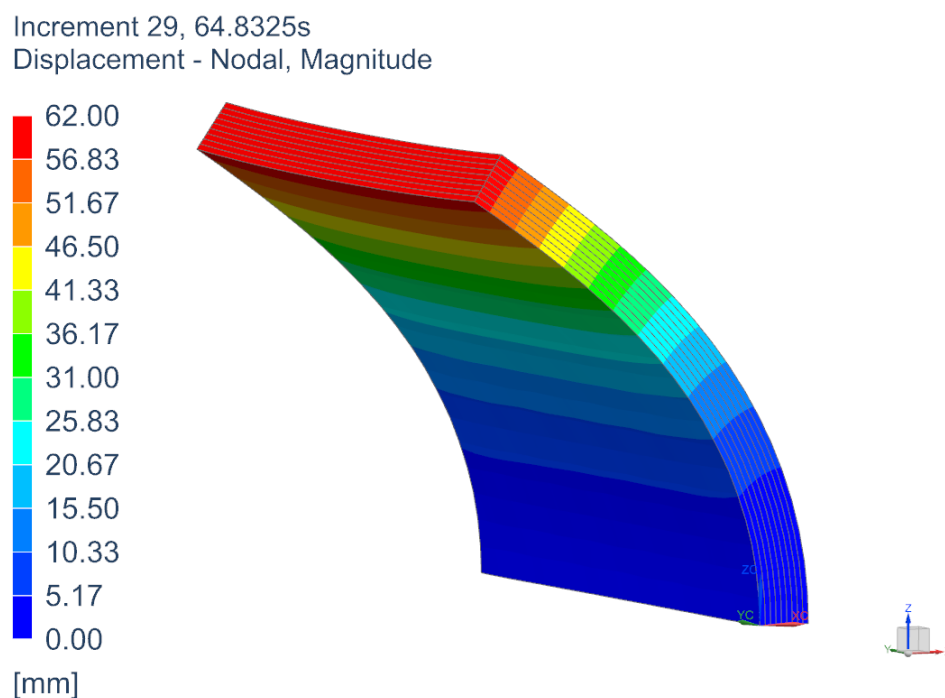
Figure 5.5: Deformation of the composite sample prior to collapse obtained with Samcef (expressed by the total displacement magnitude). No scaling of the apparent shape. Loading of 10 [MPa].
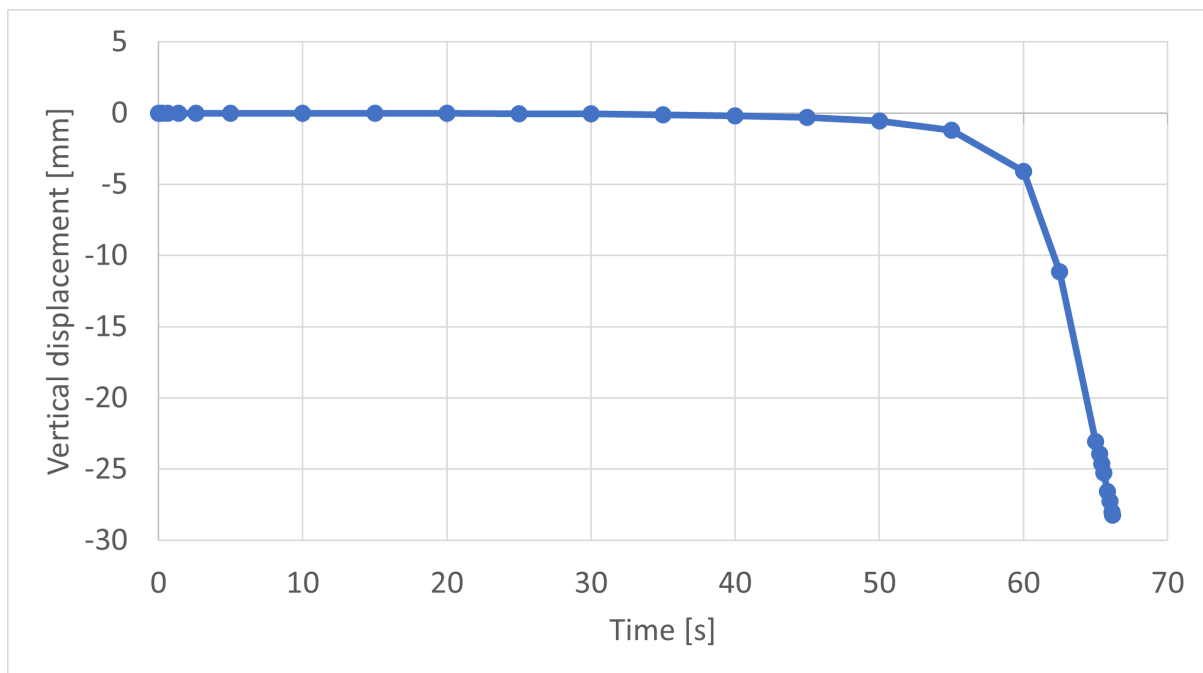
Figure 5.6: Time evolution of the sample upper edge vertical displacement (z-direction) obtained with SAMCEF. Loading of 10 [MPa].
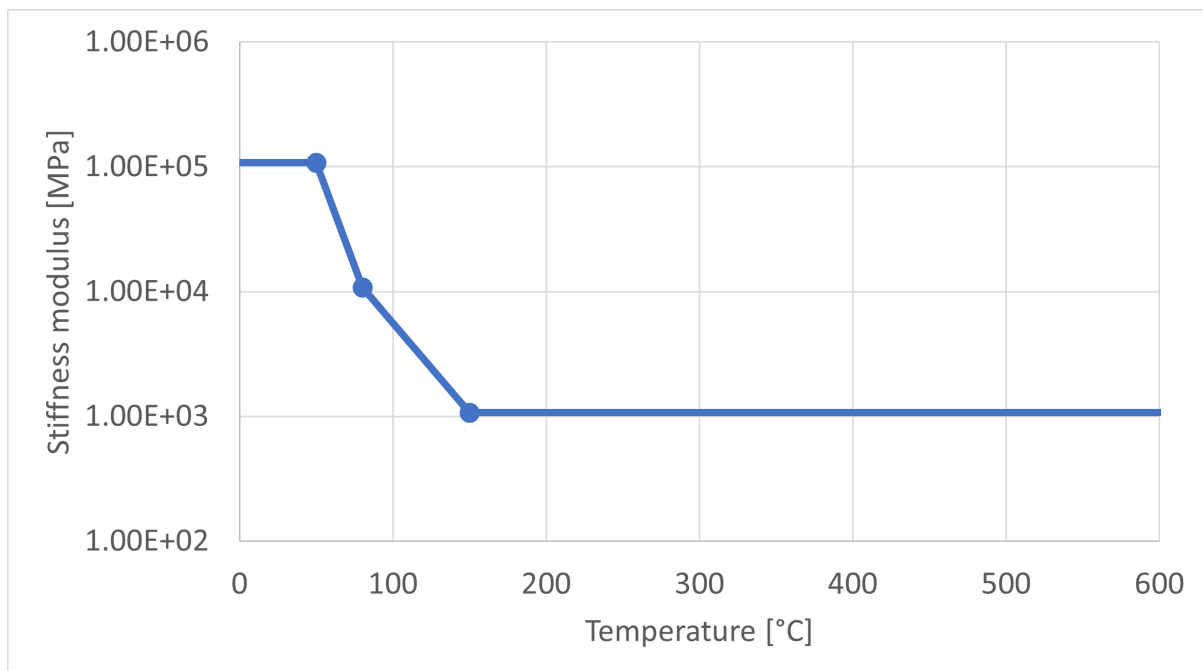

Figure 5.7: Evolution of the stiffness modulus E_1 in the fibers direction as a function of temperature defined in SAMCEF.

5.3 Advanced material model

The model can be improved by using a more advanced material definition developed by Ladevèze [34]. It takes into account the damage and the plasticity appearing in the laminate based on the Continuum Damage Mechanics theory (see Section 3.3.2).

The response of the material due to temperature only (without loading) is very similar to the one obtained in the previous section for the elastic model. Therefore, the discussion made about Fig. 5.3 and 5.4 is still valid in this case.

Regarding the advanced material, it is interesting to highlight the evolution of the damage variable when the sample is subjected to loading (10 [MPa]). This is indeed one of the additional variable that is not taken into account in the simple elastic model. Fig. 5.8 shows the damage level of each element for the ply at the unexposed face. A value of 1 means that the element is totally damaged which is the case for some of them just before collapse. The damage variable highlighted in Fig. 5.8 is d_{22}. It means that the damage is present in the matrix and is parallel to the fibers.

A graph shown in Fig. 5.9 gives the time evolution of the damage variables. They are given for all the plies at the location of the bottom left red element from Fig. 5.8. It can be observed that the damage increases very slowly in a first time for plies 8 and 9. Then, just before the collapse, its value jumps to one very rapidly. The three first plies (7 to 9) starting from the unexposed face are totally damaged and ply 6 is partially damaged. All the other plies are very slightly damaged as well but almost not compared to the plies 6 to 9. Note that the model does not take into account the damage induced directly by the material decomposition. Moreover, as explained previously, the mesh should be refined in order to obtain better results. Other results such as plasticity could be studied because it also influences the composite behavior.
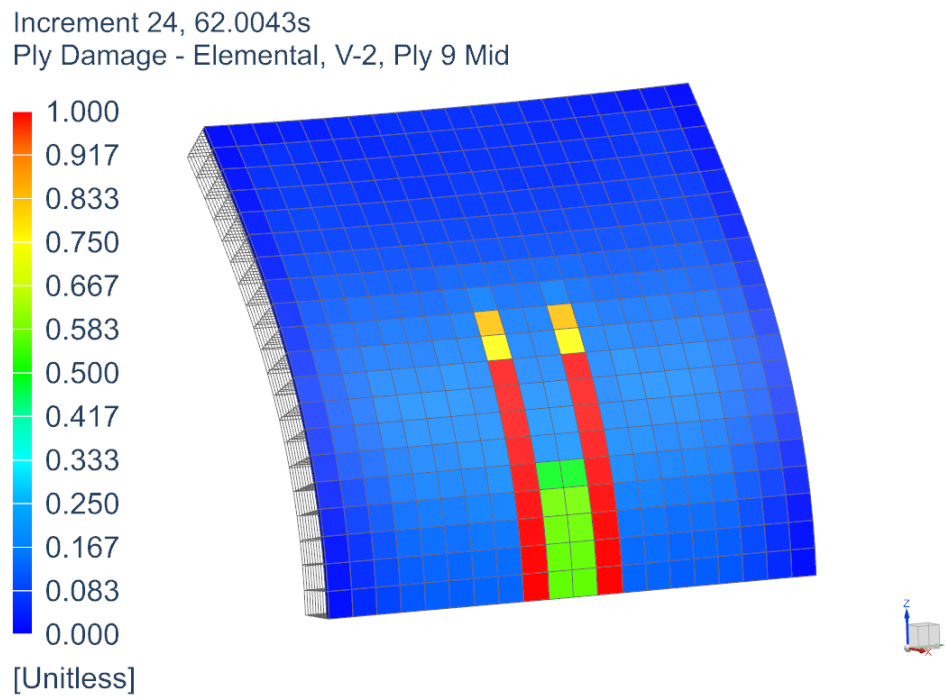
Figure 5.8: Representation of the damage variable for each element of the ply located at the unexposed face of the sample. Loading of 10 [MPa].
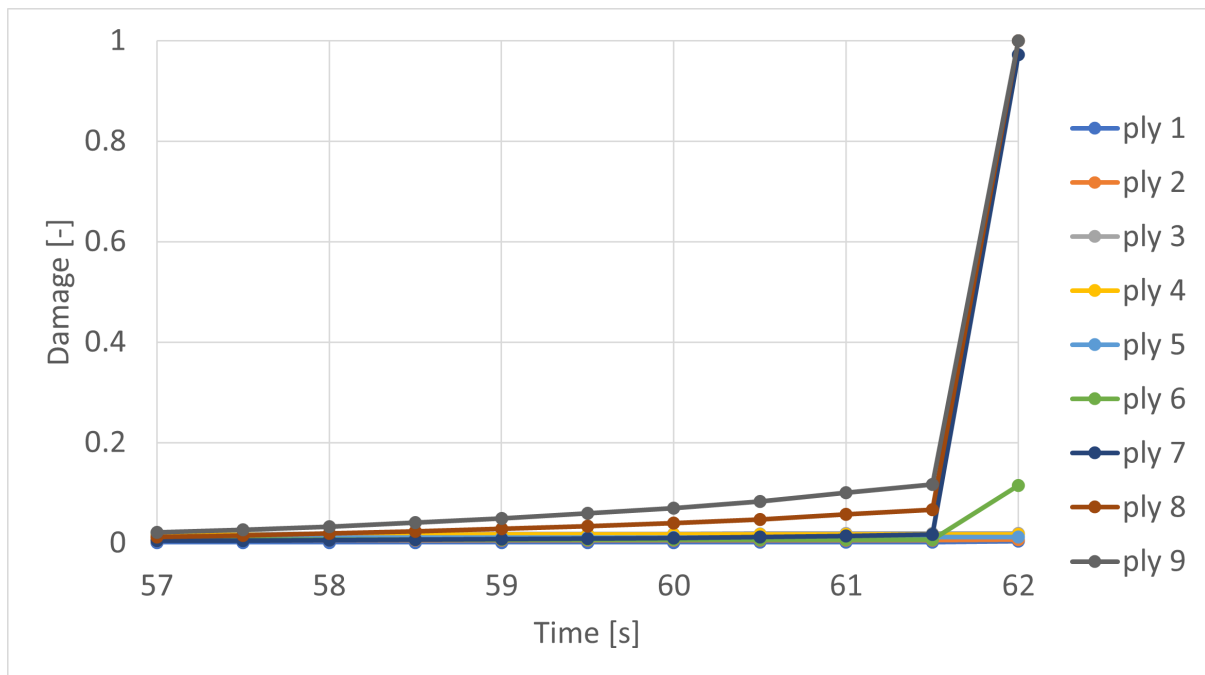

Figure 5.9: Time evolution of the damage variable for each ply at the location of the bottom left red element from Fig. 5.8. Loading of 10 [MPa].

Chapter 6

Conclusions and perspectives

The objective of this master thesis was to perform a thermo-mechanical modeling of composite materials subjected to fire. The modeling had to be done using the SAMCEF finite element solver. The thermal and the mechanical part were considered separately leading to a two-step analysis. The focus was put on the thermal part since it had never been done previously at the company GDTECH and therefore required a certain amount of work.

First, the thermo-mechanical processes occurring in composites subjected to fire have been identified. They were divided into four main categories: thermal, chemical, physical and failure processes. Then, some existing thermal models available in the literature have been discussed. One particular model developed by Henderson et al. was found to be the one most used in practice. This model is based on three main processes that govern the thermal response of composites exposed to fire. These are the heat conduction, matrix decomposition and convection from the decomposition gases. A detailed description of that model has been made regarding the material properties definition and the boundary conditions. The existing mechanical models were briefly discussed.

Then, the solver SAMCEF was used to reproduce results coming from the literature. A modeling methodology has been developed in order to adapt the default equations used in the software to the model from Henderson et al.. This methodology allowed to obtain a one-dimensional model able to predict the thermal response of composites subjected to fire. The results were assessed thanks to two publications using the same theoretical model. It was shown that the mass loss due to matrix decomposition was correctly represented by the software. Regarding the evolution of the temperature distribution inside the material, the results were not very conclusive. It was shown that the value of the energy of decomposition needed to be increased by a certain amount in order to obtain better results. No physical explanation was found for that need. Moreover, it was highlighted that complete material properties were sometimes lacking. Therefore, the numerical model required some tuning of the available parameters in order to obtain better

temperature predictions. It was observed that when the model was correctly tuned, it was able to give accurate results for different heat fluxes and level of pyrolysis.

Eventually, the mechanical part of this master thesis showed that it was possible to transfer a thermal solution into a mechanical model. The mapping of the temperature distribution worked correctly. This was also something that had never been done for composites at GDTECH and which is therefore a contribution to the company. The mechanical model used a different material than the one used for the thermal analysis. It was not optimal but proved that a thermo-mechanical modeling was possible in SAMCEF. Using an elastic material law, the results nonetheless showed the effect of the thermal expansion in case of no loading. The failure under loading due to buckling has also been observed. A more advanced model allowed to represent the damage occurring in the material.

The work realised in this master thesis give a good understanding of the thermal response of composites subjected to fire and how to predict it using SAMCEF. Moreover, it shows that a two-step thermo-mechanical modeling is feasible using the software SAMCEF. However, some perspectives of improvements have been identified and are listed here:

- User-subroutines could be implemented in order to better define the heat capacities and thermal conductivities.

- The reason for the need to increase the value of the decomposition energy should be found.

- The creation of a database containing complete thermal and mechanical properties should be created

- Regarding the thermal model from Henderson et al., it could be interesting to implement it in a software like MATLAB and compare the results with the one obtained thanks to SAMCEF.

- More composite materials should be used to validate the thermal model. This could help to identify why there are still some differences between the results given in the literature and the one computed.

- Regarding the mechanical analysis, a more rigorous study should be carried out. An identical material as the one used for the thermal part should also be used.

Appendix

A.   Governing thermal equation

The energy equation writes:

$$\frac{\partial}{\partial t}\left(mh + m_g h_g\right) = \frac{\partial}{\partial x}\left(k\frac{\partial T}{\partial x}\right)\Delta x \Delta A - \frac{\partial}{\partial x}\left(\dot{m}_g h_g\right)\Delta x - Q_i\frac{\partial m}{\partial t}.$$

Expanding the terms leads to:

$$h\frac{\partial m}{\partial t} + m\frac{\partial h}{\partial t} + h_g\frac{\partial m_g}{\partial t} + m_g\frac{\partial h_g}{\partial t} = \frac{\partial}{\partial x}\left(k\frac{\partial T}{\partial x}\right)\Delta x \Delta A - h_g\frac{\partial \dot{m}_g}{\partial x}\Delta x - \dot{m}_g\frac{\partial h_g}{\partial x}\Delta x - Q_i\frac{\partial m}{\partial t},$$

$$\Leftrightarrow\quad m\frac{\partial h}{\partial t} + m_g\frac{\partial h_g}{\partial t} = \frac{\partial}{\partial x}\left(k\frac{\partial T}{\partial x}\right)\Delta x \Delta A - \dot{m}_g\frac{\partial h_g}{\partial x}\Delta x - h_g\left(\frac{\partial m_g}{\partial t} + \frac{\partial \dot{m}_g}{\partial x}\Delta x\right) - h\frac{\partial m}{\partial t} - Q_i\frac{\partial m}{\partial t}.$$

The mass continuity equation writes:

$$-\frac{\partial m}{\partial t} = \frac{\partial m_g}{\partial t} + \frac{\partial \dot{m}_g}{\partial x}\Delta x.$$

Therefore, the energy equation becomes:

$$m\frac{\partial h}{\partial t} + m_g\frac{\partial h_g}{\partial t} = \frac{\partial}{\partial x}\left(k\frac{\partial T}{\partial x}\right)\Delta x \Delta A - \dot{m}_g\frac{\partial h_g}{\partial x}\Delta x + h_g\frac{\partial m}{\partial t} - h\frac{\partial m}{\partial t} - Q_i\frac{\partial m}{\partial t},$$

$$\Leftrightarrow\quad m\frac{\partial h}{\partial t} + m_g\frac{\partial h_g}{\partial t} = \frac{\partial}{\partial x}\left(k\frac{\partial T}{\partial x}\right)\Delta x \Delta A - \dot{m}_g\frac{\partial h_g}{\partial x}\Delta x - \frac{\partial m}{\partial t}\left(Q_i + h - h_g\right).$$

The enthalpy terms can also be developed:

$$mC\frac{\partial T}{\partial t} + m_g C_g\frac{\partial T}{\partial t} = \frac{\partial}{\partial x}\left(k\frac{\partial T}{\partial x}\right)\Delta x \Delta A - \dot{m}_g C_g\frac{\partial T}{\partial x}\Delta x - \frac{\partial m}{\partial t}\left(Q_i + h - h_g\right),$$

$$\Leftrightarrow\quad \left(mC + m_g C_g\right)\frac{\partial T}{\partial t} = \frac{\partial}{\partial x}\left(k\frac{\partial T}{\partial x}\right)\Delta x \Delta A - \dot{m}_g C_g\frac{\partial T}{\partial x}\Delta x - \frac{\partial m}{\partial t}\left(Q_i + h - h_g\right).$$

B. Volumetric heat capacity

The volumetric heat capacity term from the publication of Henderson et al. [8] must be reworked in order to be correctly defined in SAMCEF.

In the thermal equation from Henderson et al. [8], this term writes:

$$(mC + m_g C_g), \tag{6.1}$$

with

$$C = F \cdot C_v + (1 - F) \cdot C_c, \tag{6.2}$$

where $F = \frac{m - m_f}{m_0 - m_f}$.

In SAMCEF, the volumetric heat capacity term is simply:

$$\rho C, \tag{6.3}$$

where

$$\rho C = (1 - \alpha) \cdot \rho_v C_v + \alpha \cdot \rho_c C_c, \tag{6.4}$$

and $\alpha = \frac{\rho_v - \rho}{\rho_v - \rho_c}$.

Starting from the heat capacity term given in Eq. 6.1, and assuming constant volume V:

$$\frac{mC + m_g C_g}{V} = \frac{m}{V}C + \frac{m_g}{V}C_g, \tag{6.5}$$

$$= \rho C + \frac{m_g}{V}C_g, \tag{6.6}$$

$$= \rho C + \frac{\phi}{\phi}\frac{m_g}{V}C_g, \tag{6.7}$$

$$= \rho C + \phi\frac{m_g}{V_g}C_g, \tag{6.8}$$

$$= \rho C + \phi\rho_g C_g. \tag{6.9}$$

Again, assuming a constant volume, it can be written that:

$$F = \frac{m - m_f}{m_0 - m_f} = \frac{\rho - \rho_c}{\rho_v - \rho_c} = 1 - \alpha. \tag{6.10}$$

Knowing that, the expressions of the heat capacity C and the porosity ϕ of the material become respectively:

$$C = F \cdot C_v + (1 - F) \cdot C_c, \tag{6.11}$$

$$= (1 - \alpha) \cdot C_v + \alpha \cdot C_c, \tag{6.12}$$

$$\phi = F \cdot \phi_v + (1 - F) \cdot \phi_c, \tag{6.13}$$

$$= (1 - \alpha) \cdot \phi_v + \alpha \cdot \phi_c. \tag{6.14}$$

Moreover, the expression of the material density ρ is by definition:

$$\rho = (1 - \alpha) \cdot \rho_v + \alpha \cdot \rho_c. \tag{6.15}$$

The density, heat capacity and porosity variables can be replaced by their definition in Eq. 6.9 which leads to:

$$\frac{(mC + m_g C_g)}{V} = [(1 - \alpha) \cdot \rho_v + \alpha \cdot \rho_c] \times [(1 - \alpha) \cdot C_v + \alpha \cdot C_c] \\ + [(1 - \alpha) \cdot \phi_v + \alpha \cdot \phi_c] \rho_g C_g. \tag{6.16}$$

Multiplying the virgin material porosity ϕ_v by $\frac{\rho_v}{\rho_v}$ and the charred material porosity ϕ_c by $\frac{\rho_c}{\rho_c}$ yields:

$$\frac{(mC + m_g C_g)}{V} = (1 - \alpha) \cdot \rho_v \left(\frac{\phi_v}{\rho_v} \rho_g C_g + (1 - \alpha)C_v + \alpha C_c \right) \\ + \alpha \cdot \rho_c \left(\frac{\phi_c}{\rho_c} \rho_g C_g + (1 - \alpha)C_v + \alpha C_c \right). \tag{6.17}$$

Knowing the definition of the volumetric heat capacity used by SAMCEF and given by Eq. 6.4, it follows that:

$$C_v^{\text{SAMCEF}} = \frac{\phi_v}{\rho_v} \rho_g C_g + (1 - \alpha)C_v + \alpha C_c, \tag{6.18}$$

$$C_c^{\text{SAMCEF}} = \frac{\phi_c}{\rho_c} \rho_g C_g + (1 - \alpha)C_v + \alpha C_c. \tag{6.19}$$

C_v^{SAMCEF} and C_c^{SAMCEF} are the variables that must be used respectively for the virgin and charred material heat capacity definition in SAMCEF.

C. Thermal conductivity

The thermal conductivity from the publication of Henderson et al. [8] must be reworked in order to be correctly defined in SAMCEF.

In the thermal equation from Henderson et al. [8], the composite thermal conductivity writes:

$$(\phi \cdot k_g + (1 - \phi) \cdot k), \tag{6.20}$$

with

$$k = F \cdot k_v + (1 - F) \cdot k_c, \tag{6.21}$$

$$\phi = F \cdot \phi_v + (1 - F) \cdot \phi_c. \tag{6.22}$$

where $F = \frac{m - m_f}{m_0 - m_f}$.

In SAMCEF, the material thermal conductivity is simply:

$$k, \tag{6.23}$$

where

$$k = (1 - \alpha) \cdot k_v + \alpha \cdot k_c, \tag{6.24}$$

and $\alpha = \frac{\rho_v - \rho}{\rho_v - \rho_c}$.

Assuming a constant volume, it can be written that:

$$F = \frac{m - m_f}{m_0 - m_f} = \frac{\rho - \rho_c}{\rho_v - \rho_c} = 1 - \alpha. \tag{6.25}$$

Knowing that, the expressions of the thermal conductivity k given in Eq. 6.21 and the porosity ϕ of the material become respectively:

$$k = F \cdot k_v + (1 - F) \cdot k_c, \tag{6.26}$$

$$= (1 - \alpha) \cdot k_v + \alpha \cdot k_c, \tag{6.27}$$

$$\phi = F \cdot \phi_v + (1 - F) \cdot \phi_c, \tag{6.28}$$

$$= (1 - \alpha) \cdot \phi_v + \alpha \cdot \phi_c. \tag{6.29}$$

The thermal conductivity and the porosity variables can be replaced by their definition

in Eq. 6.20 which leads to:

$$(\phi \cdot k_g + (1 - \phi) \cdot k) = [(1 - \alpha) \cdot \phi_v + \alpha \cdot \phi_c] \, k_g + [1 - (1 - \alpha) \cdot \phi_v - \alpha \cdot \phi_c]$$
$$\times [(1 - \alpha) \cdot k_v + \alpha \cdot k_c] \,. \tag{6.30}$$

This equation can be rewritten in order to stick to the formulation used in SAMCEF. This leads to the following expression:

$$(\phi \cdot k_g + (1 - \phi) \cdot k) = (1 - \alpha) \cdot (k_v + k_g \phi_v - k_v [(1 - \alpha)\phi_v + \alpha\phi_c])$$
$$+ \alpha \cdot (k_c + k_g \phi_c - k_c [(1 - \alpha)\phi_v + \alpha\phi_c]) \,. \tag{6.31}$$

Knowing the definition of the thermal conductivity used by SAMCEF and given by Eq. 6.24, it follows that:

$$k_v^{\text{SAMCEF}} = k_v + k_g \phi_v - k_v [(1 - \alpha)\phi_v + \alpha\phi_c] \,, \tag{6.32}$$

$$k_c^{\text{SAMCEF}} = k_c + k_g \phi_c - k_c [(1 - \alpha)\phi_v + \alpha\phi_c] \,. \tag{6.33}$$

k_v^{SAMCEF} and k_c^{SAMCEF} are the variables that must be used respectively for the virgin and charred material thermal conductivity definition in SAMCEF.

D. Darcy law

The form of the Darcy law used in the publication from Henderson et al. [8] is given by the following equation:

$$\dot{m}_g = -\frac{\gamma m_g}{\mu \phi \Delta x} \frac{\partial P}{\partial x},$$ (6.34)

which is equivalent to:

$$\dot{m}_g'' = -\frac{\gamma m_g}{\mu \phi \Delta x \Delta A} \frac{\partial P}{\partial x}.$$ (6.35)

The pressure P is given by the following equation:

$$P = \frac{m_g RT}{M_g \phi \Delta x \Delta A}.$$ (6.36)

Isolating m_g in Eq. 6.36 and introducing it in the Darcy law given by Eq. 6.35 yields:

$$\dot{m}_g'' = -\frac{\gamma M_g P}{\mu RT} \frac{\partial P}{\partial x}.$$ (6.37)

In SAMCEF, the Darcy law is defined as follows:

$$\dot{m}_g'' = -K_P \frac{\partial P}{\partial x} \quad \text{where} \quad K_P = \frac{\gamma M_g P}{\mu RT}.$$ (6.38)

As it can be seen, Eq. 6.37 and 6.38 are totally equivalent. Therefore, the form of the Darcy law used by default in SAMCEF does not have to be modified.

E. Radiative source temperature

The boundary condition used in the model from Henderson et al. [8] for the exposed face is given in Eq. 2.16 and rewritten here:

$$-k \left. \frac{\partial T}{\partial x} \right|_{x=0} = \varepsilon_s \left(q''_{rad} - \sigma T_{s,0}^4 \right) + h_{conv,0} \left(T_\infty - T_{s,0} \right), \tag{6.39}$$

$$\text{with} \qquad q''_{rad} = \sigma \varepsilon_r T_r^4. \tag{6.40}$$

The radiative component of this boundary condition writes:

$$q'' = \varepsilon_s \left(q''_{rad} - \sigma T_{s,0}^4 \right) \tag{6.41}$$

In SAMCEF, the radiative flux boundary condition is defined as follows, assuming a gray body ($\alpha_s = \varepsilon_s$ by default in the software):

$$q'' = \sigma \left(\alpha_s T_r^4 - \varepsilon_s T_s^4 \right), \tag{6.42}$$

$$\Leftrightarrow \quad q'' = \varepsilon_s \left(\sigma T_r^4 - \sigma T_s^4 \right). \tag{6.43}$$

By analogy between Eq. 6.41 and 6.43, the expression for the radiative source temperature to be introduced in SAMCEF is:

$$T_r^{\text{SAMCEF}} = \sqrt[4]{\frac{q''_{rad}}{\sigma}}. \tag{6.44}$$

Bibliography

[1] Snorri Gudmundsson. *General Aviation Aircraft Design: Applied Methods and Procedures.* 2nd ed. San Diego: Elsevier Science & Technology, 2022. ISBN: 978-0-12-822647-6.

[2] Daniel P. Raymer. *Aircraft Design: A Conceptual Approach.* 5th ed. AIAA Education Series. Reston, VA: American Institute of Aeronautics and Astronautics, 2012. ISBN: 978-1-60086-911-2.

[3] Anthony F. Molland. *The Maritime Engineering Reference Book a Guide to Ship Design, Construction and Operation.* 1st edition. Amsterdam ; Butterworth-Heinemann, 2008. ISBN: 978-1-283-31088-8.

[4] S. Feih et al. "Modelling the Compression Strength of Polymer Laminates in Fire". In: *Composites Part A: Applied Science and Manufacturing* 38.11 (2007), pp. 2354–2365. ISSN: 1359-835X. DOI: `10.1016/j.compositesa.2007.04.013`.

[5] *Simcenter Samcef.* Siemens Industry Software. 2019.

[6] A. P. Mouritz et al. "Review of Fire Structural Modelling of Polymer Composites". In: *Composites. Part A, Applied science and manufacturing* 40.12 (2009), pp. 1800–1814. ISSN: 1359-835X. DOI: `10.1016/j.compositesa.2009.09.001`.

[7] A. P. Mouritz. *Fire Properties of Polymer Composite Materials.* 1st ed. 2006. Solid Mechanics and Its Applications, 143. Dordrecht: Springer Netherlands, 2006. ISBN: 978-1-280-74510-2. DOI: `10.1007/978-1-4020-5356-6`.

[8] J. B. Henderson, J. A. Wiebelt, and M. R. Tant. "A Model for the Thermal Response of Polymer Composite Materials with Experimental Verification". In: *Journal of Composite Materials* 19 (Jan. 1985), pp. 579–595. ISSN: 0021-9983. DOI: `10.1177/002199838501900608`.

[9] S. Feih et al. "Modelling the Tension and Compression Strengths of Polymer Laminates in Fire". In: *Composites science and technology* 67.3-4 (2007), pp. 551–564. ISSN: 0266-3538. DOI: `10.1016/j.compscitech.2006.07.038`.

[10] J.B. Henderson and T.E. Wiecek. "A Mathematical Model to Predict the Thermal Response of Decomposing, Expanding Polymer Composites". In: *Journal of Composite Materials* 21.4 (Apr. 1987), pp. 373–393. ISSN: 0021-9983, 1530-793X. DOI: `10.1177/002199838702100406`.

[11]   G. T. Egglestone and D. M. Turley. "Flammability of GRP for Use in Ship Super-
        structures". In: *Fire and Materials* 18.4 (1994), pp. 255–260. ISSN: 1099-1018. DOI:
        `10.1002/fam.810180408`.

[12]   M. J. Scudamore. "Fire Performance Studies on Glass-Reinforced Plastic Lam-
        inates". In: *Fire and Materials* 18.5 (1994), pp. 313–325. ISSN: 1099-1018. DOI:
        `10.1002/fam.810180507`.

[13]   Archibald Tewarson and Domenic P. Macaione. "Polymers and Composites- An
        Examination of Fire Spread and Generation of Heat and Fire Products". In: *Journal
        of Fire Sciences* 11.5 (Sept. 1993), pp. 421–441. ISSN: 0734-9041. DOI: `10.1177/`
        `073490419301100504`.

[14]   J. R. Brown and Z. Mathys. "Reinforcement and Matrix Effects on the Combustion
        Properties of Glass Reinforced Polymer Composites". In: *Composites. Part A, Ap-
        plied science and manufacturing* 28.7 (1997), pp. 675–681. ISSN: 1359-835X. DOI:
        `10.1016/S1359-835X(97)00018-3`.

[15]   A. G. Gibson et al. "A Model for the Thermal Performance of Thick Composite
        Laminates in Hydrocarbon Fires". In: *Revue de l'Institut Français du Pétrole* 50.1
        (Jan. 1995), pp. 69–74. ISSN: 0020-2274, 2777-3566. DOI: `10.2516/ogst:1995007`.

[16]   R. M. Sullivan and N. J. Salamon. "A Finite Element Method for the Thermo-
        chemical Decomposition of Polymeric Materials—I. Theory". In: *International Jour-
        nal of Engineering Science* 30.4 (Apr. 1992), pp. 431–441. ISSN: 0020-7225. DOI:
        `10.1016/0020-7225(92)90035-F`.

[17]   YuI Dimitrienko. "Thermomechanical Behaviour of Composite Materials and Struc-
        tures under High Temperatures: 1. Materials". In: *Composites. Part A, Applied sci-
        ence and manufacturing* 28.5 (1997), pp. 453–461. ISSN: 1359-835X. DOI: `10.1016/`
        `S1359-835X(96)00144-3`.

[18]   Changsong Luo, Wei Xie, and Paul E. DesJardin. "Fluid-Structure Simulations
        of Composite Material Response for Fire Environments". In: *Fire technology* 47.4
        (2009), pp. 887–912. ISSN: 0015-2684. DOI: `10.1007/s10694-009-0126-4`.

[19]   Wei Xie and Paul E. DesJardin. "An Embedded Upward Flame Spread Model Using
        2D Direct Numerical Simulations". In: *Combustion and flame* 156.2 (2009), pp. 522–
        530. ISSN: 0010-2180. DOI: `10.1016/j.combustflame.2008.11.011`.

[20]   Wei Xie and Paul E. DesJardin. "A Level Set Embedded Interface Method for
        Conjugate Heat Transfer Simulations of Low Speed 2D Flows". In: *Computers &
        fluids* 37.10 (2008), pp. 1262–1275. ISSN: 0045-7930. DOI: `10.1016/j.compfluid.`
        `2007.10.017`.

[21]   Thomas W. Loh, Everson Kandare, and Kate TQ Nguyen. "The Effect of Thickness
        on the Compression Failure of Composite Laminates in Fire". In: *Composite struc-
        tures* 286 (2022). ISSN: 0263-8223. DOI: `10.1016/j.compstruct.2022.115334`.

[22] Brian Y. Lattimer, Jason Ouellette, and Javier Trelles. "Thermal Response of Composite Materials to Elevated Temperatures". In: *Fire Technology* 47.4 (Oct. 2011), pp. 823–850. ISSN: 1572-8099. DOI: `10.1007/s10694-009-0121-9`.

[23] T. L. Bergman. *Incropera's Principles of Heat and Mass Transfer*. Global edition. Singapore: Wiley, 2018. ISBN: 978-1-119-38291-1.

[24] Ziqing Yu and Aixi Zhou. "Effect of Flame Heat Flux on Thermal Response and Fire Properties of Char-Forming Composite Materials". In: *Fire and materials* 38.1 (2014), pp. 100–110. ISSN: 0308-0501. DOI: `10.1002/fam.2166`.

[25] Changsong Luo and Paul E. DesJardin. "Evaluation of Thermal Transport Properties Using a Micro-Cracking Model for Woven Composite Laminates". In: (July 2009).

[26] Gaurav Agarwal and Brian Lattimer. "Method for Measuring the Standard Heat of Decomposition of Materials". In: *Thermochimica Acta* 545 (Oct. 2012), pp. 34–47. ISSN: 0040-6031. DOI: `10.1016/j.tca.2012.06.027`.

[27] Camille Mercadé. "Modélisation de la dégradation d'un matériau composite carbone-époxy soumis à une sollicitation thermo-mécanique couplée. Application aux réservoirs d'hydrogène de type IV". PhD thesis. 2017.

[28] Anne-Charlotte Goupil. "Contribution à l'étude numérique du comportement au feu d'un panneau composite pour l'industrie navale". PhD thesis. 2016.

[29] Juan Pablo Márquez Costa. "Caractérisation et modélisation des interfaces dans les composites organiques stratifiés à haute température: Application à la tenue au feu des structures aéronautiques". PhD thesis. 2021.

[30] *SAMCEF User's Manual*. URL: `https://docs.plm.automation.siemens.com/data_services/resources/nx/1899/nx_help/custom/en_US/samcef_solver_documentation/index.html`.

[31] Suhas V. Patankar. *Numerical Heat Transfer and Fluid Flow*. Series in Computational Methods in Mechanics and Thermal Sciences. Washington : New York: Hemisphere Pub. Corp. ; McGraw-Hill, 1980. ISBN: 978-0-07-048740-6.

[32] Michaël Bruyneel. *Private Communication*. 2022.

[33] Michaël Bruyneel. *Classical Lamination Theory*. Lecture Notes. Université de Liège, 2021.

[34] P. Ladeveze and E. LeDantec. "Damage Modelling of the Elementary Ply for Laminated Composites". In: *Composites Science and Technology* 43.3 (Jan. 1992), pp. 257–267. ISSN: 0266-3538. DOI: `10.1016/0266-3538(92)90097-M`.

[35] Michaël Bruyneel et al. "Damage Modeling of Laminated Composites: Validation of the Intra-Laminar Damage Law of SAMCEF at the Coupon Level for UD Plies". In: 2014.

[36]   K Joon Yoon and Ju-Sik Kim. "Thermal Deformations of Carbon/Epoxy Laminates for Temperature Variation". In: *ICCM-12, Paris* (1999).

[37]   Olivier Allix et al. "Modelling and Identification of Temperature-Dependent Mechanical Behaviour of the Elementary Ply in Carbon/Epoxy Laminates". In: *Composites science and technology* 56.7 (1996), pp. 883–888. ISSN: 0266-3538. DOI: `10.1016/0266-3538(96)00036-X`.

[38]   Jean-Charles Craveur and Philippe Jetteur. *Introduction à la mécanique non linéaire: Calcul des structures par éléments finis*. Dunod, Mar. 2020. ISBN: 978-2-10-081247-9.